

**NASA Contractor Report 4267**

**Autonomous Integrated GPS/INS  
Navigation Experiment for OMV:  
PHASE I Feasibility Study**

**Triveni N. Upadhyay, George J. Priovolos,  
and Harley Rhodehamel**

**CONTRACT NAS8-38031  
JANUARY 1990**

(NASA-DT-89-7) ADMINISTRATION  
GPS/INS NAVIGATION EXPERIMENT FOR OMV. PHASE  
I: FEASIBILITY STUDY (Mayflower  
Communications Co.) 93 p

CSCL 17G

H1/04 0271118

Unclas



NASA Contractor Report 4267

# Autonomous Integrated GPS/INS Navigation Experiment for OMV: PHASE I Feasibility Study

Triveni N. Upadhyay, George J. Priovolos,  
and Harley Rhodehamel  
*Mayflower Communications Company, Inc.*  
*Reading, Massachusetts*

Prepared for  
George C. Marshall Space Flight Center  
under Contract NAS8-38031



National Aeronautics and  
Space Administration  
Office of Management  
Scientific and Technical  
Information Division

1989



## FOREWORD

The research results described in this report was sponsored by NASA Marshall Space Flight Center, Marshall Space Flight Center, AL under the SBIR Phase I Program, Contract No. NAS8-38031. The NASA COTR on the program was Mr. A. Wayne Deaton, EL23.

The research was carried out by Mayflower Communications Company, Inc. during the period February - August 1989. The Principal Investigator on the project was Dr. Triveni N. Upadhyay.

Several individuals and organizations provided technical data and support which were essential to the successful completion of the Phase I research. Mr. Wayne Deaton EL23, and Mr. Larry Brandon, of NASA MSFC provided us data on GPS navigation requirements for future advanced STSs and the data on NASA atmospheric drag models. Mr. Chuck Shortwell and Mr. Albert T. Monulki, TRW OMV Program, were helpful in providing OMV GN&C description including preliminary definition of the telemetry data and interface to the OMV OBC.

Excellent administration support in the preparation of the report was provided by Ms. Joan Beaulieu and Ms. Angela Russo.

# AUTONOMOUS INTEGRATED GPS/INS NAVIGATION EXPERIMENT FOR OMV

## TABLE OF CONTENTS

Section	Title	Page
1	INTRODUCTION	1
1.1	Background	1
1.2	Outline of the Report	4
2	PHASE I TECHNICAL OBJECTIVES AND APPROACH	5
3	PHASE I RESULTS	9
3.1	Common GN&C Requirements	10
3.2	OMV OBC Interface Requirements	13
3.3	Integrated GPS/INS Navigation Filter Design	15
3.3.1	Navigation and Attitude Sources	17
3.3.2	Gravity and Atmospheric Drag Models	19
3.3.3	GPS Satellite Visibility	30
3.3.4	Navigation Filter Implementation	43
3.3.5	Performance Results	59
3.6	Memory and Throughput Analysis	72
3.7	Experiment Validation Test Plan	78
4	SUMMARY - CONCLUSIONS	80
5	REFERENCES	86

## SECTION 1

### INTRODUCTION

Mayflower Communications Company, Inc., has prepared this final report on the basis of the results of its SBIR Phase I research, Topic No. 88-1-09.10, of the same title. The Phase I research was carried out under Contract No. NAS8-38031.

#### 1.1 Background

The emphasis on space-based autonomous systems to support government and commercial needs is expected to continue into the future. Future space missions will require increased automation, up to fully autonomous operations, to meet the need for faster decisions, continual coverage and increased survivability [1, 10, 11]. The cost of ground tracking and contingency mission planning to support these missions is expected to be very high. Furthermore, the tracking accuracy and coverage of these ground stations, as well as space-based tracking stations such as TDRSS, will need to be improved to support future missions, e.g., NASA TOPEX [21], which will further increase the cost.

The requirement for improved spacecraft navigation accuracy and autonomy has resulted in heavy reliance on GPS satellite signals [2-5, 9, 28]. Previous efforts [8, 9] have not fully explored the synergism between GPS and an Inertial Navigation System (INS) to obtain the best accuracy out of these two sensors for spacecraft applications. The proposed autonomous, integrated GPS/INS navigation system experiment is an integrated Kalman filter that combines several GPS-based attitude determination techniques to obtain an accurate, continuous, navigation solution for all phases of a spacecraft

mission, thereby providing improved accuracy and extreme flexibility in mission planning.

The Phase I research focused on the experiment definition. A successful experiment demonstration, via a Phase II Program, will pave the way for developing an autonomous, integrated GPS/INS navigation system to improve the total navigation performance of advanced Space Transportation Systems (STSS) such as OMV, STV and Space Station. A tightly-integrated GPS/INS navigation filter design was analyzed in Phase I and was shown, via detailed computer simulation, to provide precise position, velocity and attitude data to support absolute navigation (orbit determination), relative navigation (rendezvous and docking) and attitude control (pointing and tracking) requirements of future NASA missions. The application of the integrated GPS/INS navigation filter was also shown to provide the opportunity to calibrate inertial instrument errors which is particularly useful in reducing INS error growth during times of GPS outages. Feasibility of implementing a reconfigurable integrated GPS/INS navigation filter was analyzed in Phase I. Mayflower is currently developing a rule-based expert Resource System Manager for an Advanced GPS Receiver program under Air Force sponsorship.

Phase I analysis and simulation results indicate that an attitude accuracy of 0.1 degrees or better (1-sigma) can be achieved during an orbit maneuver (thrust phase) as well as during the coast phase using a 2-channel sequential GPS receiver. Application of this technique is expected to provide further improvement in attitude determination accuracies (better than 0.1 degree) for higher thrust vehicles, such as STV (Space Transfer Vehicle).

During the course of the Phase I research it was established that the proposed GPS/INS navigation processing technology applies to a wide class of NASA missions, e.g., OMV, Space Station, Space Transfer Vehicle (STV). While in many spacecraft applications (such as OMV) GPS is viewed as an augmentation to the existing GN&C sensors, in some advanced applications (such as STV), only GPS may provide the required mission accuracies. The very-tight flight-path angle requirements for STV for entry point into the atmosphere ( $- 4.5^\circ \pm .036^\circ$  at 65 nmi) for aerobraking may require an accurate GPS navigation solution at high altitude (geosynchronous). The entry point into the atmosphere for a given flight-path angle must be precise, with an altitude tolerance in the order of  $\pm 280$  m for a flexible aerobrake [5]. A more stringent entry corridor altitude requirement will result in reduced exit velocity error.

In Phase I we proposed to use the OMV as the demonstration platform for this experiment since it is already planned to have onboard IMUs, two GPS receivers and two GPS antennae. Furthermore, the OMV GPS receiver will have the measurements and other data available in an appropriate output format for implementing the proposed integrated navigation filter. While OMV provides a good target platform for demonstration and for possible flight implementation to provide improved capability, a successful proof-of-concept ground demonstration can be obtained using any simulated mission scenario data, such as STV, Shuttle-C, Space Station, Earth Observation Systems (EOS). A follow-on Phase III program is expected to implement the Phase II developed software design and navigation processing technology in a future NASA/DoD mission.

## 1.2 Outline of the Report

Section 2 of the report describes the Phase I technical objectives and our approach to accomplish these objectives.

Section 3 summarizes the Phase I results. The primary result in this section is the design and implementation of the integrated GPS/INS navigation filter. Simulation results for an OMV high-thrust trajectory using this filter are presented in this section. Finally, preliminary results of a memory and throughput analysis of this filter for a real-time implementation are also discussed.

Section 4 summarizes the main findings of the Phase I research and outlines the plan for a follow-on program to demonstrate this experiment.

## SECTION 2

### PHASE I TECHNICAL OBJECTIVES AND APPROACH

The focus of the Phase I research was an Experiment Definition Study. The primary objective of the study was to ascertain the feasibility of the proposed integrated GPS/INS navigation processing for the OMV to provide improved total navigation performance and flexibility in mission planning. Specific technical objectives of the Phase I study were:

1. Identify the required interfaces between the OMV and the integrated GPS/Inertial filter and determine that the data (telemetry) will be available at the required rate/format to evaluate the proposed navigation algorithms.
2. Analyze and evaluate the real-time implementation issues.
3. Identify the scope of specific application and test software to be developed during the Phase II effort, define the algorithms, and develop a test validation plan.

All of the Phase I objectives have been met. Close cooperation and excellent working relationship between Mayflower, NASA MSFC and TRW personnel was established which was instrumental in achieving the planned objectives.

The Phase I technical approach consisted of configuring the experiment such that it can maximally utilize the GN&C sensors and data available onboard the OMV and such that it be

executed on a non-interfering basis to the prime OMV development effort.

The current baseline OMV GPS/INS navigation processing is shown in Figure 1. Figure 1 shows the primary OMV navigation sensors which consist of IMU sensors (gyros and accelerometers), sun and horizon attitude update sensors and GPS receiver/processor. The current approach to use GPS onboard the OMV consists of using the GPS navigation solution (position, velocity and time estimates) at 1 second rate to reset the inertial navigation solution. The current (baseline) processing approach does not attempt to integrate the two sensors and exploit their inherent synergism to obtain improved performance. The proposed autonomous, integrated GPS/INS navigation experiment, shown in Figure 2, as dotted functional block, was developed as a wraparound to the baseline approach of Figure 1. The proposed experiment tightly integrates the GPS and INS sensors, processes GPS receiver pseudo-range and delta-range measurements from one or both antennae (when available) and the INS navigation solution to obtain an improved estimate of OMV position, velocity, attitude and time. Furthermore, the integrated navigation filter estimates the significant INS instrument parameters, such as gyro bias drift, accelerometer bias and scale factor. The latter feature provides an improved accuracy INS navigation solution at times of GPS outages.

The Phase I approach to meet the first objective, namely interface definition, consisted of conducting technical interchange meetings at NASA Marshall Space Flight Center (10 March 1989) and at TRW, Redondo Beach, CA (4 April 1989). The interfaces between the OMV Onboard Computer (OBC) and the proposed experiment were reviewed at these meetings. From the results of these meetings it was determined that the current

## CURRENT BASELINE GPS/INS NAVIGATION PROCESSING FOR THE OMV

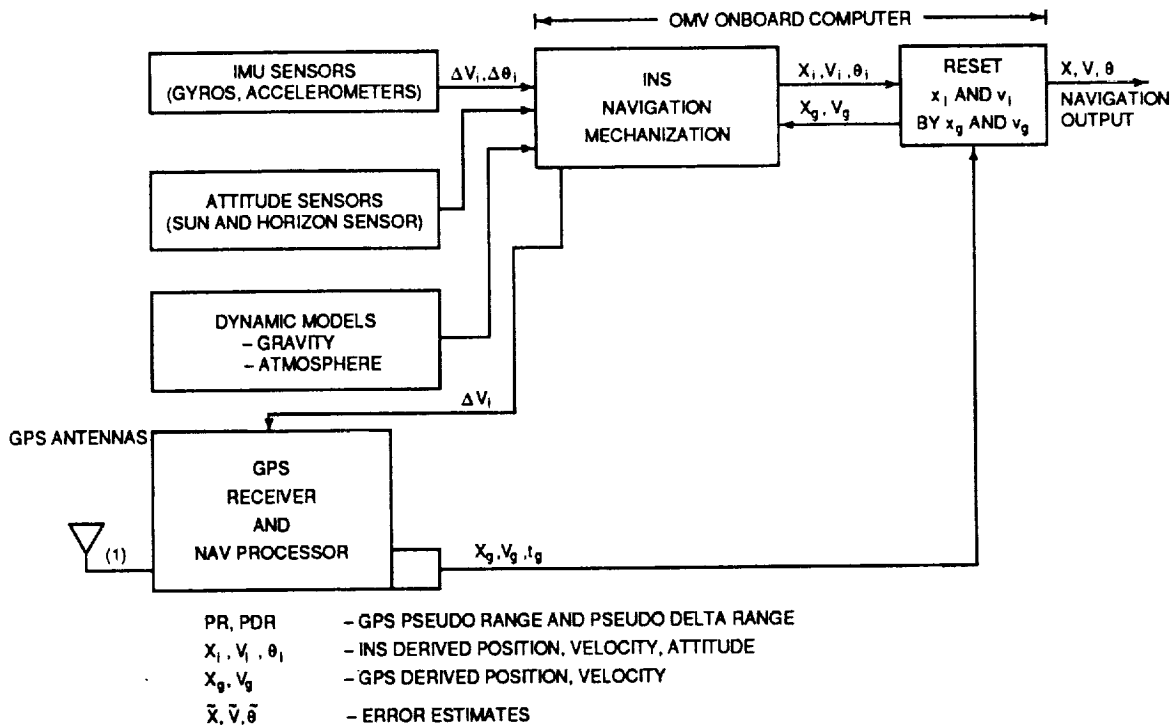


FIGURE 1

## AUTONOMOUS INTEGRATED GPS/INS NAVIGATION PROCESSING FOR THE OMV (Proof-Of-Concept Demonstration)

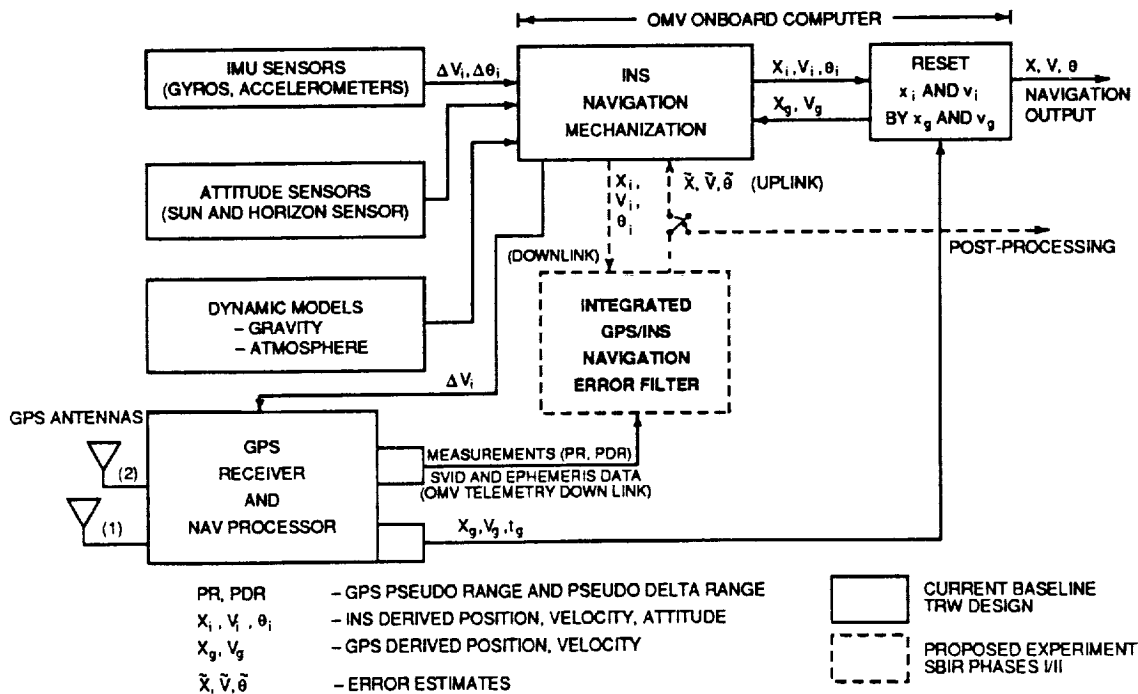


FIGURE 2

OMV telemetry data plan includes all the data required to implement the proposed integrated GPS/INS navigation experiment.

The integrated navigation filter design and real-time implementation issues were addressed during the Phase I study. The primary tool for analysis and evaluation of the integrated filter performance was the Mayflower GINSS (GPS/Inertial Navigation System Simulation) software package. This computer program has been developed by Mayflower over several years and has been applied successfully on other government programs. The approach to address the real-time implementation issues consisted of : (1) converting the conventional Kalman filter equations to a more robust U-D factor implementation [14] which requires only single precision word length for preserving numerical accuracy, and (2) developing a memory and throughput estimate for the integrated navigation filter using OMV OBC instruction times.

Our approach to meeting the third technical objective, namely identifying the application and test software, and developing a test and validation plan has followed the TRW OMV GN&C Guidance and Navigation Design Validation Test Plan outlined in the OMV PDR Document [8]. The approach consisted of validating the navigation filter algorithms using our GINSS software package. The navigation filter algorithm was verified in Phase I by carrying out extensive evaluation using different system parameters and initial conditions.

## SECTION 3

### PHASE I RESULTS

Specific results of the Phase I Experiment Definition and Feasibility Study are presented in this section. In order to facilitate the reading and evaluation of Phase I results we have patterned this section to match the Phase I Statement of Work (SOW), that is, a subsection number below corresponds to a task of the same number in the Phase I SOW.

The primary result described in this section concerns the design, implementation and evaluation of the proposed integrated GPS/INS navigation filter. The filter design involved models of IMU sensor errors, GPS receiver measurement errors, gravity and atmospheric drag models, and Kalman filter equations implemented in the U-D factor form. The interface design between the OMV OBC, which implements the INS navigation mechanization equations, and the integrated GPS/INS filter (Figure 2) utilizing the OMV telemetry data was developed. These interfaces are discussed in Section 3.2. The GPS and INS navigation sensors and the gravity and atmospheric drag models and their effect on the orbit prediction accuracy are described in Section 3.3. This section also includes the results of GPS satellite visibility for the OMV. The performance evaluation results for two specific test cases : (1) good initial conditions and (2) poor initial conditions are reported in Section 3.3.5 for a high-thrust trajectory. The first test case (good initial conditions) corresponds to an orbit transfer phase where GPS was assumed to be available during the coast phase prior to the start of the burn. The second test case (poor initial conditions or a worst-case analysis) assumes GPS outage during the coast phase and, therefore, initial conditions for the

orbit transfer phase correspond to a pure INS solution. Excellent position, velocity and attitude accuracy was demonstrated for both the test cases. Similar results were also obtained for an OMV low-thrust trajectory.

Applicability of the proposed experiment to a wide class of NASA missions is described next.

### **3.1 Common GN&C Requirements for Advanced STSS**

The navigation and attitude update requirements for several NASA missions were reviewed during the Phase I study. The objective was to assess how the results of the proposed experiment can be used to support the goal of developing autonomous, fault-tolerant GN&C systems for future NASA missions. Specific attention was devoted to the OMV, Space Station, OTV and NASA's Earth Science Geostationary Platforms. Navigation accuracy requirements of these missions are summarized in this section.

The OMV orbit navigation accuracy requirements described in Table 1 [8] can be significantly improved by employing the proposed integrated navigation filter algorithm. Simulation results for OMV trajectories, and OMV navigation sensors' parameters are described in Section 3.3.5.

The NASA GPS navigation requirements for the Space Station are summarized in Table 2. Recent studies by Hughes, Axiomatix and Texas Instruments [9] have concluded that these Space Station navigation and attitude update requirements can be met by GPS tracking of the Space Station.

**Table 1 OMV Navigation Requirements [8]**

Navigation Mode	Accuracy Requirement (rms 1-sigma)
Absolute Navigation Accuracy	100 meters 0.15 m/s
Relative Navigation Accuracy  - Beginning of Rendezvous Transfer  - Final Midcourse  - Final Rendezvous Injection	150 meters, 0.15 m/s  11 meters, 0.05 m/s  8 meters, 0.05 m/s
Attitude Reference Update	0.16 deg per axis

A preliminary review of the OTV/STV aeroassist GN&C requirements [12] and Geostationary Platform [17] requirements was also conducted. The absolute navigation requirements for these missions are much tighter than for the OMV and the Space Station. Another complicating factor which makes these missions more challenging for GPS applications is the limited availability of GPS satellites at higher altitudes. The OMV and the Space Station are classified as a low-earth orbit (LEO) users for which the GPS availability is excellent (see Section 3.3.3). The OTV and the Geostationary Platforms are classified as GEO users where GPS availability is restricted. Several candidate techniques [4, 5] can be employed to alleviate this limitation. The feasibility of these techniques for STV will be pursued in Phase II via a cost-performance tradeoff study.

**Table 2 NASA Space Station Navigation Requirements [9]**

Navigation Mode	Accuracy (rms 1-sigma)
Target Absolute Navigation [28]	10 meters (1-sigma)
Relative Navigation [28] at Docking/Berthing	3 meters (1-sigma)
Relative Navigation without Docking Maneuvers [9]	30 meters (1-sigma) or 1% of the range between the two spacecrafts, which- ever is the greater
Attitude Update [9]	0.01 degree

The preliminary navigation requirements for the OTV and Geostationary Platform are given below.

	GEOSTATIONARY PLATFORM [12]	OTV AEROASSIST PHASE [17]
Position/Velocity Accuracy	5m -50 m (3 $\sigma$ ) depending on pointing and control system requirements	15 m (3- $\sigma$ ) LEO 0.02 m/s 340 m (3- $\sigma$ ) GEO 0.03 m/s
Attitude Alignment Accuracy	----	0.074 degree (3- $\sigma$ ) 15 minutes after stellar update

This brief review of advanced STSS navigation requirements supports the claim of general applicability of the proposed experiment to a wide class of future NASA missions.

### 3.2 OMV OBC Interface Requirements

An important aspect of the Phase I feasibility study was to ensure that appropriate interfaces between the GPS receiver, OMV OBC and telemetry data will be available for experiment demonstration. Review of OMV documents and conversation with TRW personnel verified that OMV onboard GPS receiver will output its pseudo-range and delta-range measurements along with the navigation solution, computed within the receiver processor, at 1 second rate. This data along with other slower rate data, such as satellite ephemerides, satellite ID, receiver signal-to-noise power estimates will be put on the telemetry downlink. The OMV downlink data will also contain the onboard INS navigation solution and the instrument  $\Delta V$  and  $\Delta\theta$  output. This data set was determined to be adequate for a ground demonstration of the proposed navigation system experiment. The GPS receiver data output blocks are listed below [8]:

#### Block I    Tracking and Navigation Data Block

- BIT status
- Mode status (standby, navigate)
- $C/N_0$  estimate
- NDS/ONS vehicle ID
- pseudo-range
- delta pseudo-range
- time tag (GMT) of pseudo-data
- position, velocity vector
- time tag (GMT) of navigation state
- navigation status
- data quality (navigation position, velocity error covariance matrix)

## Block II Almanac and Ephemeris Data Block

The corrections to the navigation state vector estimated by the filter can be computed in real-time on a ground computer and these corrections can be uploaded to the host vehicle to form a closed loop system around the experiment (Figure 2).

### 3.3 Integrated GPS/INS Navigation Filter Design

A tightly-integrated GPS/INS navigation filter design is presented in this section. The navigation filter equations, implemented in the U-D factor form, are described here. The proposed integrated GPS/INS navigation filter combines several GPS-based attitude determination techniques to obtain an accurate and continuous navigation solution for all phases of a spacecraft mission, thereby providing improved accuracy and extreme flexibility in mission planning. The three GPS-based attitude determination techniques employed here are:

1. Velocity vector matching technique employing one GPS antenna during spacecraft orbit maneuvers
2. Interferometric GPS carrier phase processing technique using two or more antennae during spacecraft coast and maneuver phases
3. Attitude vector matching technique employing one GPS antenna during spacecraft rotation maneuvers

The autonomous integrated GPS/INS navigation experiment will use a combination of these techniques for providing improved total navigation solution. The focus of the presentation in this section is on the first technique which is considered the primary technique for the OMV attitude determination. Modifications to the navigation filter to implement the other two techniques are also identified.

Location of the two GPS antennae on the OMV is shown in Figure 3. The two antennae are separated in Y axis by approximately 5 meters in the fully deployed position.



LOW GAIN ANTENNA ASSEMBLY  
(REVISED PLUME IMPINGEMENT CONFIGURATION)



ORIGINAL PAGE IS  
OF POOR QUALITY

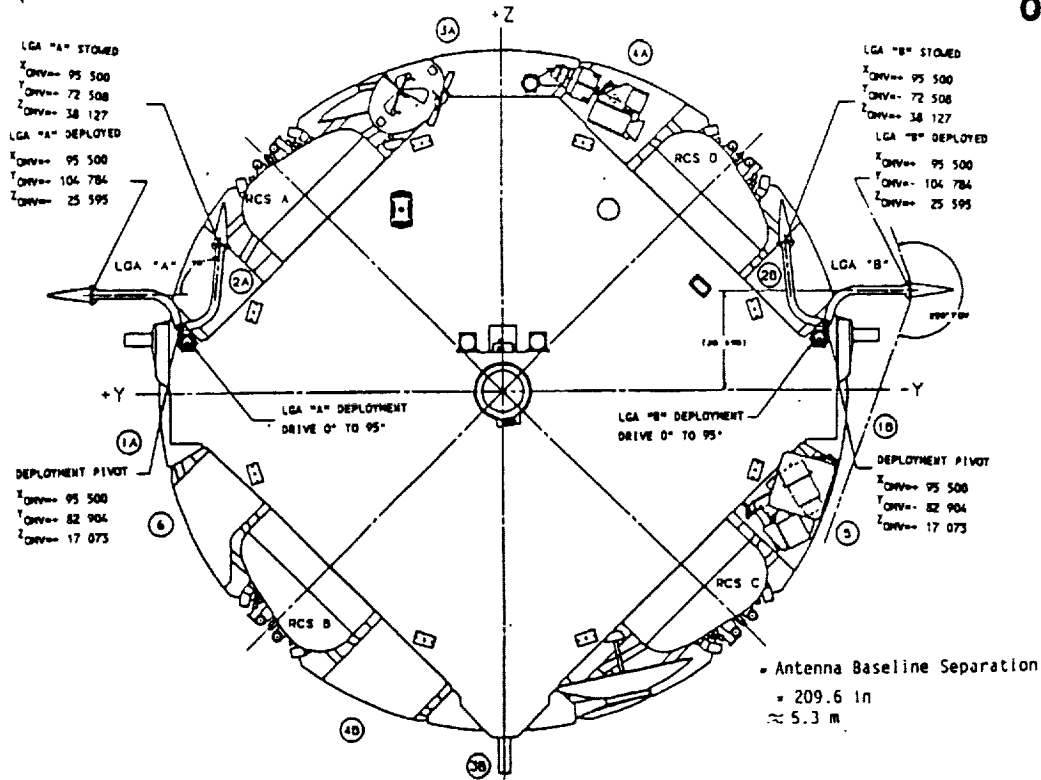


Fig. 3 : Location of the GPS Antennae on the OMV.



GN&C HARDWARE BLOCK DIAGRAM

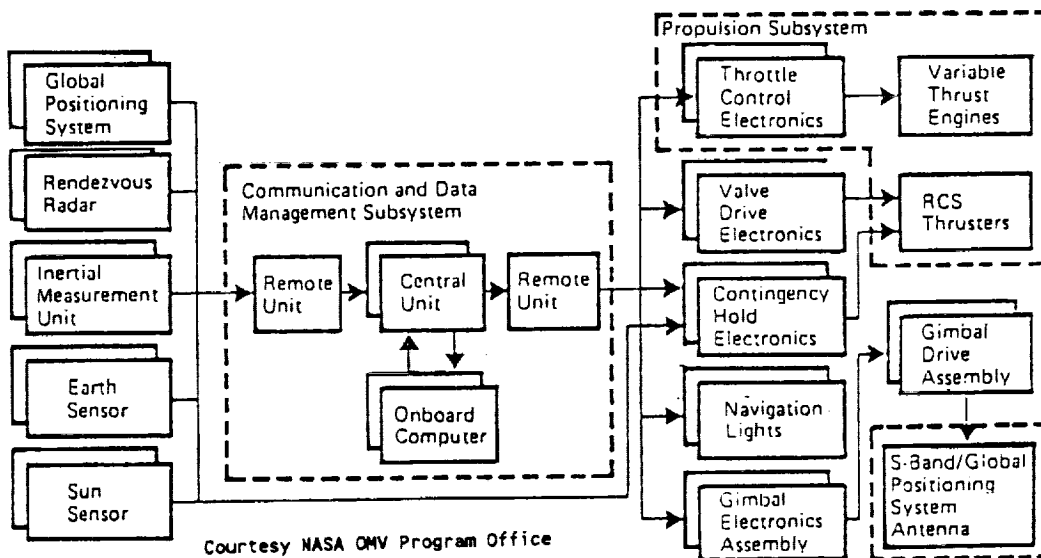


Fig. 4 : Simplified GN&C Block Diagram.

### **3.3.1 Navigation and Attitude Sensors - GPS and INS**

The OMV guidance, navigation and control (GN&C) subsystem performs completely automatic spacecraft operation for orbit change, rendezvous and station keeping [15; p. 112]. A simplified block diagram of the GN&C subsystem is shown in Figure 4.

Redundant sensor assemblies provide the information required by the onboard computer (OBC) software to guide and control the OMV automatically through its mission phases. Each sensor complement consists of a GPS receiver, a rendezvous radar, an inertial measurement unit (IMU), an Earth sensor and a sun sensor.

The primary navigation sensor on the OMV is the GPS receiver [8; p. 2-5]. It provides accurate flight vehicle position and velocity in Earth centered coordinates. Inertial attitude reference is obtained by the IMU gyros and is propagated by a closed-form integration algorithm using quaternions. The Earth and sun sensors provide periodic attitude reference updates to correct for gyro drifts. The overall attitude accuracy achieved with this design is better than 1° per axis [15; p. 113].

Ground tracking of the spacecraft provides a means to estimate the navigation errors and upload the corrections. Tracking of GPS satellites by the OMV GPS receiver provides an autonomous capability to update the INS position and velocity [16; p. 8].

OMV orbital position and velocity (ephemeris calculation) is propagated by the OBC using a fourth order numerical integrator of the Runge-Kutta type for the numerical

integration of the differential equations of motion [8; p. 2-5].

### OMV Global Positioning System (GPS) Receiver

The OMV GPS receiver is a 2-channel sequential receiver being developed by Rockwell International, Satellite and Space Electronics Division. The size, power and weight estimates are 9.9" x 7.1" x 2.3", 13 Watts and 6 lbs, respectively.

The receiver will output data at a rate of 1 per second. The accuracy of the receiver-computed position is 393 ft (3- $\sigma$ ) per axis using C/A code and 367 ft (3- $\sigma$ ) per axis using P-Code (GDOP=4.3). The velocity accuracy is 0.86 ft/sec (3- $\sigma$ ) per axis (GDOP=4.3). The GPS receiver measurement error model (1- $\sigma$ ) for the integrated navigation filter evaluation is given below:

Receiver Pseudo-Range Measurement Noise	= 1.8 m
Receiver Delta-Range Measurement Noise	= 2.5 cm
Clock Frequency Drift Rate	= $10^{-8}$ sec/sec
Delta Range Integration Interval	= 0.1 sec

GPS environment errors (e.g., satellite ephemeris error, satellite clock error, iono/tropospheric errors and multipath errors) used in this evaluation are described in [2].

### OMV Inertial Measurement Unit (IMU)

The OMV IMU is the modified SKIRU IV produced by Singer-Kearfott. The unit contains two MOD II E/S GYROFLEX gyros, which are 2-Degree-of-Freedom, dry tuned-rotor gyros, without temperature control. The gyro performance characteristics are as follows:

Gyro Bias Drift	0.022 deg/hr, 3- $\sigma$
Input Axis Alignment	7 arcsec , 3- $\sigma$
Scale Factor Linearity and Asymmetry	40 ppm
Scale Factor Stability	93 ppm , 3- $\sigma$

The unit also contains three MOD VII accelerometers, which are single-axis, subminiature, linear, pendulus devices. The accelerometer performance characteristics are as follows:

Bias Stability	27 micro-g, 3- $\sigma$
Scale Factor Linearity and Asymmetry	0.155%

### 3.3.2 Gravity and Atmospheric Drag Models

There are times during the OMV mission when prediction of the vehicle orbit is required (e.g., rendezvous and docking). The two prominent perturbing accelerations at the OMV altitudes are the ones induced by the geopotential and the atmospheric drag.

Currently, the OMV OBC orbit predictor utilizes a second degree zonal harmonic ( $J_2$ ) model to compute the orbital perturbations due to the non-central part of the Earth's gravitational field, whereas the magnitude of the atmospheric drag perturbing acceleration is an input constant [8; p. 2-5]. The effects of ignoring terms, other than  $J_2$ , in the reference geopotential model on the OMV orbit prediction were analyzed. It was shown that inclusion of a (2,2) model will significantly improve the orbit prediction accuracy at a minimal computational cost.

## Effects of the Geopotential Modeling

In order to study the effects of the geopotential modeling on the OMV orbit prediction accuracy we generated three orbital arcs. The first one, termed the (8,8) orbit, was designated as our reference orbit. It was generated assuming that the Earth is completely modeled by the Goddard Earth Model T1 (GEM-T1) to degree and order 8 [19]. The second orbit, termed the  $J_2$  orbit, was generated assuming that the Earth is an ellipsoid of revolution with the GEM-T1 fundamental parameters. The third orbit, termed the (2,2) orbit, was generated assuming that the Earth is completely modeled by GEM-T1 to degree and order 2. The duration of each orbit was six hours and a new point was computed every five minutes. The orbital eccentricity  $e=0.001$  and the inclination  $i=35^\circ$  was assumed for all three arcs. Each orbit was generated at two altitudes, namely 150 nmi (277.8 km) and 250 nmi (463 km), which correspond to orbital periods of approximately 89 min and 94 min respectively.

The Root Sum Square (RSS) differences in coordinates and velocities between the (8,8) and  $J_2$ , and the (8,8) and (2,2) orbits for an orbital altitude of 150 nmi are shown in Figures 5, 6, 7 and 8, whereas the same differences at an orbital altitude of 250 nmi are shown in Figures 9, 10, 11 and 12. Examination of Figures 5, 6, 7 and 8 indicates that at an orbital altitude of 150 nmi the RSS coordinate difference (with respect to the (8,8) reference model) is 3.6 km for the  $J_2$  orbit and 1.4 km for the (2,2) orbit, whereas the corresponding RSS velocity difference is 4 m/sec for the  $J_2$  orbit and 1.4 m/sec for the (2,2) orbit. Furthermore, inspection of Figures 9, 10, 11 and 12 indicates that at an orbital altitude of 250 nmi, the RSS coordinate difference is 3.0 km for the  $J_2$  orbit and 0.9 km for the (2,2) orbit whereas

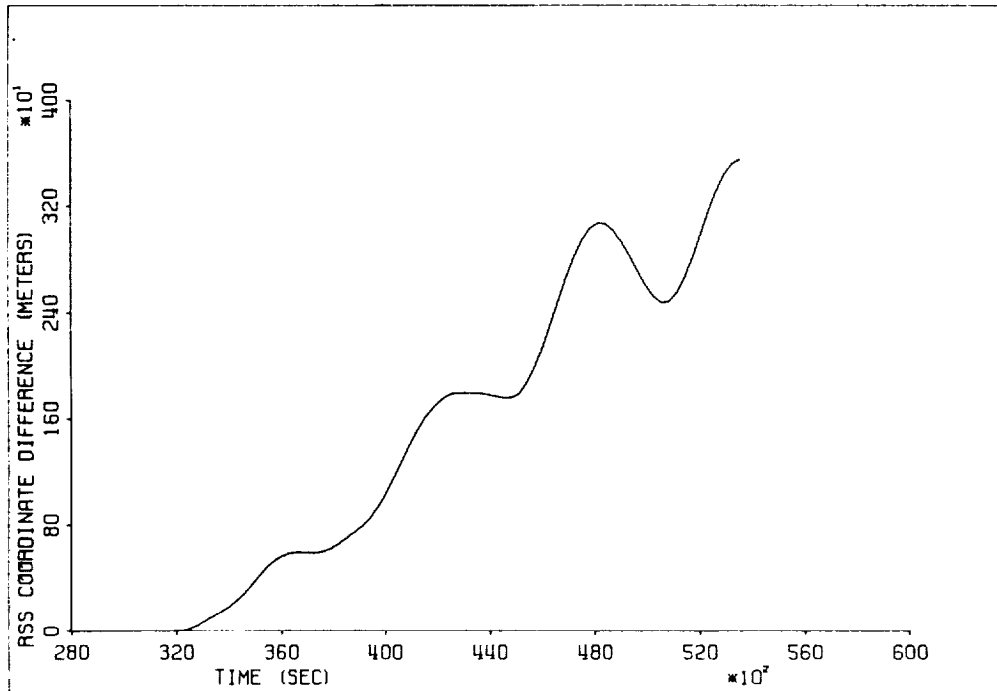


Fig. 5 : Root Sum Square Coordinate Differences of an (8,8)  
Minus a J2 Orbit. Orbital Altitude = 150 n.mi.

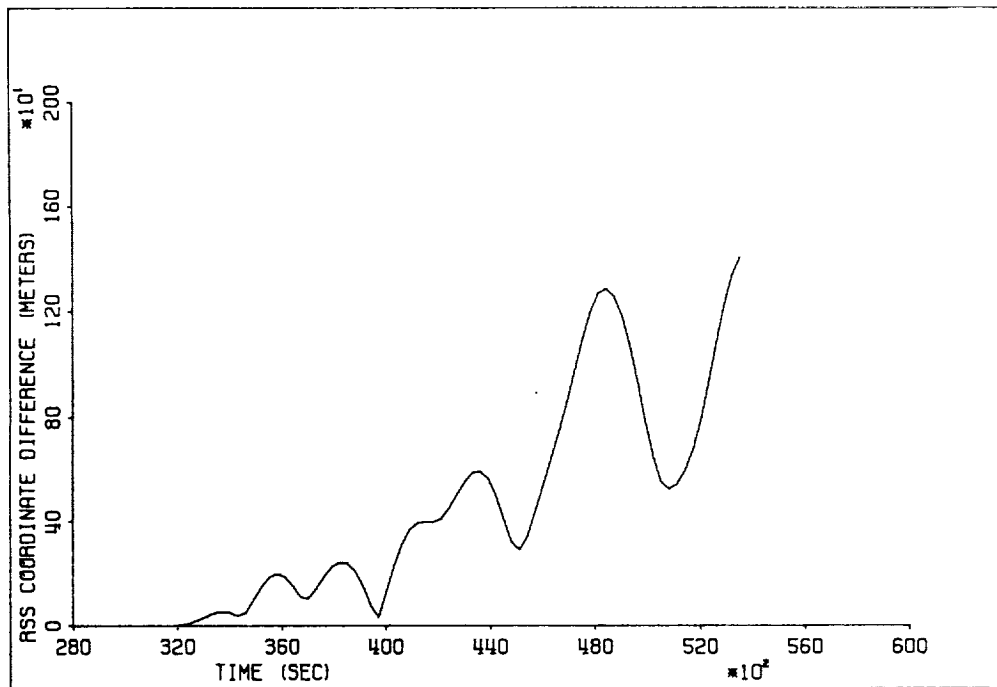


Fig. 6 : Root Sum Square Coordinate Differences of an (8,8)  
Minus a (2,2) Orbit. Orbital Altitude = 150 n.mi.

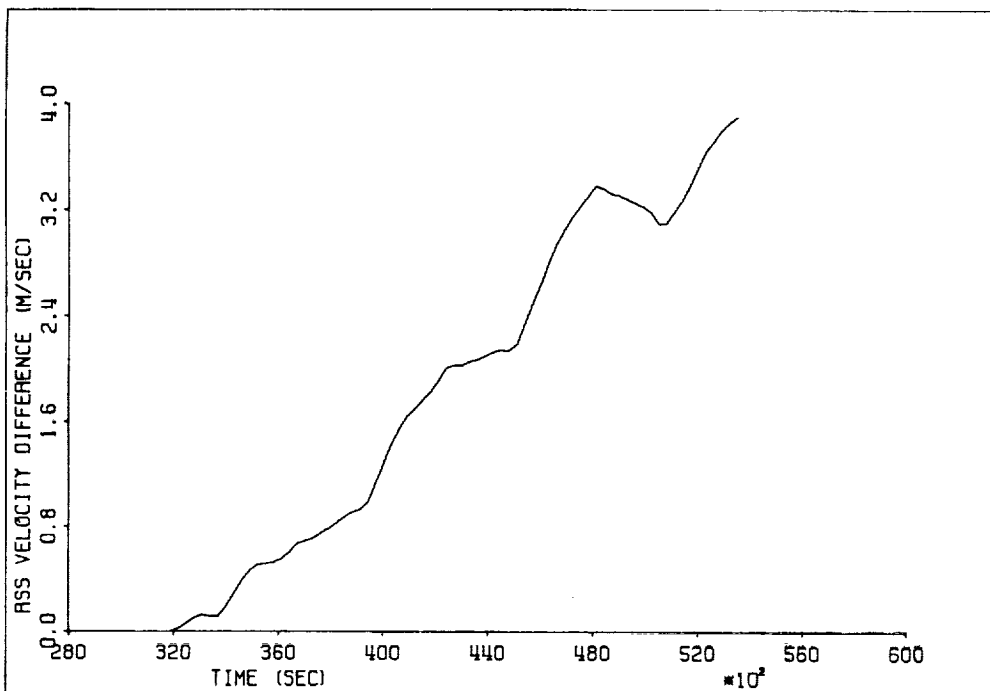


Fig. 7 : Root Sum Square Velocity Differences of an (8,8)  
Minus a J2 Orbit. Orbital Altitude = 150 n.mi.

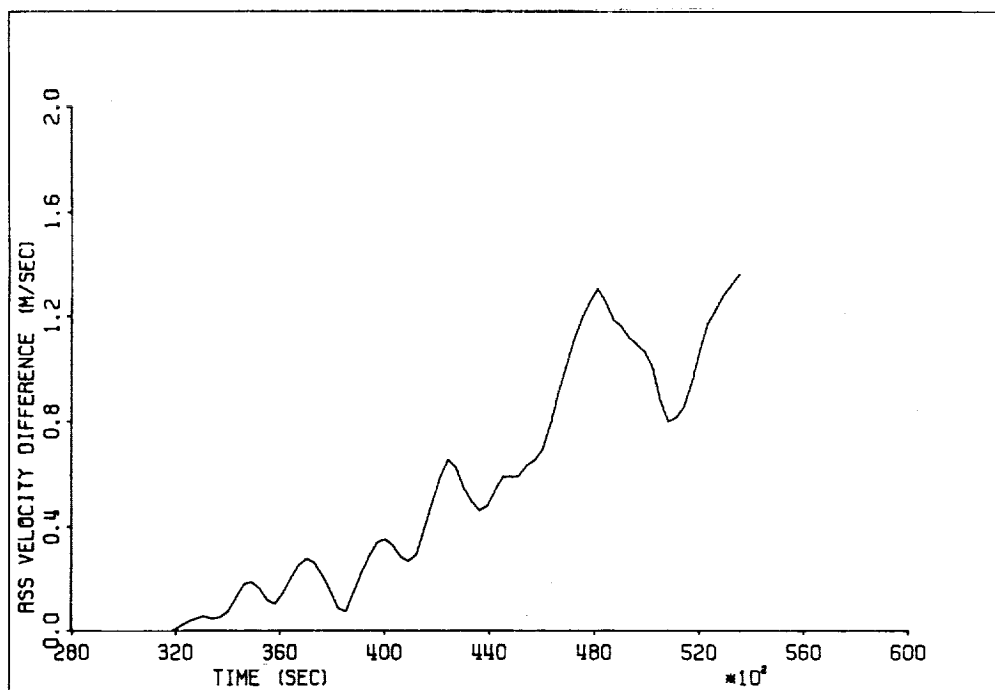
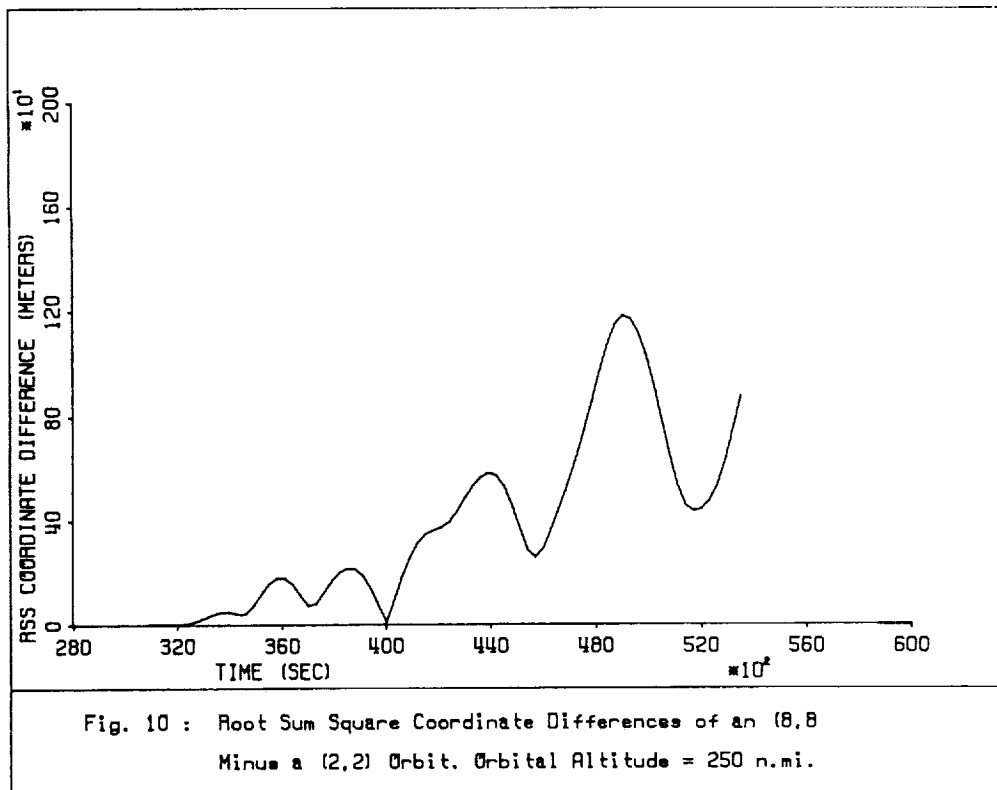
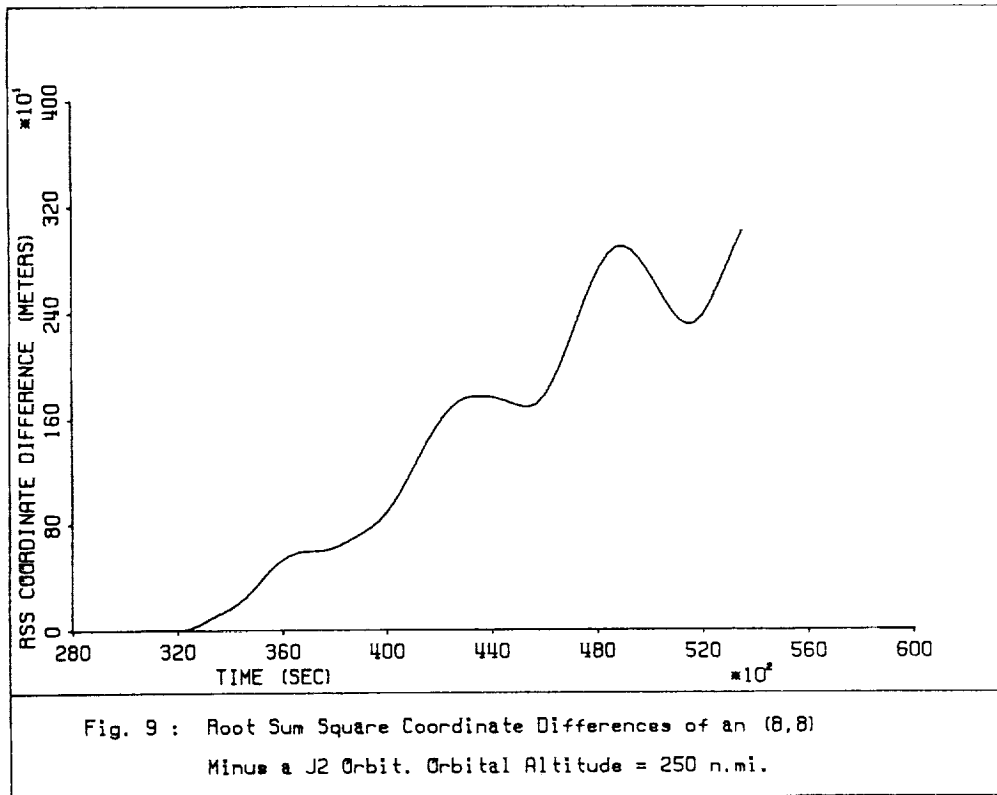
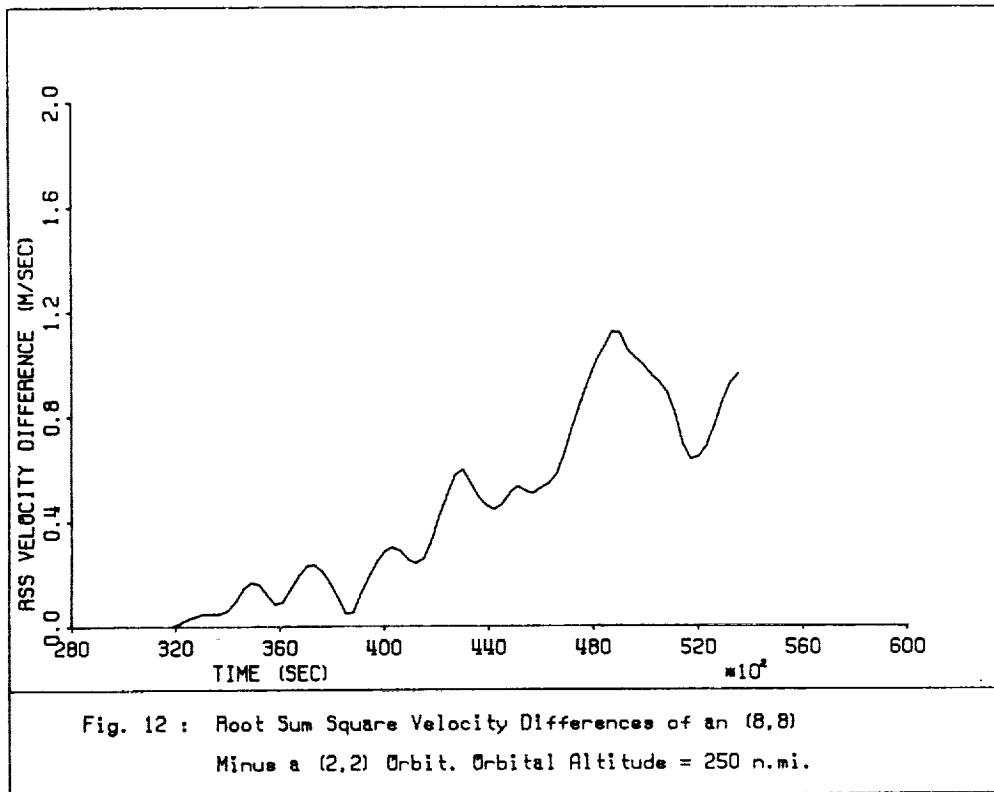
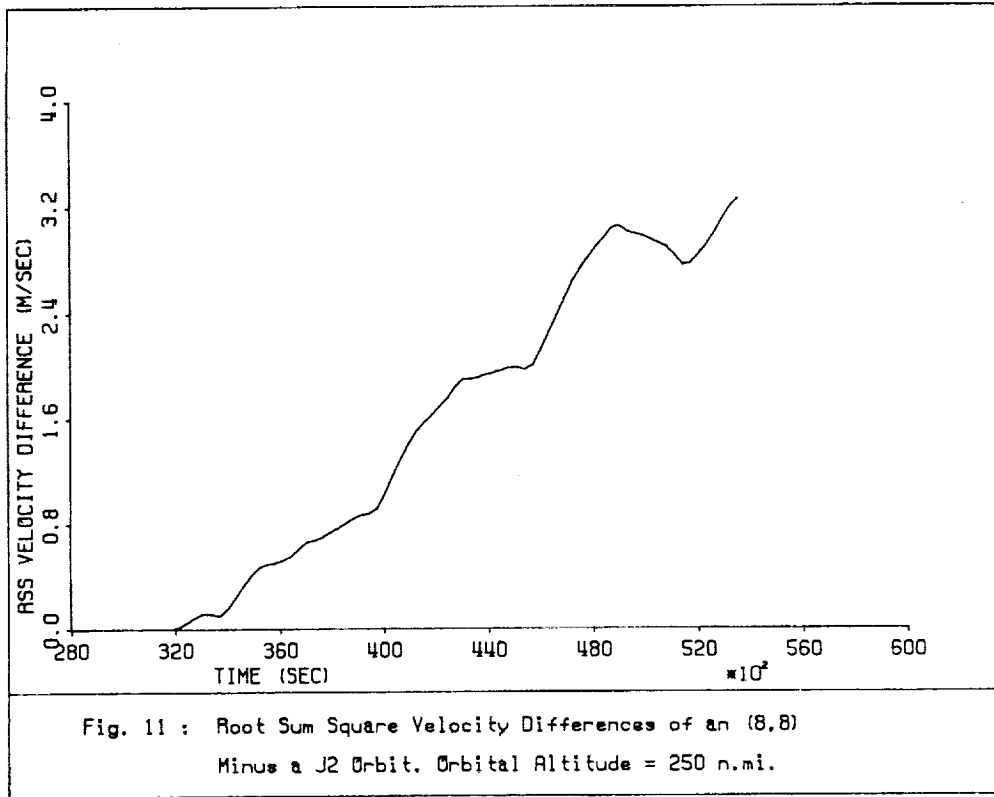


Fig. 8 : Root Sum Square Velocity Differences of an (8,8)  
Minus a (2,2) Orbit. Orbital Altitude = 150 n.mi.





the RSS velocity difference is 3.2 m/sec for the  $J_2$  orbit and 1.0 m/sec for the (2,2) orbit. From the aforementioned results it is apparent that the (2,2) orbit is better (smaller prediction error over a 6 hour arc) than the  $J_2$  orbit by a factor of 2.5 or higher.

The substantial improvement of the orbit prediction using the (2,2) field, as opposed to using the second degree zonal harmonic  $J_2$  only, suggested that one evaluate the additional throughput required for the (2,2) orbit implementation versus the  $J_2$  orbit implementation. The computation of the perturbing acceleration due to the non-central part of the geopotential field  $V$  encompasses the calculation of the derivatives of  $V$  with respect to the geocentric radius  $r$ , the geocentric latitude  $\phi$  and the longitude  $\lambda$  of the OMV. One has [18]

$$\frac{\partial V}{\partial r} = -\frac{GM}{r^2} \sum_{n=2}^{\infty} (n+1) \left(\frac{a}{r}\right)^n \sum_{m=0}^n (C_{nm} \cos m\lambda + S_{nm} \sin m\lambda) P_{nm}(\sin\phi) \quad (1)$$

$$\frac{\partial V}{\partial \phi} = \frac{GM}{r} \sum_{n=2}^{\infty} \left(\frac{a}{r}\right)^n \sum_{m=0}^n (C_{nm} \cos m\lambda + S_{nm} \sin m\lambda) \frac{\partial P_{nm}}{\partial \phi} \quad (2)$$

$$\frac{\partial V}{\partial \lambda} = \frac{GM}{r} \sum_{n=2}^{\infty} \left(\frac{a}{r}\right)^n \sum_{m=0}^n [m(S_{nm} \cos m\lambda - C_{nm} \sin m\lambda)] P_{nm}(\sin\phi) \quad (3)$$

where

$C_{nm}, S_{nm}$  = fully normalized potential coefficients

$P_{nm}(\sin\phi)$  = fully normalized associated Legendre functions

GM = geocentric gravitational constant

a = scaling parameter associated with  $C_{nm}$ ,  $S_{nm}$ .

For the  $J_2$  Orbit, the derivatives in (1), (2), and (3) become

$$\left( \frac{\partial V}{\partial r} \right)_{J_2} = - \frac{GM}{r^2} 3 \left( \frac{a}{r} \right)^2 C_{20} P_{20}(\sin \phi) \quad (4)$$

$$\left( \frac{\partial V}{\partial u} \right)_{J_2} = \frac{GM}{r} \left( \frac{a}{r} \right)^2 C_{20} \frac{\partial P_{20}}{\partial \phi} \quad (5)$$

$$\left( \frac{\partial V}{\partial k} \right)_{J_2} = 0 \quad (6)$$

where  $C_{20} = - J_2/\sqrt{5}$ .

On the other hand, GEM-T1 has its tesserals of the second degree equal to zero (i.e.,  $C_{21} = S_{21} = 0$ ), therefore the derivatives for the (2,2) orbit are

$$\left( \frac{\partial V}{\partial r} \right)_{(2,2)} = - \frac{GM}{r^2} 3 \left( \frac{a}{r} \right)^2 [C_{20} P_{20} + (C_{22} \cos 2\lambda + S_{22} \sin 2\lambda) P_{22}] \quad (7)$$

$$\left( \frac{\partial V}{\partial \phi} \right)_{(2,2)} = \frac{GM}{r} \left( \frac{a}{r} \right)^2 \left[ C_{20} \frac{\partial P_{20}}{\partial \phi} + (C_{22} \cos 2\lambda + S_{22} \sin 2\lambda) \frac{\partial P_{22}}{\partial \phi} \right] \quad (8)$$

$$\left( \frac{\partial V}{\partial \lambda} \right)_{(2,2)} = \frac{GM}{r} \left( \frac{a}{r} \right)^2 [S_{22} \cos 2\lambda - C_{22} \sin 2\lambda] P_{22}(\sin \phi) \quad (9)$$

Comparison of (4) to (7), (5) to (8) and (6) to (9) indicates that the additional throughput required is due to the

sectorials  $C_{22}$ ,  $S_{22}$  of the second degree. The explicit terms are

$$[C_{22} \cos 2\lambda + S_{22} \sin 2\lambda] P_{22} \quad (10)$$

$$[C_{22} \cos 2\lambda + S_{22} \sin 2\lambda] \partial P_{22} / \partial \phi \quad (11)$$

$$\partial V / \partial \lambda \quad (12)$$

Once  $\sin \lambda$  and  $\cos \lambda$  are computed, the additional throughput is (FA=floating-point addition, FM=floating-point multiplication)

$\cos 2\lambda$	$= 2\cos^2 \lambda - 1$	2 FM, 1 FA
$\sin 2\lambda$	$= 2\sin \lambda \cos \lambda$	2 FM
$P_{22}$	$= ((\sqrt{15}/2) \cos \phi) \cos \phi$	2 FM (assuming $\sqrt{15}/2$ is stored)
$\partial P_{22} / \partial \phi$	$= ((\sqrt{15}/2) \cos \phi) \sin \phi$	1 FM (assuming $(\sqrt{15}/2) \cos \phi$ is available from the previous operation)
$A = C_{22} \cos 2\lambda + S_{22} \sin 2\lambda$		2 FM, 1 FA
$AP_{22}$		1 FM (assuming that A is available from the previous operation)
$A \partial P_{22} / \partial \phi$		1 FM (assuming that A is available from previously)
$\frac{\partial V}{\partial \lambda}$		5 FM, 1 FA (assuming $GM/r(a/r)^2$ is stored from previously)

The grand total is 16 multiplications and 3 additions. Based on the TRW specifications of a 1750A processor for the OMV onboard computer with an internal clock frequency of 6 MHz one can estimate the additional throughput as follows:

$$16FM + 3FA = 16 \times 13 + 3 \times 15 = 253 \quad \text{clock cycles}$$

hence

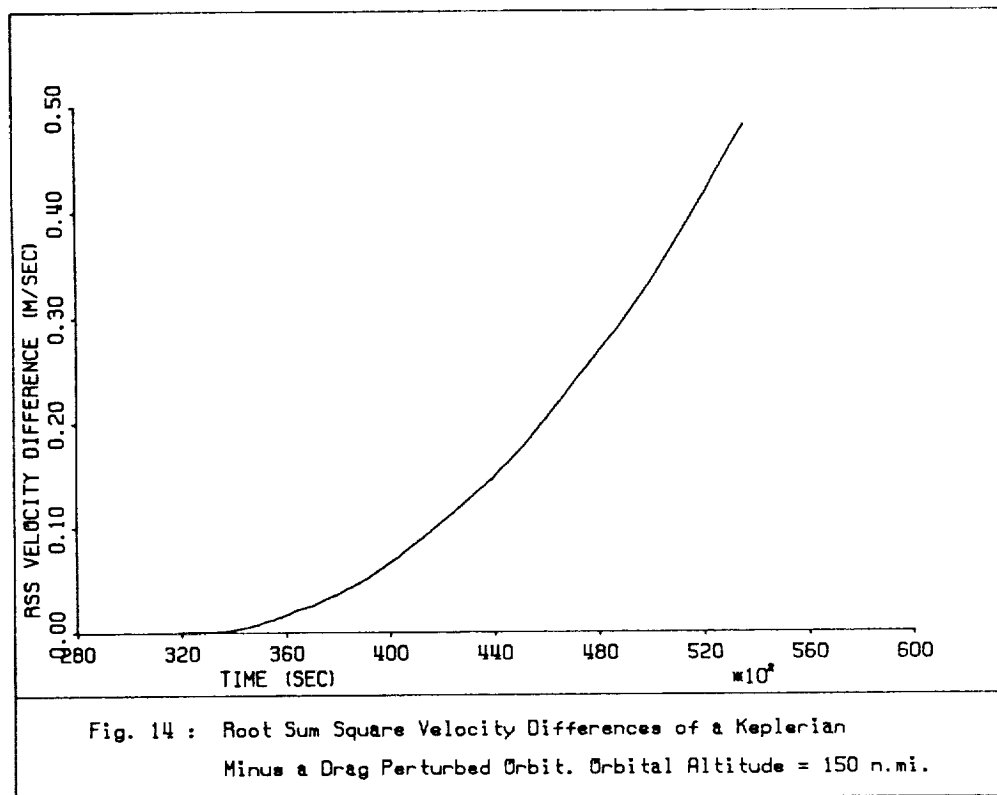
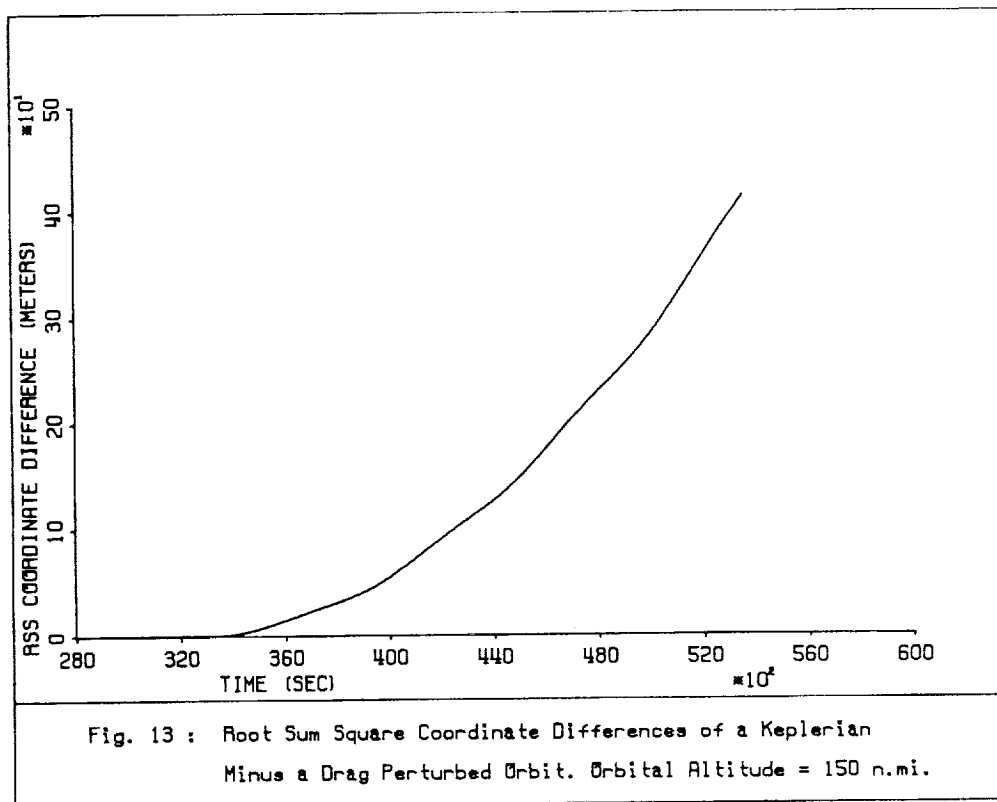
$$\text{Throughput} = 253 \times (1/6) \times 10^{-6} \text{ sec} = 42.17 \text{ } \mu\text{sec per update}$$

This additional throughput estimate appears to be negligible in light of the resulting improvement of the orbit by a factor of 2.5.

### Effects of the Atmospheric Drag

In order to study the effects of the atmospheric drag on the OMV orbit prediction accuracy we generated two six hour orbital arcs, computing a new point every five minutes. The first orbit was Keplerian, whereas the second one was perturbed by the atmospheric drag. The orbital eccentricity was  $e=0.001$ , the inclination was  $i=35^\circ$  and the altitude was 150 nmi for both orbits. The air density required for the computation of the perturbing acceleration due to the atmospheric drag was computed assuming a Jacchia-Groves atmospheric model (Global Reference Atmospheric Model-GRAM) [20] as implemented by the subroutine "GRAM". The RSS differences in coordinates and velocities between the two orbits are shown in Figures 13 and 14.

In Figures 13 and 14 one can observe a secular behavior of the atmospheric drag effects. The RSS coordinate difference grows to approximately 400 m and the RSS velocity difference grows to 0.5 m/sec at the end of the six hour arc. This is a significant effect. However, implementation of the GRAM routine in the onboard computer of the OMV is a formidable task due to both the memory required by the routine and its associated files and the throughput required for the



operation of the routine. Therefore, alternate models to describe the atmosphere should be examined such that both the drag effect is reduced and the computational burden on the OBC of the OMV is contained to within feasible limits.

### **3.3.3 GPS Satellite Visibility-One Antenna**

A study to determine the visibility of the GPS satellites to the OMV GPS antennae was carried out. The primary GPS constellation of 21 satellites [27] was used for this investigation. Twelve hour orbital arcs were generated to cover a full period of the GPS satellites. An antenna look angle of  $110^\circ$  and two OMV orbital altitudes (250 nmi and 1000 nmi) and two inclinations ( $27^\circ$  and  $55^\circ$ ) were utilized. The GPS satellite selection and the computation of the Geometric Dilution of Precision (GDOP) was carried out once per minute, due to the rapidly changing geometry.

The visibility study was carried out assuming that there was no rotation of the OMV body frame with respect to inertial space, such that its Y-axis was always parallel to the Y-axis of the inertial frame. This may not be a realistic assumption, since the OMV will probably be oriented towards the sun at all times for power reasons. However, while on one hand the above assumption has practically no influence on the visibility study due to the homogeneity of the GPS constellation, on the other hand, this assumption can be very easily relaxed by incorporating attitude data in our analysis (e.g., quaternions or Euler angles).

In the course of our study an interesting notion came about, namely that of antenna switching. Since the OMV has two GPS antennae, the effect of antenna switching on the GPS satellite visibility was analyzed. The idea is that software

commands on the OMV OBC or ground control commands could be utilized to switch from one GPS antenna to the other to ensure the best possible visibility of the GPS constellation. Figure 15 shows the geometry with antenna switching, whereas Figure 16 shows the geometry without antenna switching.

For the case of antenna switching (Fig. 15), let the coordinates of the GPS satellite S be  $(X_S, Y_S, Z_S)$  in the inertial frame and let the coordinates of the OMV's antenna A be  $(X_A, Y_A, Z_A)$  in the same frame. The visibility criterion is

$$\theta \leq z$$

where  $z$  is the antenna look angle of 110 degrees. Now

$$\theta = \cos^{-1} \langle i_{AZ}, i_{AS} \rangle$$

where  $i_{AZ}$  and  $i_{AS}$  are the unit vectors along the antenna zenith and along the direction AS respectively. One has

$$i_{AZ} = [ 0 \ 1 \ 0 ]^T$$

and

$$i_{AS} = [ X_S - X_A, Y_S - Y_A, Z_S - Z_A ]^T / r_{AS}$$

where

$$r_{AS} = [(X_S - X_A)^2 + (Y_S - Y_A)^2 + (Z_S - Z_A)^2]^{1/2}$$

Hence the visibility criterion becomes

$$\cos^{-1} [(Y_S - Y_A) / r_{AS}] \leq z$$

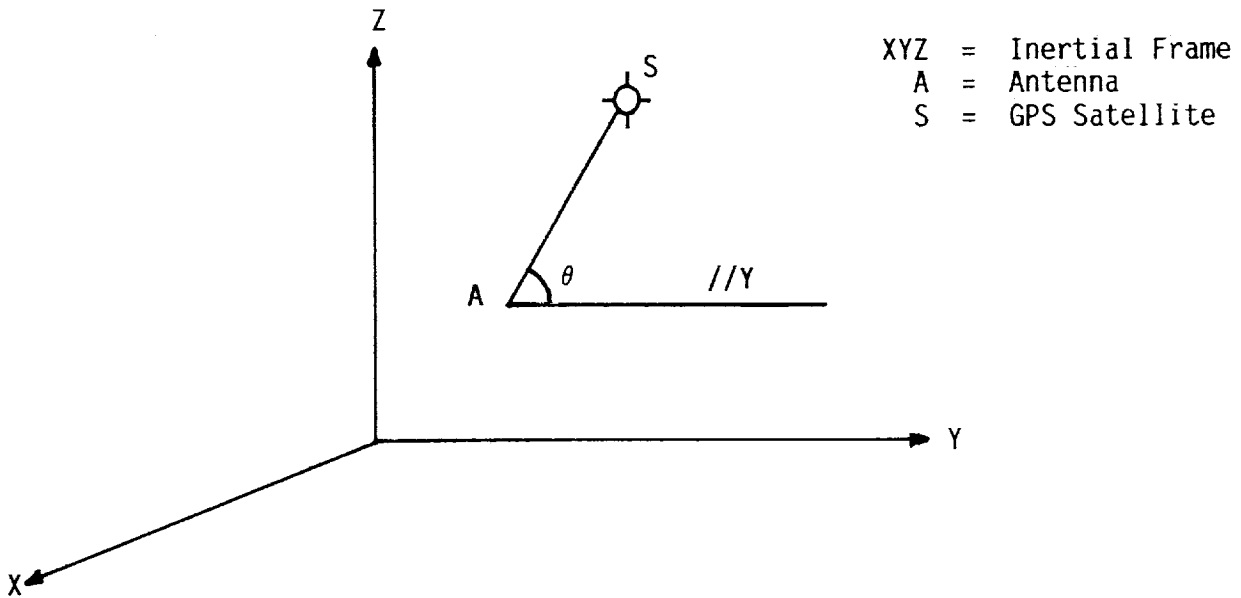


Fig. 15: GPS Satellite Visibility - Antenna Switching

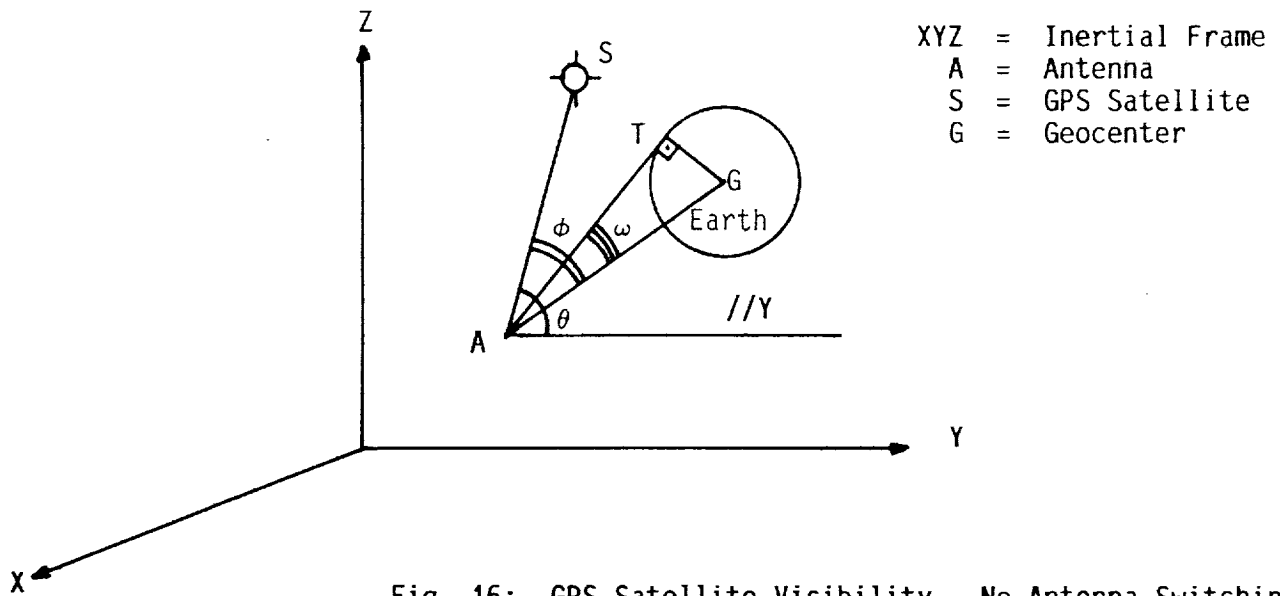


Fig. 16: GPS Satellite Visibility - No Antenna Switching

For the case of no antenna switching (Fig. 16), let the inertial coordinates of the OMV antenna A, of the GPS satellite S and of the Geocenter G be  $(X_A, Y_A, Z_A)$ ,  $(X_S, Y_S, Z_S)$  and  $(X_G, Y_G, Z_G)$  respectively. The visibility criterion is

$$(\theta \leq z \quad \text{and} \quad \phi \geq \omega)$$

We will only examine the additional condition  $\phi \geq \omega$ . The angle  $\omega$  is

$$\omega = \cos^{-1}(|\underline{AT}|/|\underline{AG}|), \text{ or}$$

$$\omega = \cos^{-1} \frac{[(X_G - X_A)^2 + (Y_G - Y_A)^2 + (Z_G - Z_A)^2 - R_E^2]^{1/2}}{[(X_G - X_A)^2 + (Y_G - Y_A)^2 + (Z_G - Z_A)^2]^{1/2}}$$

where  $R_E$  is the mean Earth radius equal to 6371 km. Also

$$\phi = \cos^{-1}(\langle \underline{AS}, \underline{AG} \rangle / (|\underline{AS}| |\underline{AG}|)), \text{ or}$$

$$\phi = \cos^{-1}(N/D)$$

where

$$N = (X_S - X_A)(X_G - X_A) + (Y_S - Y_A)(Y_G - Y_A) + (Z_S - Z_A)(Z_G - Z_A)$$

and

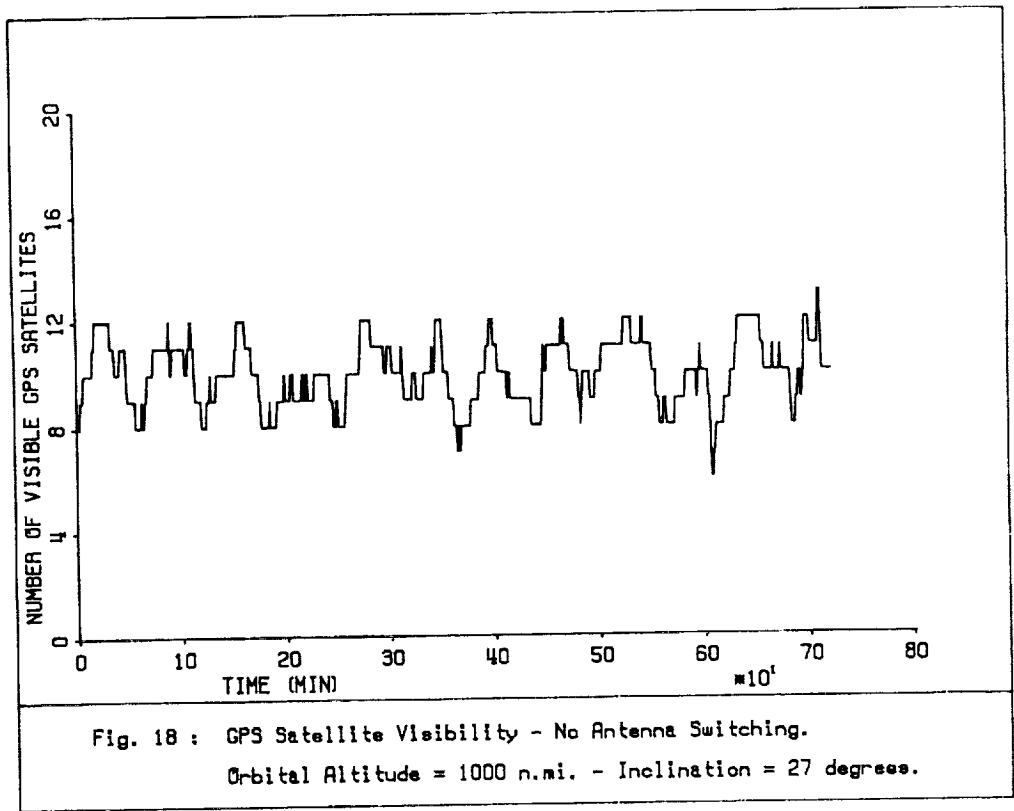
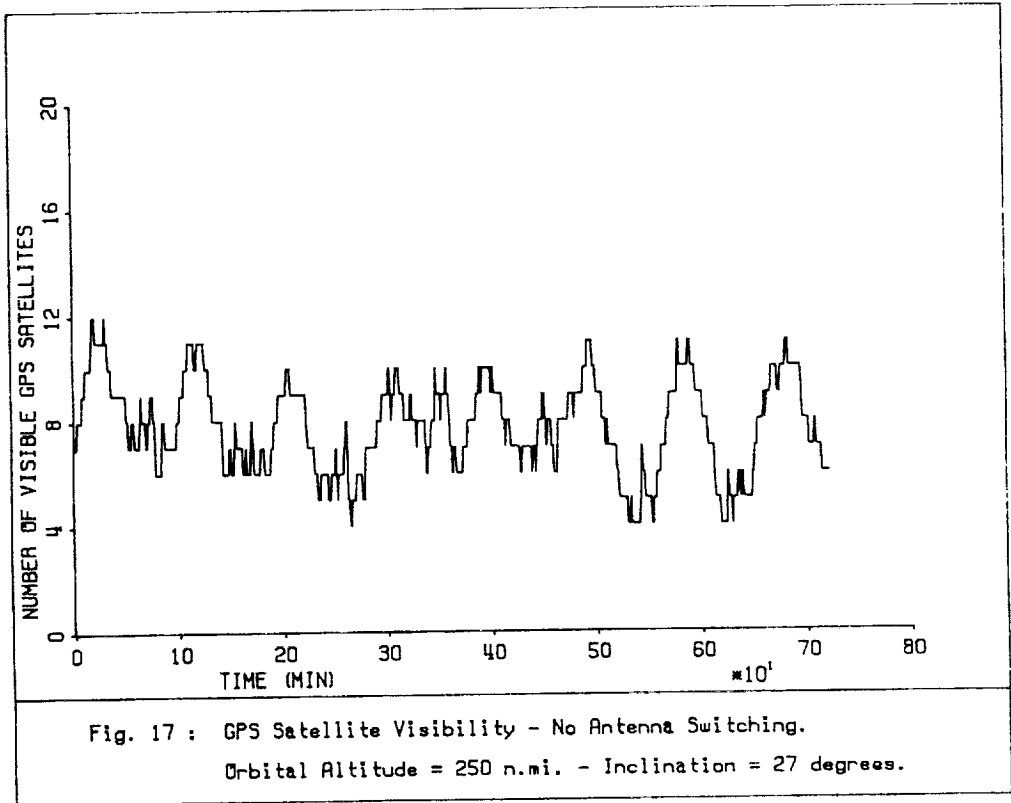
$$D = [(X_S - X_A)^2 + (Y_S - Y_A)^2 + (Z_S - Z_A)^2]^{1/2}$$

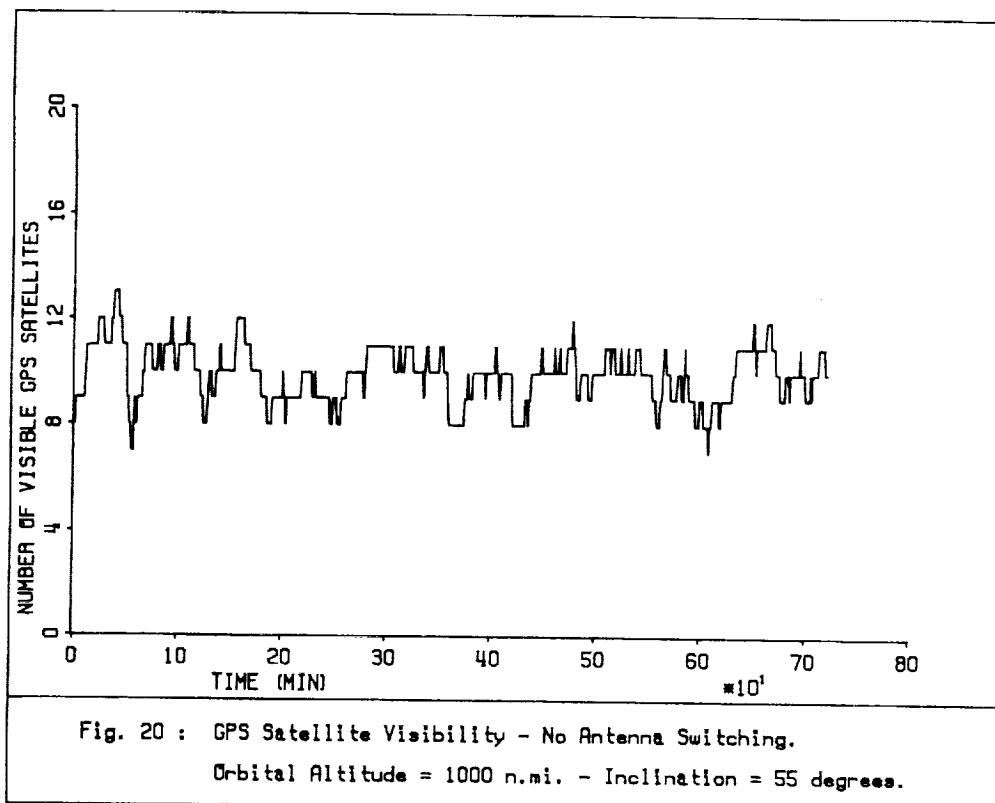
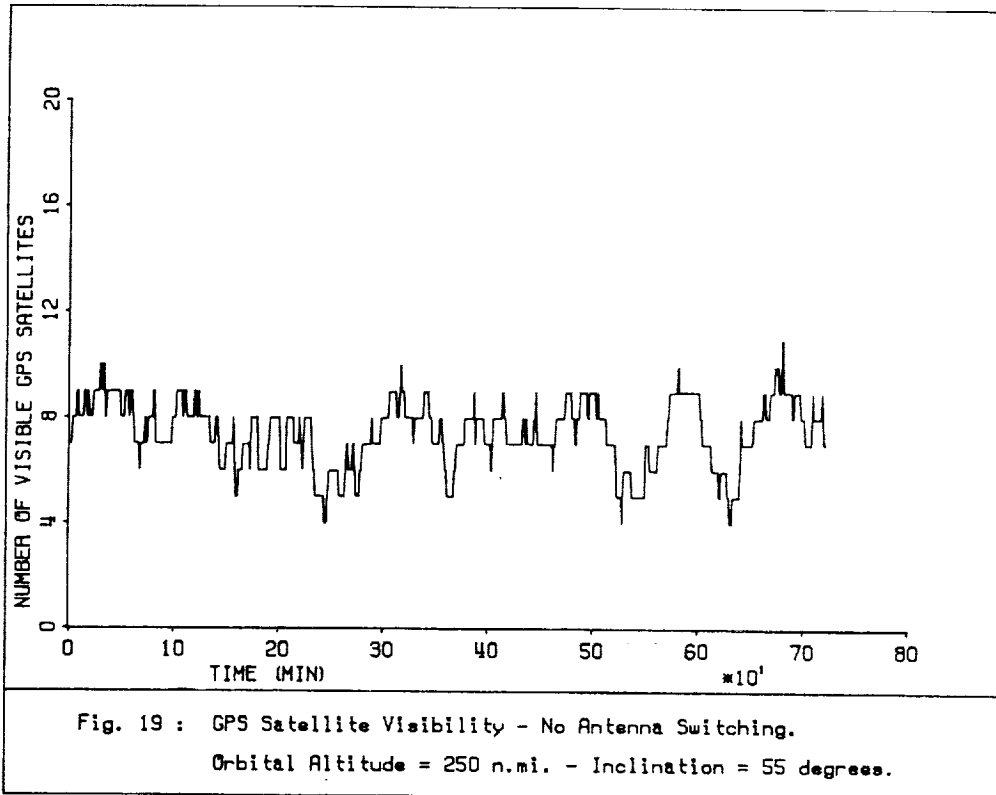
$$* [(X_G - X_A)^2 + (Y_G - Y_A)^2 + (Z_G - Z_A)^2]^{1/2}$$

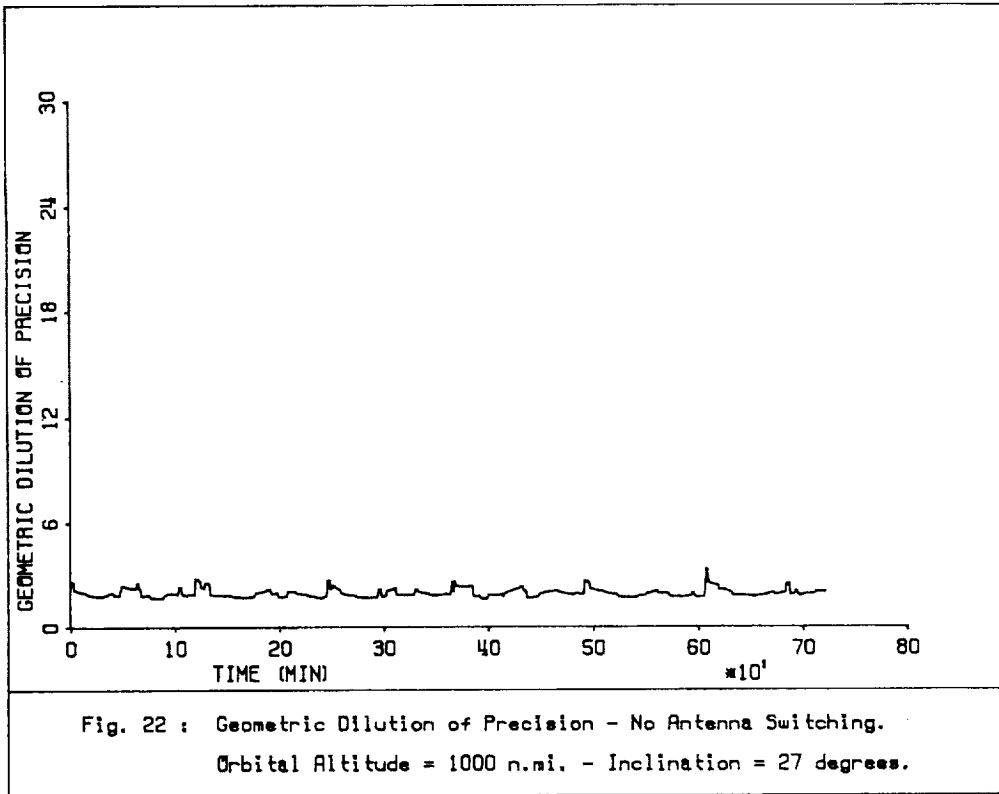
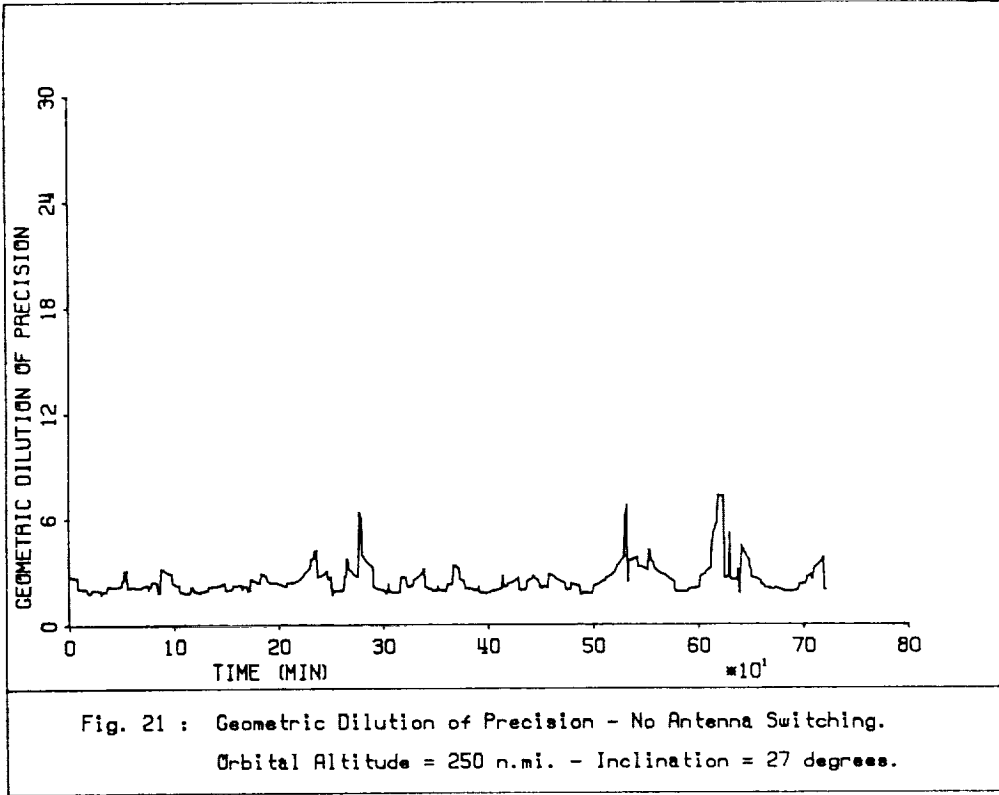
Figures 17 through 20 show the visibility results without antenna switching for the two different altitudes and the two inclinations. Figures 21 through 24 show the corresponding GDOP for the respective altitudes and inclinations. Furthermore, Figures 25 through 32 are similar to 17 through 24 but with antenna switching.

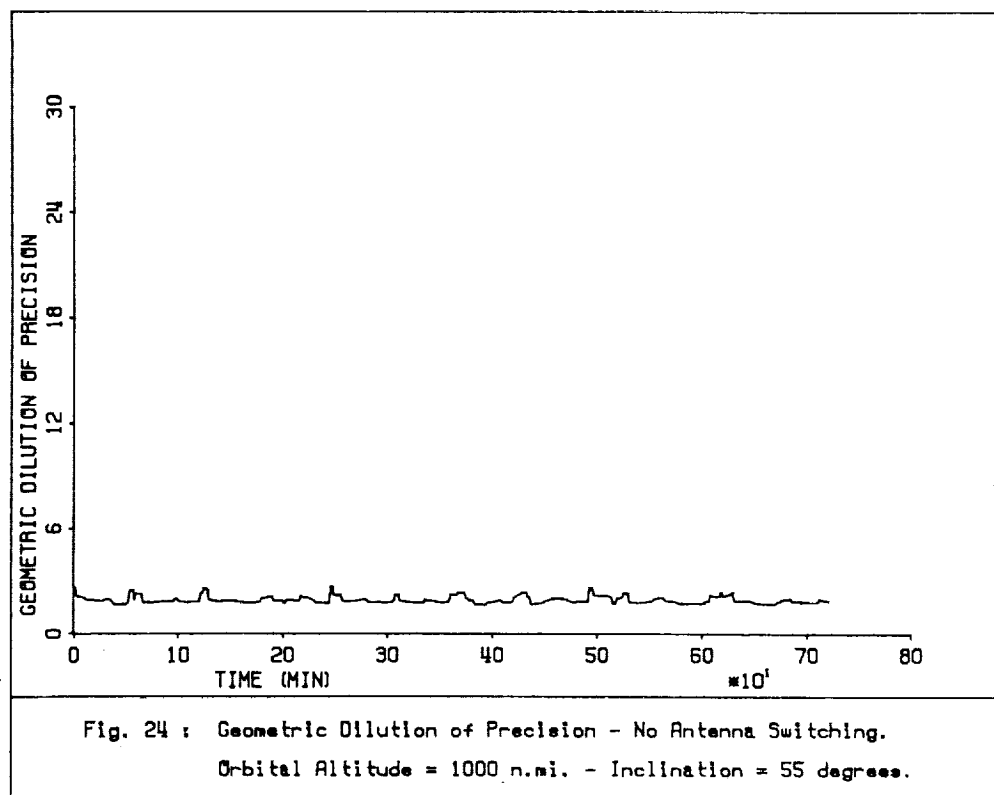
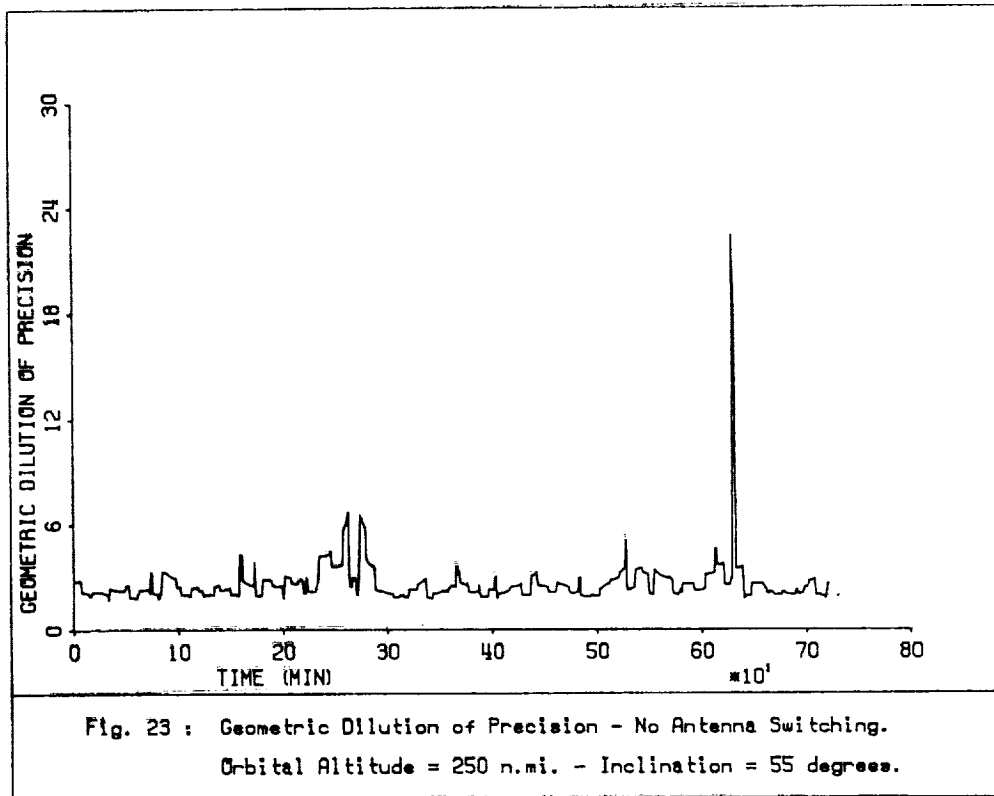
From Fig. 17 one can observe that the average number of visible GPS satellites at an altitude of 250 nmi and at an inclination of  $27^\circ$  is approximately 7, whereas the minimum is 4 and the maximum is 12. From Fig. 18 one can see that at an altitude of 1000 nmi and at the same inclination, the average number of visible satellites is approximately 9 with a minimum of 6 and a maximum of 13, i.e., the visibility is better at the higher altitude. This result is also apparent from comparison of Fig. 19 to 20. On the other hand, comparison of Fig. 17 to 19 and 18 to 20 indicates practically no influence of the inclination on the visibility. Inspection and comparison of Figures 21 through 24 indicate similar influence of the altitude and the inclination on the GDOP, and that at the 1000 nmi altitude, the GDOP upper bound is approximately 3.

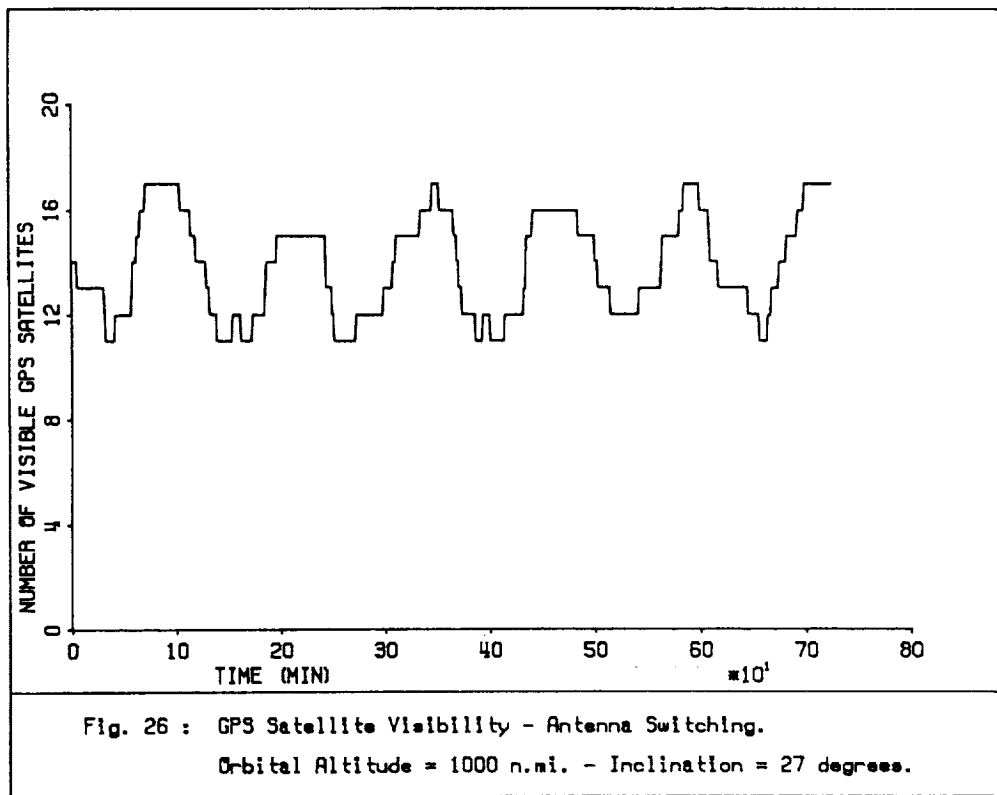
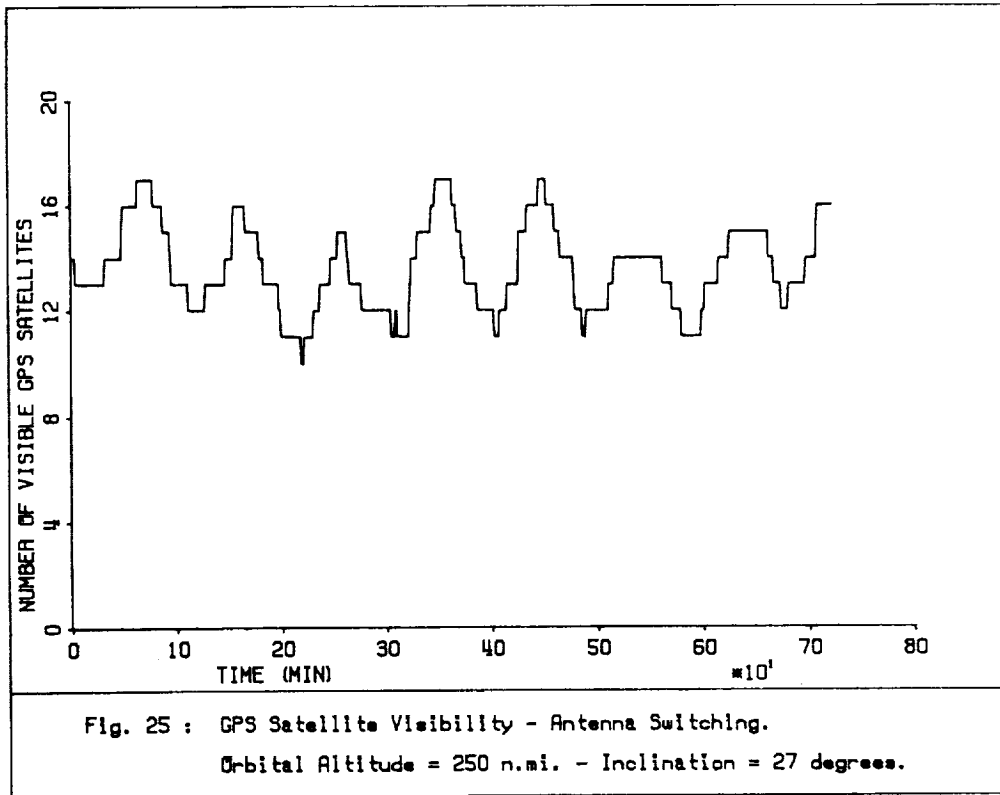
From Figures 25 through 28 one can observe an average number of 13 visible satellites with no less than 10 and as much as 17 always in view. Furthermore, it is also interesting to note that the altitude influences the results much less in this case. Moreover, from Figures 29 through 32 one can see that the GDOP has an upper bound of approximately 2.5 without any poor geometry regions (such as the ones in Figures 21 and 23) and that the influence of the altitude is only marginal.

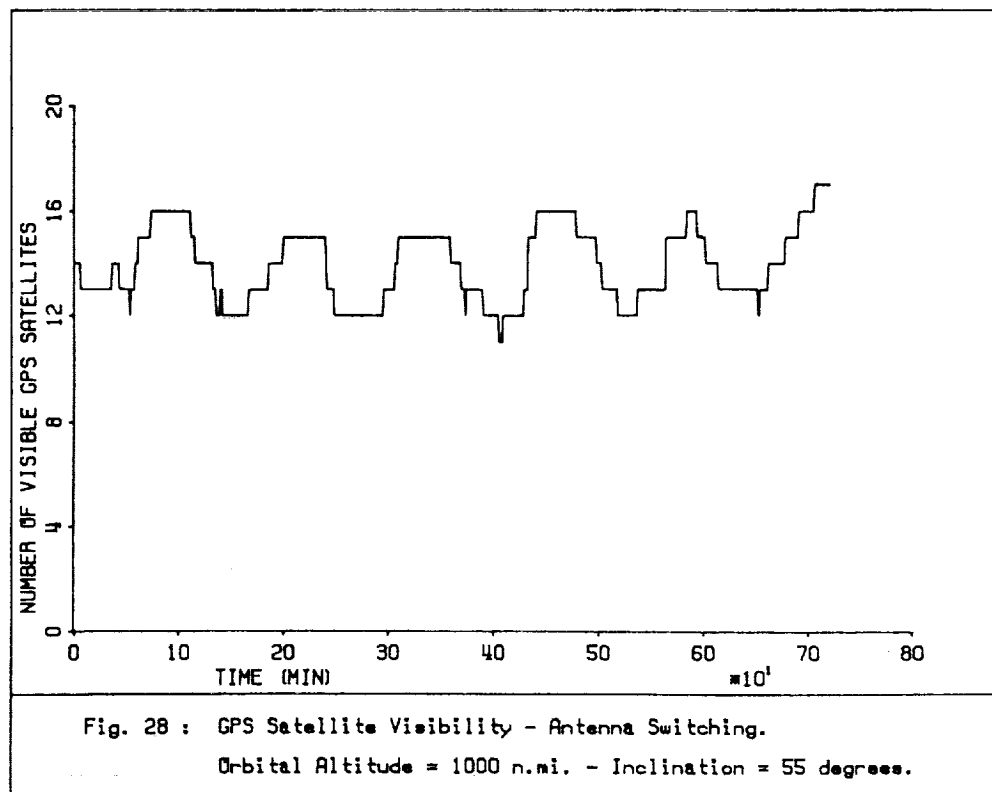
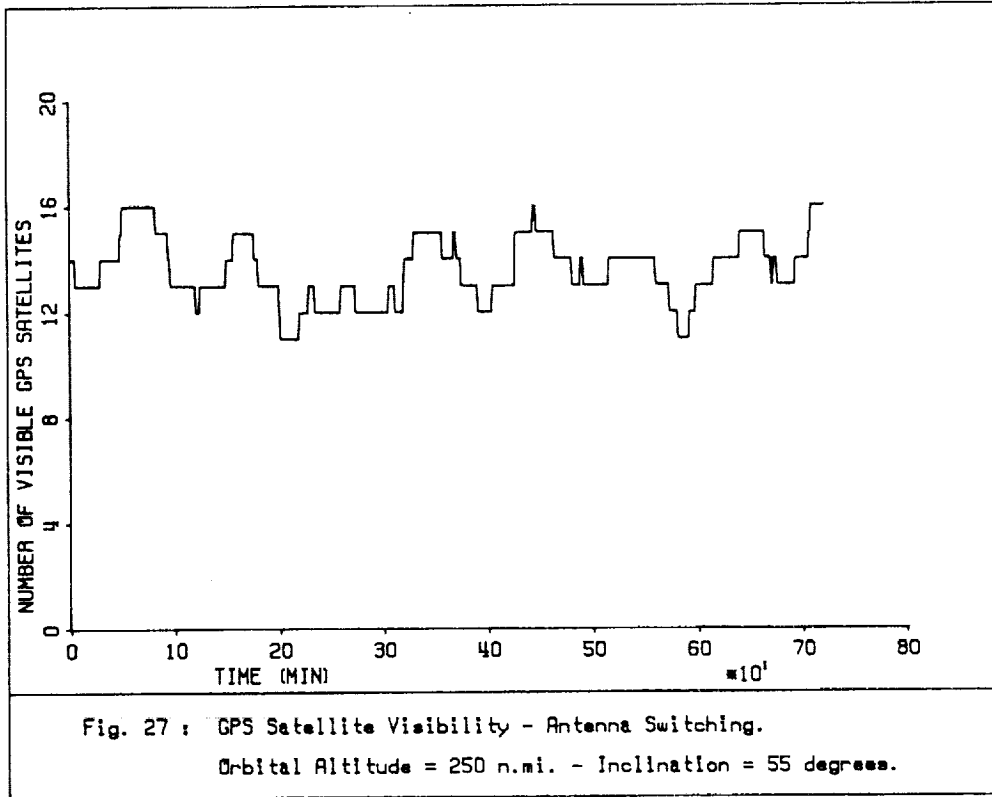


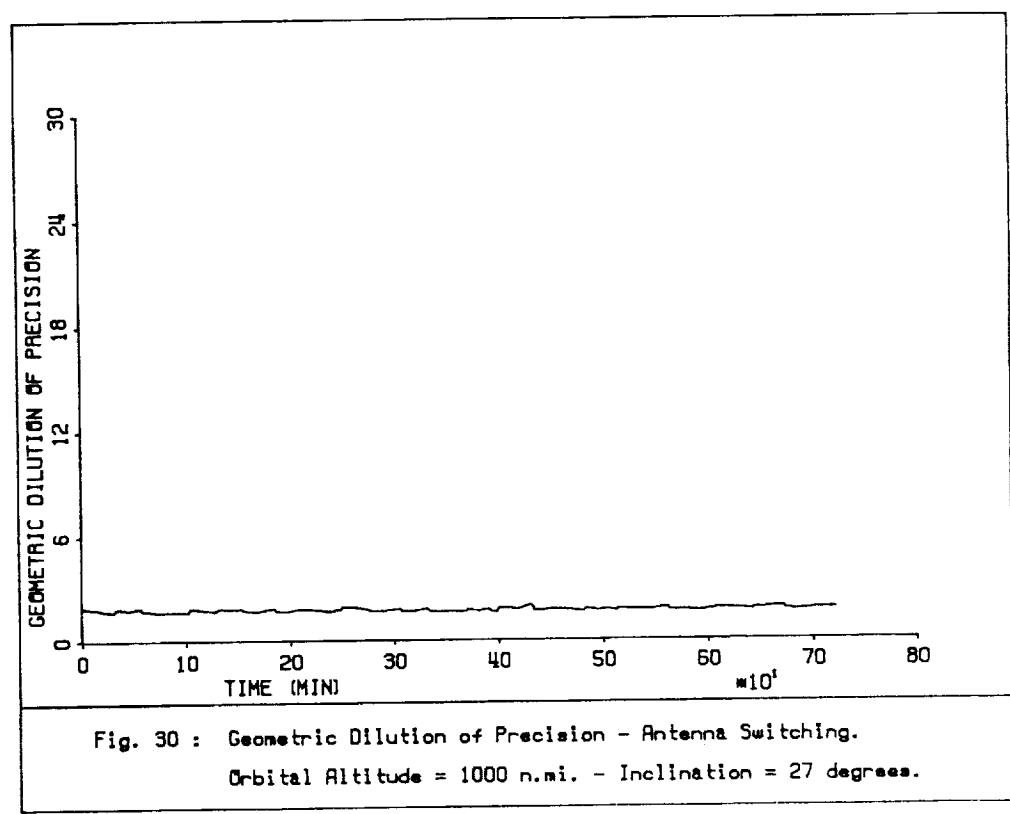
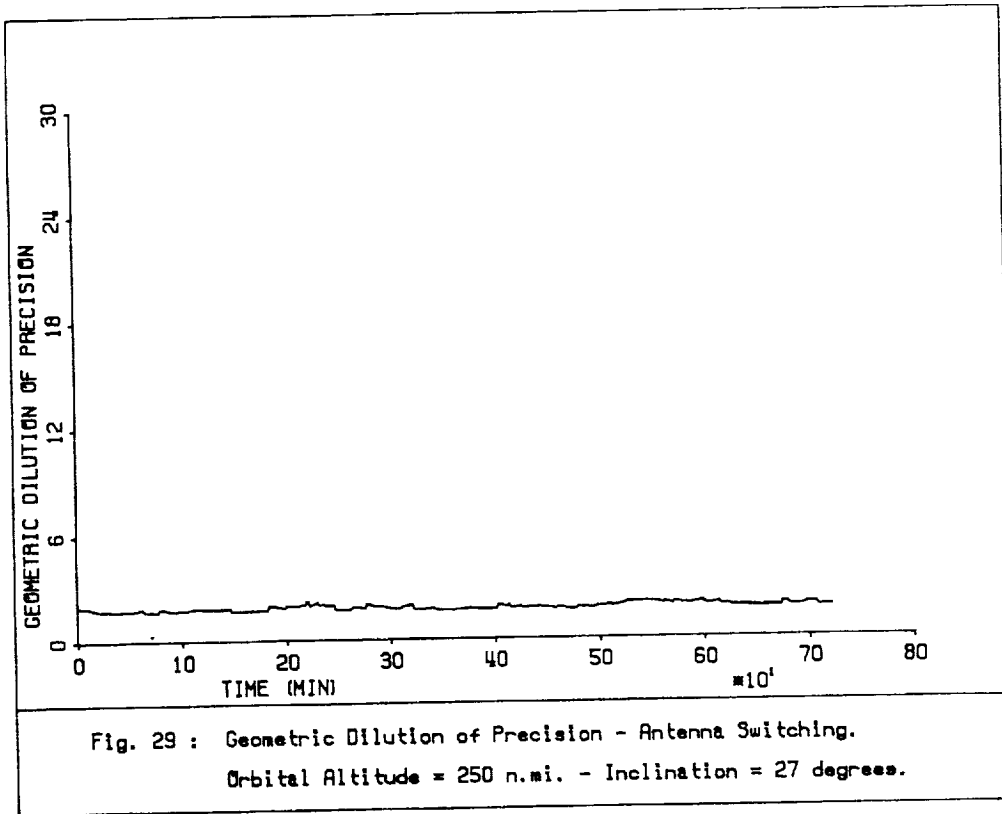


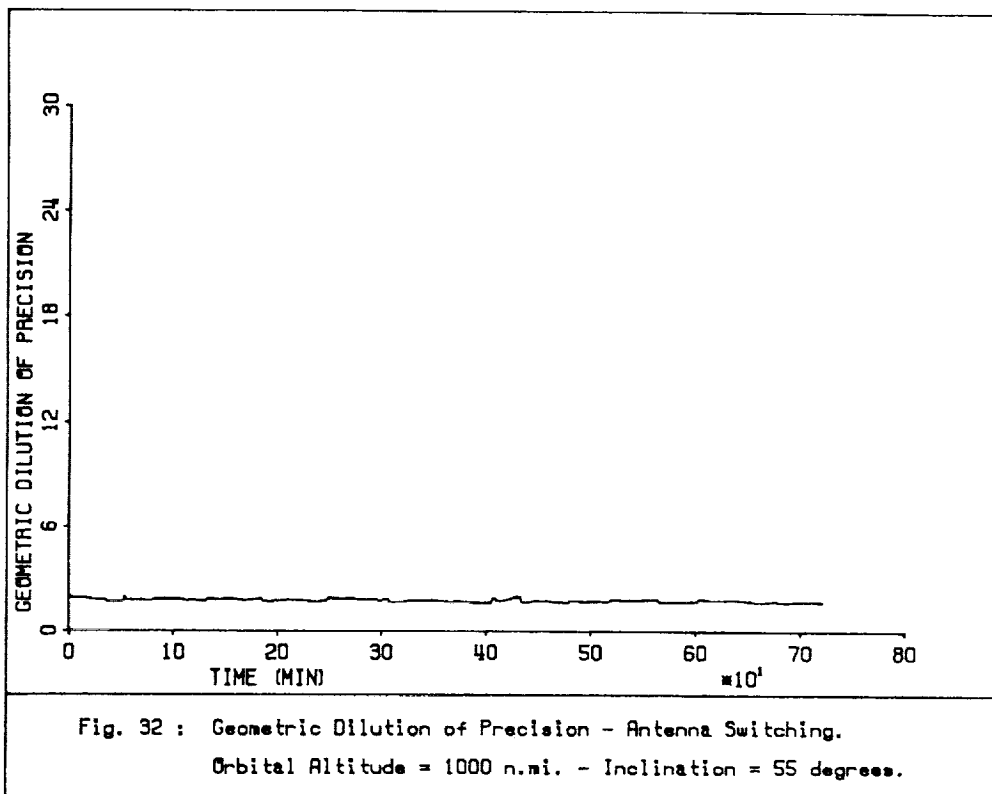
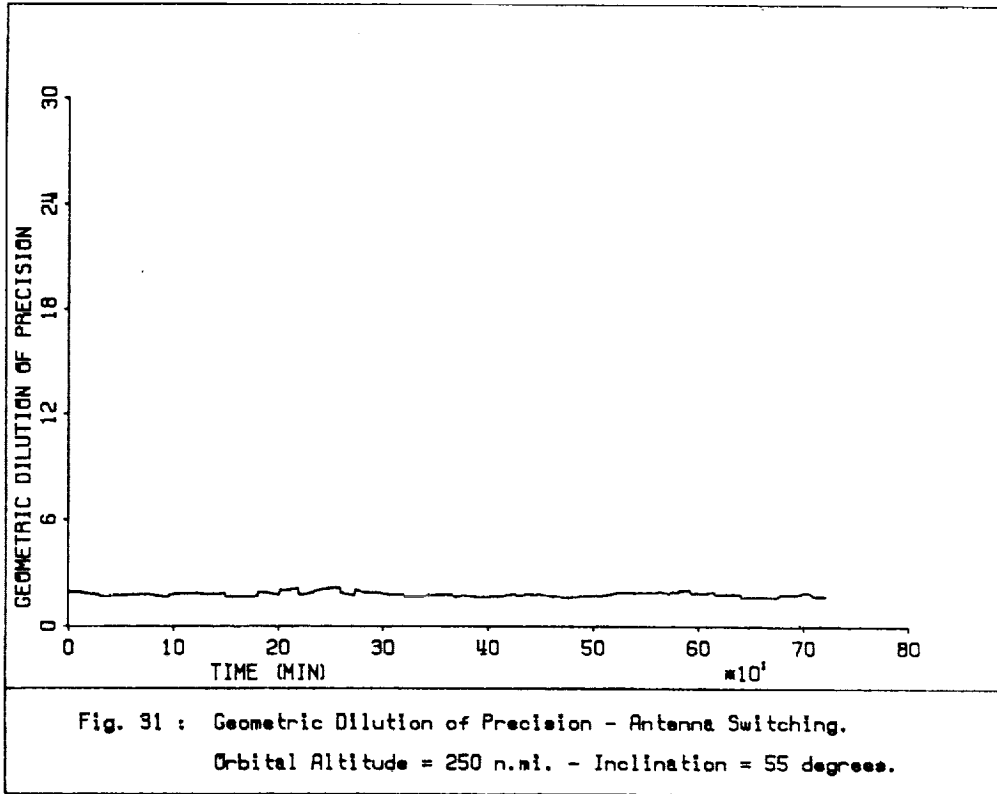












Comparison of the results without and with antennae switching indicates that the latter yields an improvement of the results by a factor of 1.5.

### 3.3.4 Navigation Filter Implementation

The integrated GPS/INS navigation filter is implemented as an extended-Kalman filter for simultaneously estimating the navigation error states and dominant IMU instrument errors. For the Phase I analysis involving OMV, the IMU instrument errors included in the filter states are the gyro bias drift and the accelerometer scale factor errors. For this application, the accelerometer bias errors were not considered significant [7]. The integrated filter implementation is based on the functional block diagram shown in Figure 2. The filter incorporates GPS receiver measurements of pseudo-range (code phase) and delta-range (integrated carrier phase) to estimate the filter states. The error states included in the navigation filter for the OMV application are:

Position	3
Velocity	3
Alignment	3
Gyro bias drift	3
Accelerometer scale factor	3
GPS clock time bias and frequency drift	2
Total	<u>17</u>

We introduced two new features in our navigation filter. The first one was the implementation of the filter in its U-D factor formulation. The second one was the incorporation of

the second degree zonal harmonic in the filter. The first feature improves the numerical stability (robustness) of the filter while working with single precision numbers. The second feature improves the navigation performance of the system.

### U-D Factors

The implementation of the integrated GPS/INS navigation filter in the on-board computer of the OMV places an additional memory and throughput requirement on the mission. Consequently, any effort to reduce the aforementioned burden is desirable. From the filter standpoint, an important step towards reducing memory and computation requirements is the implementation of the U-D factor formulation of the filter as opposed to its conventional Kalman formulation. In this section the conventional Kalman filter equations and the U-D factors equations for the Kalman filter are presented. A comparison between the two formulations is also presented here.

### Conventional Kalman Filter Formulation

The conventional formulation of the discrete Kalman filter is [22; p. 110]

#### (i) Time Update:

$$\hat{\underline{X}}_k^{(-)} = \Phi_{k,k-1} \hat{\underline{X}}_{k-1}^{(+)} \quad (13)$$

$$P_k^{(-)} = \Phi_{k,k-1} P_{k-1}^{(+T)} \Phi_{k,k-1}^T + Q_{k-1} \quad (14)$$

(ii) Measurement Update:

$$\hat{X}_k^{(+)} = \hat{X}_k^{(-)} + K_k (\underline{z}_k - H_k \hat{X}_k^{(-)}) \quad (15)$$

$$P_k^{(+)} = (I - K_k H_k) P_k^{(-)} \quad (16)$$

$$K_k = P_k^{(-T)} H_k^T (H_k P_k^{(-T)} H_k^T + R_k)^{-1} \quad (17)$$

where  $\Phi_{k,k-1}$  is the state transition matrix, related to the system's dynamics matrix  $F$  by

$$\Phi_{k,k-1} = I + \Delta t F + 1/2 \Delta t^2 F^2 + \dots \quad (18)$$

$Q_k$  is the system's noise covariance,  $\underline{z}_k$  is the observation vector,  $H_k$  is the design or observation matrix,  $R_k$  is the measurement noise covariance matrix and  $K_k$  is the Kalman gain matrix.

### U-D Factor Formulation

The foundation of the U-D factor formulation is that given a covariance matrix  $P$ , one can compute a unit upper triangular matrix  $U$  and a diagonal matrix  $D$  such that [14]

$$P = U D U^T \quad (19)$$

where a unit upper triangular matrix is defined as an upper triangular matrix whose entries in the main diagonal are all equal to 1.

(i) Time Update:

Let U and D be the U-D factors of  $P_{k-1}^{(+)}$  such that

$$P_{k-1}^{(+)} = U D U^T \quad (20)$$

and define

$$W = [\Phi_{k,k-1}U \quad I] \quad (21)$$

$$B = \begin{bmatrix} D & 0 \\ 0 & Q_k \end{bmatrix} \quad (22)$$

then

$$\begin{aligned} WBW^T &= [\Phi_{k,k-1}U \quad I] \begin{bmatrix} D & 0 \\ 0 & Q_k \end{bmatrix} \begin{bmatrix} U^T & \Phi_{k,k-1}^T \\ & I \end{bmatrix} \\ &= [\Phi_{k,k-1}U \quad I] \begin{bmatrix} D U^T & \Phi_{k,k-1}^T \\ & Q_k \end{bmatrix} \\ &= \Phi_{k,k-1} U D U^T \Phi_{k,k-1}^T + Q_k \\ &= \Phi_{k,k-1} P_{k-1}^{(+)} \Phi_{k,k-1}^T + Q_k \end{aligned}$$

i.e.,

$$P_k^{(-)} = WBW^T \quad (23)$$

so that the problem of computing the U-D factors of  $P_k^{(-)}$  given  
the U-D factors of  $P_{k-1}^{(+)}$  (covariance time update) is reduced to  
computing the U-D factors of the expression  $WBW^T$ .

Now, let  $V$  be a unit upper triangular matrix such that

$$W = VX \quad (24)$$

where the columns of the matrix  $X$  are orthogonal elements of a  
weighted inner product space  $S$ . The weighted inner product of  
 $S$  is defined as:

$$\langle a, b \rangle_B = a^T B b; \quad a, b \in S \quad (25)$$

The orthogonality with respect to this inner product is  
defined as follows: Let  $a, b \in S$ , then

$$(a, b \text{ orthogonal}) \iff \langle a, b \rangle_B = 0 \quad (26)$$

Now, let

$$X = [X_1 \ X_2 \ \dots \ X_n] \quad (27)$$

The columns of  $X$  are orthogonal with respect to  $\langle \cdot, \cdot \rangle_B$ ,  
i.e.,

$$\langle X_i, X_j \rangle_B = X_i^T B X_j = 0 \quad \text{if } i \neq j \quad (28a)$$

$$\langle X_i, X_j \rangle_B = X_i^T B X_j = B_j \quad \text{if } i=j \quad (28b)$$

From (28), one immediately deduces that

$$XBX^T = \Lambda \quad (29)$$

where  $\Lambda$  is diagonal, therefore  $V$  and  $\Lambda$  are the U-D factors of  $P_k^{(-)}$  since  $V$  is unit upper triangular,  $\Lambda$  is diagonal and

$$P_k^{(-)} = WBW^T = VXBX^TV^T = V\Lambda V^T \quad \text{q.e.d.}$$

Therefore, the covariance time update problem is now reduced to computing a unit upper triangular matrix  $V$  and a matrix  $X$  with orthogonal columns with respect to  $\langle \cdot, \cdot \rangle_B$ , such that (24) is satisfied. This is accomplished via a Gram-Schmidt orthogonalization process. The method, as well as an algorithm to implement it are described in [14]. In summary, the algorithm is:

Given: (a)  $U, D$  such that  $P_{k-1}^{(+)} = UDU^T$   
 (b)  $\Phi_{k,k-1}; Q_k$

Needed:  $V, \Lambda$  such that  $P_k^{(-)} = V\Lambda V^T$

1. Compute  $W = [\Phi_{k,k-1}U \quad I] = [W_1 \ W_2 \ \dots \ W_n]$

2. Compute

$$B = \begin{bmatrix} D & 0 \\ 0 & Q_k \end{bmatrix}$$

3. Compute  $V, \Lambda$  with the following scheme

$$\Lambda_j = \langle W_j^{(n-j)}, W_j^{(n-j)} \rangle_B$$

$$V_{i,j} = \frac{1}{\Lambda_j} \langle W_i^{(n-j)}, W_j^{(n-j)} \rangle_B, \quad i=1,2,\dots,j-1$$

$$W_i^{(n-j+1)} = W_i^{(n-j)} - V_{i,j} W_j^{(n-j)}$$

$$\Lambda_1 = \langle W_1^{(n-1)}, W_1^{(n-1)} \rangle_B$$

where  $W_i^{(0)} = W_i$  for  $i=1,2,\dots,n$

Note that when  $\Lambda_j = 0$ , the choice of  $V_{i,j}$  is arbitrary and one usually sets  $V_{i,j}$  equal to the unit vector.

(ii) Measurement Update:

Let  $U$  and  $D$  be the U-D factors of  $P_k^{(-)}$ . Substituting (17) in (16) one has

$$\begin{aligned} P_k^{(+)} &= P_k^{(-)} - K_k H_k P_k^{(-)} = P_k^{(-)} - P_k^{(-)} H_k^T (H_k P_k^{(-)} H_k + R_k)^{-1} H_k P_k^{(-)} \\ &= U [D - D U^T H_k^T (H_k U D U^T H_k^T + R_k)^{-1} H_k U D] U^T \end{aligned} \quad (30)$$

Let us denote

$$A = D - D U^T H_k^T (H_k U D U^T H_k^T + R_k)^{-1} H_k U D \quad (31)$$

If  $V$  and  $B$  are the U-D factors of  $A$ , such that

$$A = VBV^T \quad (32)$$

and

$$W = UV \quad (33)$$

then  $W$  and  $B$  are the U-D factors of  $P_k^{(+)}$ , since:

$$WBW^T = UVBV^T U^T = UAU^T = P_k^{(+)}, \text{ or}$$

$$P_k^{(+)} = WBW^T \quad (34)$$

Therefore, the problem of computing the U-D factors of  $P_k^{(+)}$  given the U-D factors  $U$  and  $D$  of  $P_k^{(-)}$  (covariance measurement update) is reduced to computing the U-D factors  $V$  and  $B$  of the matrix  $A$ , because given  $V$  and  $B$  one can compute  $W$  from (33). The algorithm is [14]:

**Given:** (a)  $U, D$  such that  $P_k^{(-)} = UDU^T$   
 (b)  $H_k; R_k$

**Needed:**  $W, B$  such that  $P_k^{(+)} = WBW^T$

1. Compute  $f = U^T H_k^T$

$$g = Df = DU^T H_k^T$$

2. Set  $a_0 = R_k$ , then, for  $j=1, 2, \dots, n$ :

$$a_j = a_{j-1} + f_j g_j$$

$$B_j = \frac{a_{j-1}}{a_j} D_j \quad (B_j = D_j \text{ if } a_j=0)$$

$$l_j = g_j$$

$$\lambda = \frac{f_j}{a_{j-1}} \quad (\lambda = 0 \text{ if } a_{j-1} = 0)$$

$$W_{ij} = V_{ij} + l_i \lambda \quad ; i=1,2,\dots,j-1$$

set  $l_i$  equal to  $l_i + V_{ij} l_j$

$$3. \text{ Compute } \hat{X}_k^{(+)} = \hat{X}_k^{(-)} + l(z - H_k X_k^{(-)})$$

### Comparison of the Conventional and the U-D Factor Formulation of the Filter

An inherent shortcoming of the conventional formulation of the Kalman filter is related to indefinite covariance matrices. Examination of (16) indicates that there may be instances, where, due to numerical instabilities, the covariance matrix can have negative elements in its main diagonal. On the other hand, the U-D factor formulation was designed not to suffer from similar shortcomings.

Another advantage of the U-D formulation is near double precision accuracy with simple precision arithmetic. Extensive tests ran by [14; pp. 238-239] indicated that the U-D factor formulation in single precision arithmetic gave results that were close to double precision reference cases, whereas the conventional Kalman formulation performed poorly. The advantage is obvious in terms of memory, since single precision arithmetic is performed on 4-byte words, whereas double precision arithmetic is performed on 8-byte words, thus approximately half the storage area is required for single precision.

In terms of CPU time requirements, the conventional formulation is more efficient than the U-D formulation, however, the additional requirement represents only a modest (less than 10%) increase in CPU time, especially when covariances are not computed at every step. Moreover, the single precision arithmetic of the U-D formulation minimizes the CPU time (over the double precision) and makes it comparable to the conventional Kalman filter.

### Incorporation of the Second Degree Zonal Harmonic in the Filter

It can be shown that the vehicle velocity with respect to the rotating Earth expressed in local coordinates is governed by [23; p. 10]

$$\dot{V}_N = f_N + g_N - (\omega_Z + \Omega_Z)V_E + \omega_E V_V \quad (35)$$

$$\dot{V}_E = f_E + g_E - (\omega_N + \Omega_N)V_V + (\omega_V + \Omega_V)V_N \quad (36)$$

$$\dot{V}_V = f_V + g_V - \omega_E V_N + (\omega_N + \Omega_N)V_E \quad (37)$$

where

$[V_N \ V_E \ V_V]^T$  = velocity vector with respect to the Earth

$[f_N \ f_E \ f_V]^T$  = specific force vector

$[g_N \ g_E \ g_V]^T$  = gravity vector

$[\omega_N \ \omega_E \ \omega_V]^T$  = angular velocity of the local frame with respect to inertial space

$[\Omega_N \ \Omega_E \ \Omega_V]^T$  = angular velocity of the Earth with respect to inertial space

or, using the relationships of Table 3-2 in [23, p. 27], one has

$$\dot{V}_N = f_N + g_N - V_E^2 \tan \phi / r - 2\Omega V_E \sin \phi - V_N V_V / r \quad (38)$$

$$\dot{V}_E = f_E + g_E - V_E V_V / r - 2\Omega V_V \cos \phi + V_E V_N \tan \phi / r + 2\Omega V_N \sin \phi \quad (39)$$

$$\dot{V}_V = f_V + g_V + V_N^2 / r + V_E^2 / r + 2\Omega V_E \cos \phi \quad (40)$$

where

$r$  = geocentric radius of the vehicle

$\phi$  = latitude of the vehicle

$\Omega$  = Earth rotation rate.

Taking the total differentials of (38), (39) and (40) yields the differential equations governing the velocity errors. One has

$$\begin{aligned} \delta \dot{V}_N = & -[(V_E / r \cos \phi)^2 + 2\Omega V_E \cos \phi / r] \delta X_N + (V_E^2 \tan \phi + V_N V_V) \delta X_V / r^2 \\ & - (2V_E \tan \phi / r + 2\Omega \sin \phi) \delta V_E - V_V \delta V_N / r - V_N \delta V_V / r + \delta g_N \end{aligned} \quad (41)$$

$$\delta \dot{V}_E = (V_E V_N / (r \cos \phi)^2 + 2\Omega V_V \sin \phi / r + 2\Omega V_N \cos \phi / r) \delta X_N$$

$$\begin{aligned}
& + (V_V V_E - V_E V_N \tan \phi) \delta X_V / r^2 + (V_N \tan \phi - V_V) \delta V_E / r \\
& + (V_E \tan \phi / r + 2\Omega \sin \phi) \delta V_N - (2\Omega \cos \phi + V_E / r) \delta V_V + \delta g_E
\end{aligned} \tag{42}$$

$$\begin{aligned}
\delta V_V = & -2\Omega V_E \sin \phi \delta X_N / r - (V_N^2 + V_E^2) \delta X_V / r^2 + (2\Omega \cos \phi + 2V_E / r) \delta V_E \\
& + 2V_N \delta V_N / r + \delta g_V
\end{aligned} \tag{43}$$

The terms  $\delta g_N$ ,  $\delta g_E$  and  $\delta g_V$  in (41), (42) and (43) are the gravity computation errors due to evaluating gravity at the indicated rather than the true position [23; pp. 23 and 133]. The omission error and the local variations in the gravity vector (vertical deflections and gravity anomalies) are usually modeled as first order Markov processes [23, p. 133] and are not included in (41), (42) and (43).

One usually assumes that the Earth is a sphere, thus

$$g_N = g_E = 0; g_V = -g = -GM/r^2$$

where  $g$  is the magnitude of the gravity vector. Hence

$$\delta g_N = \delta g_E = 0; \delta g_V = 2g/r \tag{44}$$

However, more precisely, the Earth's gravity vector can be represented as

$$g_N = \frac{GM}{r^2} \sum_{n=2}^{\infty} \left( \frac{a}{r} \right)^n \sum_{m=0}^n (C_{nm} \cos m\lambda + S_{nm} \sin m\lambda) \partial P_{nm} / \partial \phi + c_N$$

$$g_E = \frac{GM}{r^2 \cos\phi} \sum_{n=2}^{\infty} \left(\frac{a}{r}\right)^n \sum_{m=0}^n [m(S_{nm}\cos m\lambda - C_{nm}\sin m\lambda)] P_{nm}(\sin\phi) + c_E$$

$$g_V = -\frac{GM}{r^2} \left[ 1 + \sum_{n=2}^{\infty} (n+1) \left(\frac{a}{r}\right)^n \sum_{m=0}^n (C_{nm}\cos m\lambda + S_{nm}\sin m\lambda) P_{nm}(\sin\phi) \right] + c_V$$

where  $c_N, c_E$  and  $c_V$  are the components of the centrifugal force vector  $c$  along the North, East and Up local coordinate system. The centrifugal force in an Earth-fixed XYZ coordinate system is given by [24; p. 47]

$$c = [\Omega^2 X, \Omega^2 Y, 0]^T$$

and the rotation matrix from XYZ to N,E,V is [25; p. 70]

$$R = \begin{bmatrix} -\sin\phi\cos\lambda & -\sin\phi\sin\lambda & \cos\phi \\ -\sin\lambda & \cos\lambda & 0 \\ \cos\phi\cos\lambda & \cos\phi\sin\lambda & \sin\phi \end{bmatrix}$$

where  $\phi$  and  $\lambda$  are the latitude and longitude of the origin of the N, E, V system. Moreover, the Cartesian geocentric coordinates X and Y are given by [26; p. 16]

$$X = r\cos\phi\cos\lambda$$

$$Y = r\cos\phi\sin\lambda$$

where  $r$  is the geocentric distance to the point of interest. Thus

$$c_N = -\Omega r \sin\phi \cos\lambda$$

$$c_E = 0$$

$$c_V = \Omega r \cos^2 \phi$$

On the other hand [25; p. 41]

$$\delta \phi = \delta X_N / r; \quad \delta \lambda = \delta X_E / r \cos \phi$$

and  $\delta h = \delta X_V$ .

Now, the gravity errors are the total differentials of the gravity vector components with respect to the local coordinates. One has

$$\delta g_N = (\partial g_N / \partial \phi) \delta \phi + (\partial g_N / \partial \lambda) \delta \lambda + (\partial g_N / \partial h) \delta h$$

and similarly for  $\delta g_E$  and  $\delta g_V$ . The final result is

$$\begin{aligned} \delta g_N = & [K \sum_{n=2}^{\infty} A_n \sum_{m=0}^n B_{nm} F_{nm} - \Omega^2 \cos 2\phi] \delta X_N \\ & + [K \sum_{n=2}^{\infty} A_n \sum_{m=0}^n m G_{nm} E_{nm}] \delta X_E / \cos \phi \\ & - [K \sum_{n=2}^{\infty} (n+2) A_n \sum_{m=0}^n B_{nm} E_{nm} + \Omega^2 \sin 2\phi / 2] \delta X_V \end{aligned} \quad (45)$$

$$\begin{aligned} \delta g_E = & K \sum_{n=2}^{\infty} A_n \sum_{m=0}^n m G_{nm} (E_{nm} + \tan \phi D_{nm}) \delta X_N / \cos \phi \\ & - K \sum_{n=2}^{\infty} A_n \sum_{m=0}^n m^2 B_{nm} D_{nm} \delta X_E / \cos^2 \phi \\ & - K \sum_{n=2}^{\infty} (n+2) A_n \sum_{m=0}^n m G_{nm} D_{nm} \delta X_V / \cos \phi \end{aligned} \quad (46)$$

$$\begin{aligned}
\delta g_V = & - \left[ K \sum_{n=2}^{\infty} (n+1) A_n \sum_{m=0}^n B_{nm} E_{nm} + \Omega^2 \sin 2\phi \right] \delta X_N \\
& - K \sum_{n=2}^{\infty} (n+1) A_n \sum_{m=0}^n m G_{nm} D_{nm} \delta X_E / \cos \phi \\
& + \left[ K \left( 2 + \sum_{n=2}^{\infty} (n+1)(n+2) A_n \sum_{m=0}^n B_{nm} D_{nm} \right) + \Omega^2 \cos^2 \phi \right] \delta X_V \quad (47)
\end{aligned}$$

where

$$\begin{aligned}
K &= GM/r^3 \\
A_n &= (a/r)^n \\
B_{nm} &= C_{nm} \cos m\lambda + S_{nm} \sin m\lambda \\
D_{nm} &= P_{nm}(\sin \phi) \\
E_{nm} &= \partial P_{nm}(\sin \phi) / \partial \phi \\
F_{nm} &= \partial^2 P_{nm}(\sin \phi) / \partial \phi^2 \\
G_{nm} &= S_{nm} \cos m\lambda - C_{nm} \sin m\lambda
\end{aligned}$$

The Legendre functions  $P_{nm}$  are given by

$$P_{nm} = L_{nm} \sin \phi P_{n-1,m} - M_{nm} P_{n-2,m} \quad \text{for } m < n$$

with

$$\begin{aligned}
L_{nm} &= [(2n+1)(2n-1)]^{1/2} / [(n+m)(n-m)]^{1/2} \\
M_{nm} &= [(2n+1)(n+m-1)(n-m-1)]^{1/2} / [(2n-3)(n+m)(n-m)]^{1/2} \\
P_{00} &= 1, \quad P_{10} = \sqrt{3} \sin \phi, \quad P_{11} = \sqrt{3} \cos \phi
\end{aligned}$$

and

$$P_{nn} = [(2n+1)/2n]^{1/2} \cos \phi P_{n-1,n-1}$$

The first derivatives of the Legendre functions are given by

$$\begin{aligned} \partial P_{nm}/\partial\phi &= [(2n+1)(n+m)(n-m)/(2n-1)]^{1/2} P_{n-1,m}/\cos\phi \\ &\quad - n\tan\phi P_{nm} \quad \text{for } m < n \end{aligned}$$

with

$$\partial P_{00}/\partial\phi = 0, \quad \partial P_{10}/\partial\phi = \sqrt{3}\cos\phi, \quad \partial P_{11}/\partial\phi = -\sqrt{3}\sin\phi$$

and

$$\partial P_{nn}/\partial\phi = (2n+1/2n)^{1/2} [\cos\phi \partial P_{n-1,n-1}/\partial\phi - \sin\phi P_{n-1,n-1}]$$

The second derivatives of the Legendre functions are given by

$$\begin{aligned} \partial^2 P_{nm}/\partial\phi^2 &= [n^2 \sin^2\phi - n - (n+m)(n-m)] P_{nm}/\cos^2\phi \\ &\quad + [(2n+1)(n+m)(n-m)/(2n-1)]^{1/2} \tan\phi P_{n-1,m}/\cos\phi \quad \text{for } m < n \end{aligned}$$

with

$$\partial^2 P_{00}/\partial\phi^2 = 0, \quad \partial^2 P_{10}/\partial\phi^2 = -\sqrt{3}\sin\phi, \quad \partial^2 P_{11}/\partial\phi^2 = -\sqrt{3}\cos\phi,$$

and

$$\begin{aligned} \partial^2 P_{nn}/\partial\phi^2 &= [(2n+1)/2n]^{1/2} [\cos\phi (\partial^2 P_{n-1,n-1}/\partial\phi^2 - P_{n-1,n-1}) \\ &\quad - 2\sin\phi \partial P_{n-1,n-1}/\partial\phi] \end{aligned}$$

and  $C_{nm}$ ,  $S_{nm}$  are the fully normalized potential coefficients describing the model geopotential field.

In the event that only the second degree zonal harmonic  $J_2$  needs to be considered one has  $C_{nm} = S_{nm} = 0$  except for  $C_{20} = -J_2/\sqrt{5}$ . Thus, considering that

$$P_{20} = \sqrt{5}(3\sin^2\phi-1)/2, \quad \partial P_{20}/\partial\phi = 3\sqrt{5}\sin 2\phi/2 \text{ and}$$

$$\partial^2 P_{20}/\partial\phi^2 = 3\sqrt{5}\cos 2\phi/2$$

the gravity error equations become

$$\begin{aligned} \delta g_N = & -\left[3\frac{GM}{r^3}\left(\frac{a}{r}\right)^2 J_2 \cos 2\phi + \Omega^2 \cos 2\phi\right] \delta X_N \\ & + \left[6\frac{GM}{r^3}\left(\frac{a}{r}\right)^2 J_2 \sin 2\phi + \Omega^2 \sin 2\phi/2\right] \delta X_V \end{aligned} \quad (48)$$

$$\delta g_E = 0 \quad (49)$$

$$\begin{aligned} \delta g_V = & \left[\frac{9GM}{2r^3}\left(\frac{a}{r}\right)^2 J_2 - \Omega^2\right] \sin 2\phi \delta X_N \\ & + \left[\frac{GM}{r^3} \left[2-6\left(\frac{a}{r}\right)^2 J_2 (3\sin^2\phi-1)\right] + \Omega^2 \cos^2\phi\right] \delta X_V \end{aligned} \quad (50)$$

Equations (48), (49) and (50) were incorporated in our navigation filter in order to consider the  $J_2$  effects. However, equations (45), (46) and (47) can be implemented if the incorporation of a higher resolution and accuracy field is desired. The value of  $J_2$  used in the filter is 0.0010826258 which corresponds to the GEM-T1 model.

### 3.3.5 Performance Results

We used the GPS Inertial Navigation System Simulation (GINSS) software to evaluate the performance of the integrated

navigation filter for the OMV high-thrust trajectory [16]. Two cases were considered. In the first case it was assumed that a GPS update was available prior to the start of the burn such that the position, velocity, tilt and clock bias were accurately known (Good Initial Conditions). In the second case it was assumed that a period of GPS outage had elapsed and there was a deterioration of the navigation parameters (Poor Initial Conditions). The latter case corresponds to a GPS signal acquisition specification [6]. The initial conditions for the two cases were:

	Case I Good Initial Conditions	Case II Poor Initial Conditions
Position	15 m (1- $\sigma$ )	150 km (3- $\sigma$ )
Velocity	0.1 m/sec (1- $\sigma$ )	200 m/sec (3- $\sigma$ )
Tilt	1° (1- $\sigma$ )	15° (3- $\sigma$ )
Clock bias	1 $\mu$ sec (1- $\sigma$ )	1 sec (3- $\sigma$ )

The performance of the filter for the first case is shown in Figures 33 through 41, whereas for the second case it is shown in Figures 42 through 50. In the aforementioned figures the time histories of the errors in position, velocity and tilt as well as their covariance time histories are shown.

From Figures 33, 34 and 35 one can observe that within 10 seconds of GPS measurement processing by the GPS/INS navigation filter, the position errors are less than 5m. At the end of the 5.5 min period the errors in position are less than 2m. From Figures 36, 37 and 38 one can observe that initially the velocity covariances increase (up to approximately 0.2m/sec for the vertical component at the first 30 seconds and then they improve to approximately 0.03m/sec. From Figures 39, 40, and 41 one can observe that the tilt errors reduce rather slowly, with the exception of the

vertical tilt error which is approximately  $0^{\circ}.3$  within 1 min. At the end of the 5.5 min period the error covariances are approximately  $0^{\circ}.2$  for the North and East tilts and  $0^{\circ}.04$  for the vertical tilt. Comparison of the navigation filter performance to the OMV navigation performance specification, presented earlier in Table 1, clearly demonstrates that incorporation of the proposed GPS/INS navigation filter in the OMV OBC will provide the required position, velocity and attitude update accuracy with ample margin. Furthermore, attitude update accuracy comparable to horizon and sun sensors can be achieved without the restriction of maneuvering the flight vehicle to point the sun sensor within 2 degrees of the sun [8].

The second test case results provide further evidence of the exceptional capability of the integrated navigation filter to obtain good accuracy in the presence of large initial condition errors. The excellent performance of the filter for this test case can be observed in Figures 42 through 50. It is indeed remarkable that even with such poor initial conditions as mentioned earlier for position, velocity, tilt and clock bias, one minute of GPS data, processed in a tightly-integrated GPS/INS filter, are capable of reducing the errors to less than 3m in position and to less than 0.2m/sec in velocity. After the 5.5 min period, the position error is less than 2m, the velocity error is less than 0.03m/sec and the tilt error is less than  $0^{\circ}.3$  in each axis.

These results are representative of the excellent performance of the proposed integrated navigation filter.

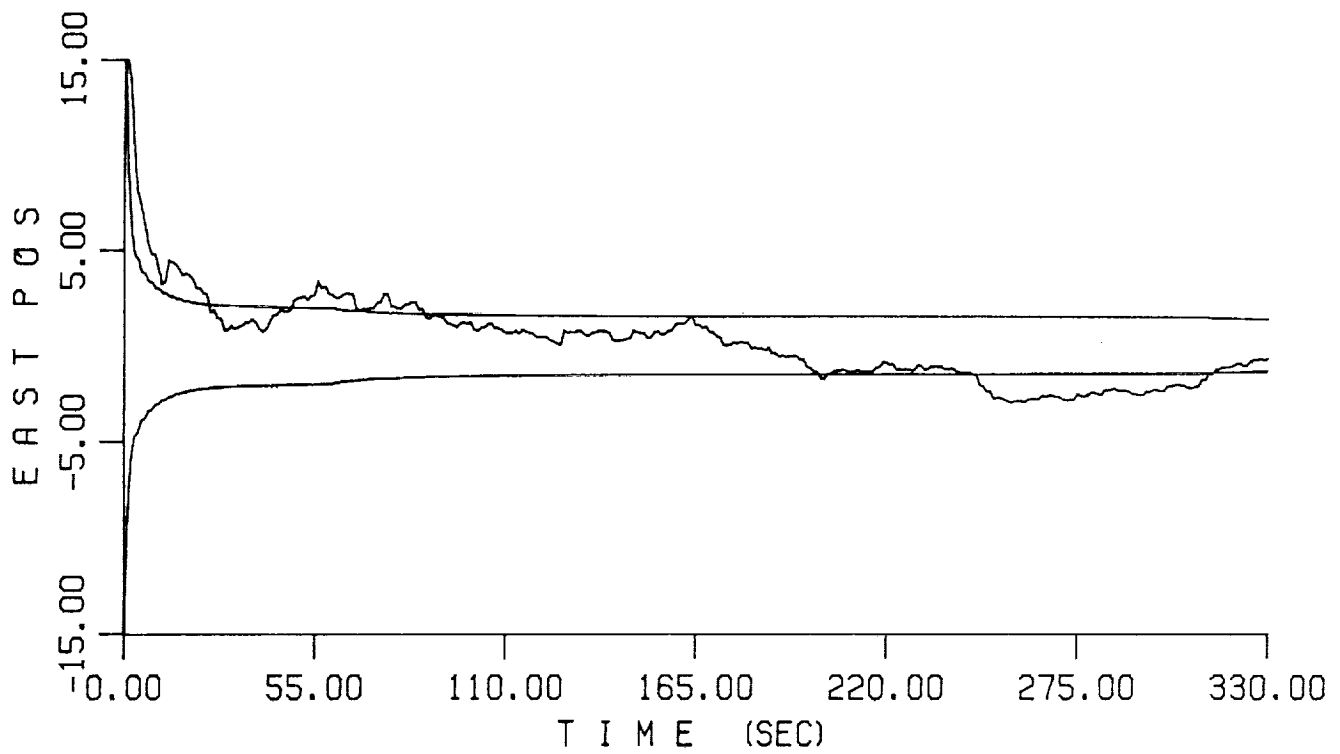


Fig. 33 : Time History of the East Position Error and its Covariance. Case I : Good Initial Conditions.

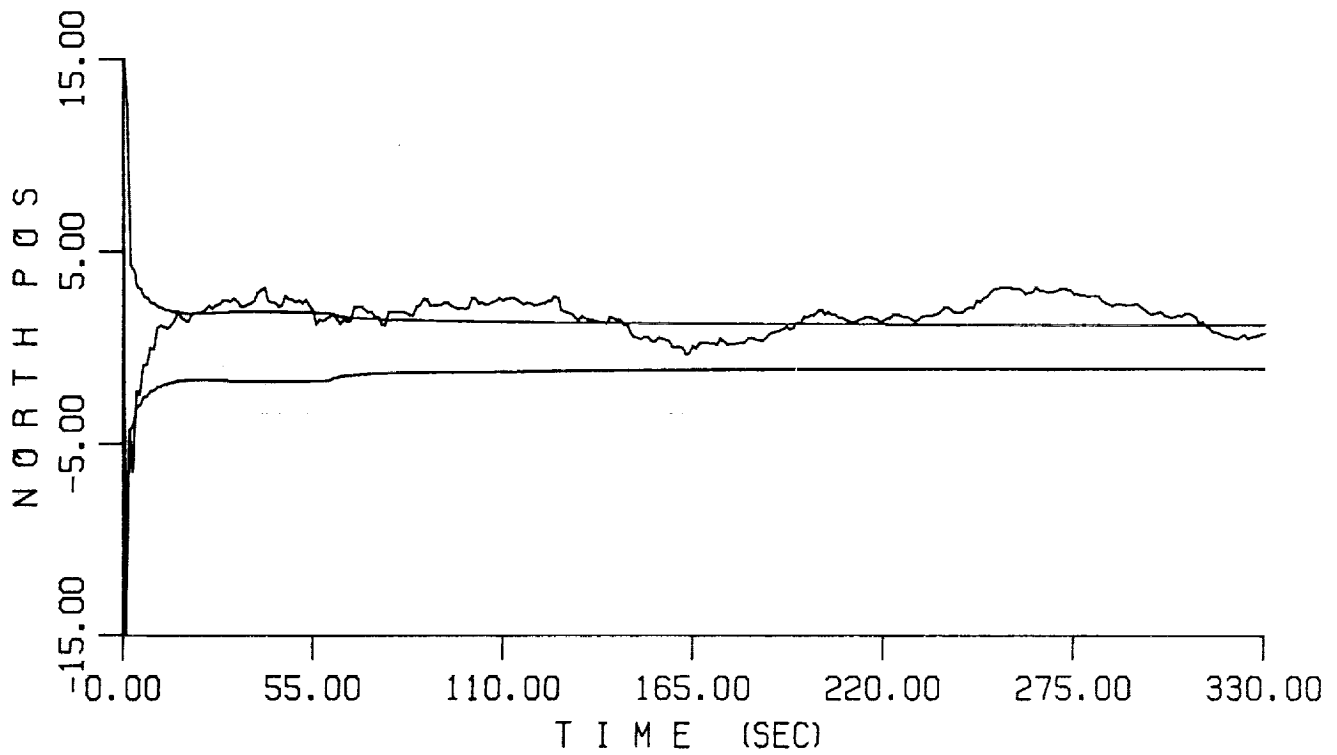


Fig. 34 : Time History of the North Position Error and its Covariance. Case I : Good Initial Conditions.

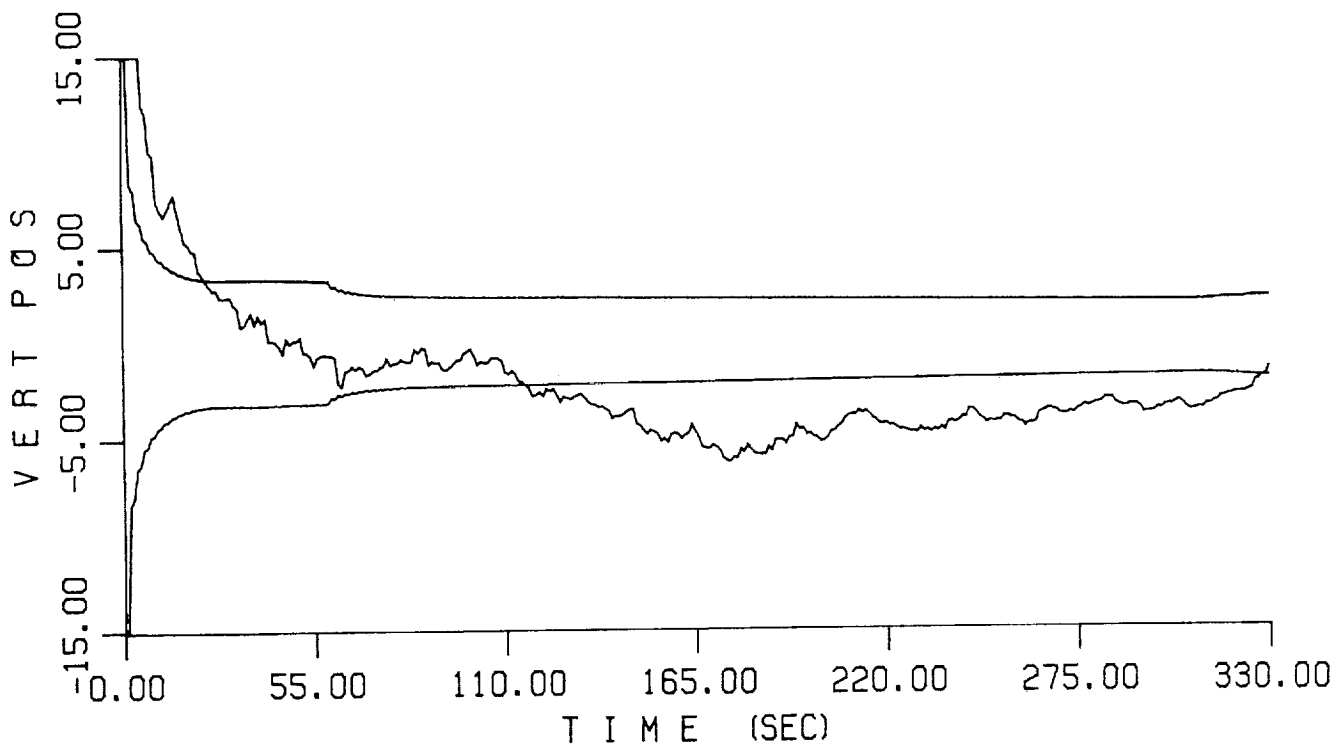


Fig. 35 : Time History of the Vertical Position Error and its Covariance. Case I : Good Initial Conditions.

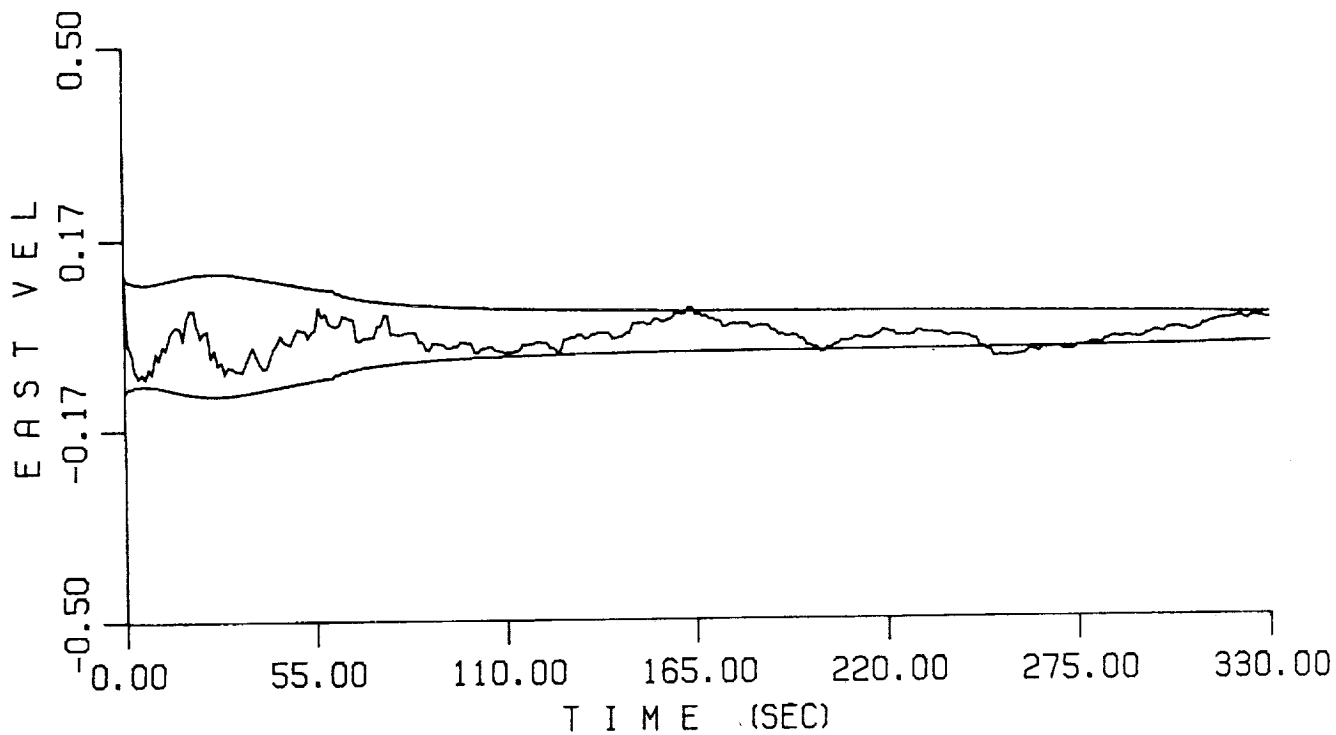


Fig. 36 : Time History of the East Velocity Error and its Covariance. Case I : Good Initial Conditions.

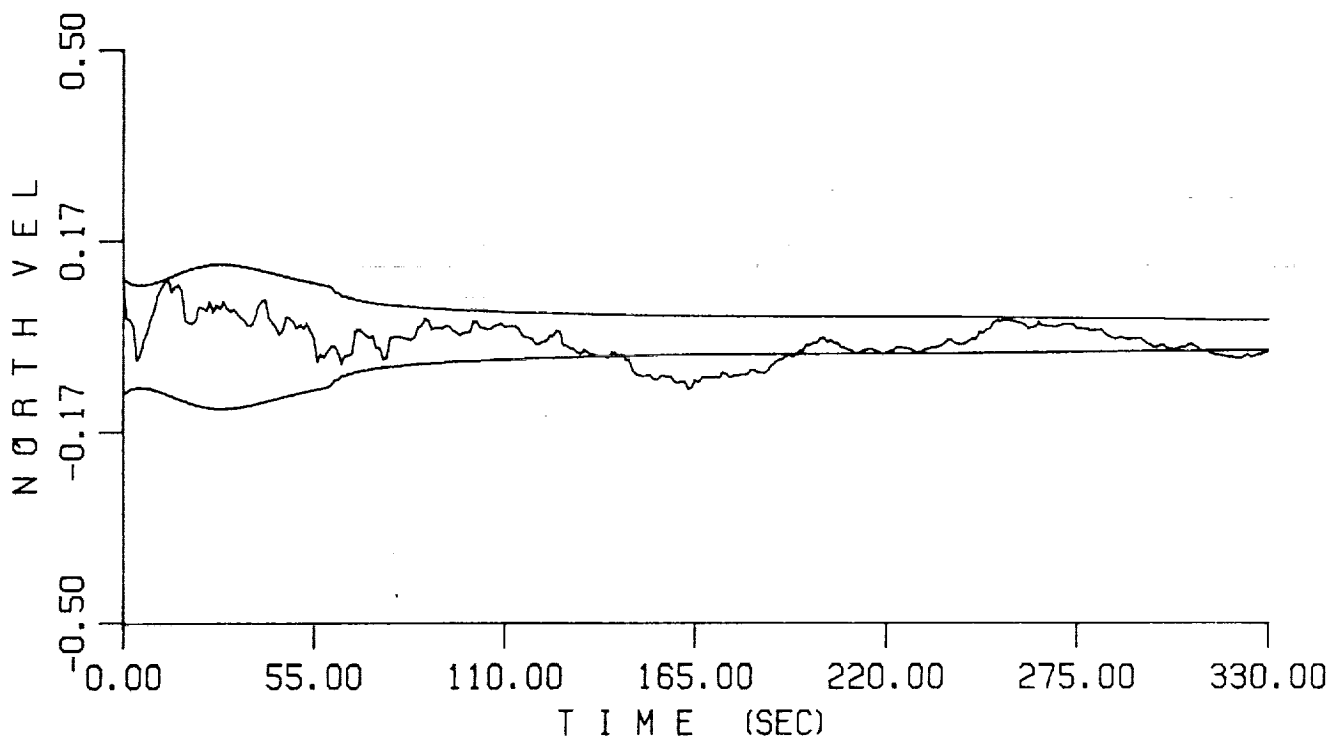


Fig. 37 : Time History of the North Velocity Error and its Covariance. Case I : Good Initial Conditions.

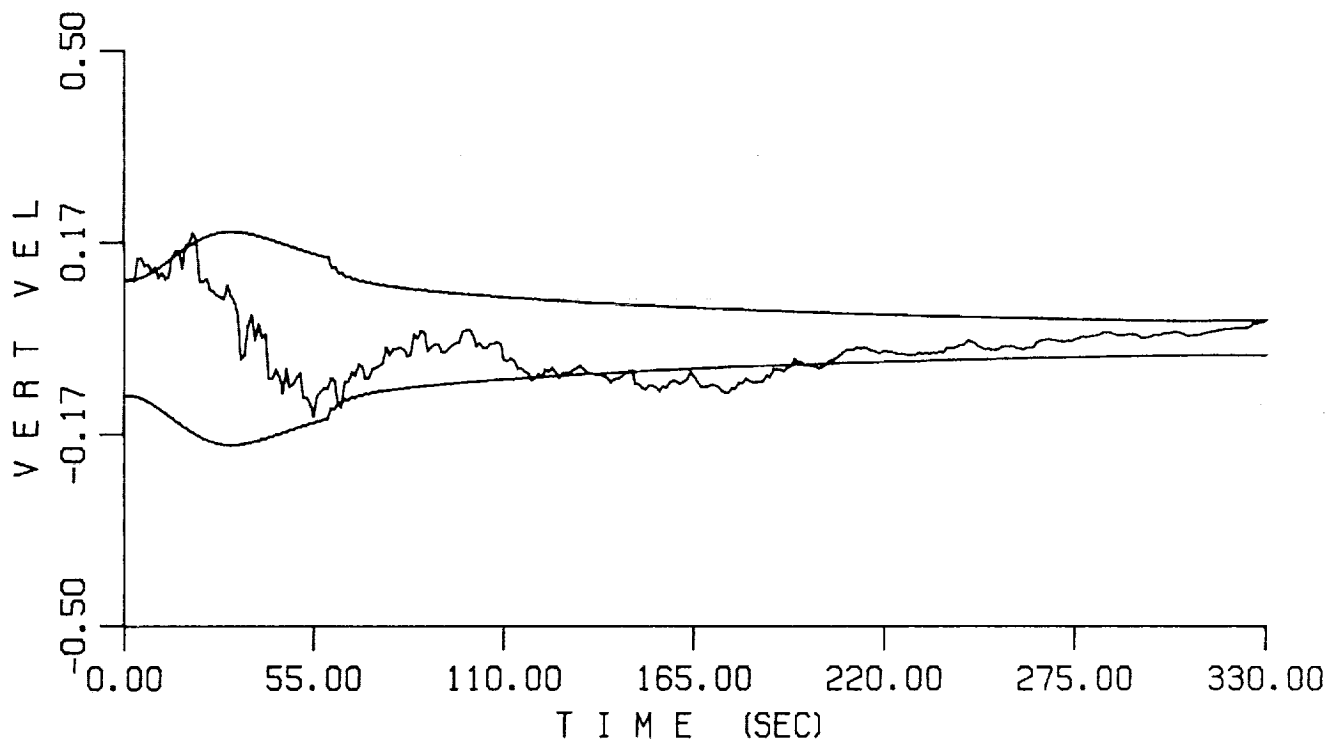


Fig. 38 : Time History of the Vertical Velocity Error and its Covariance. Case I : Good Initial Conditions.

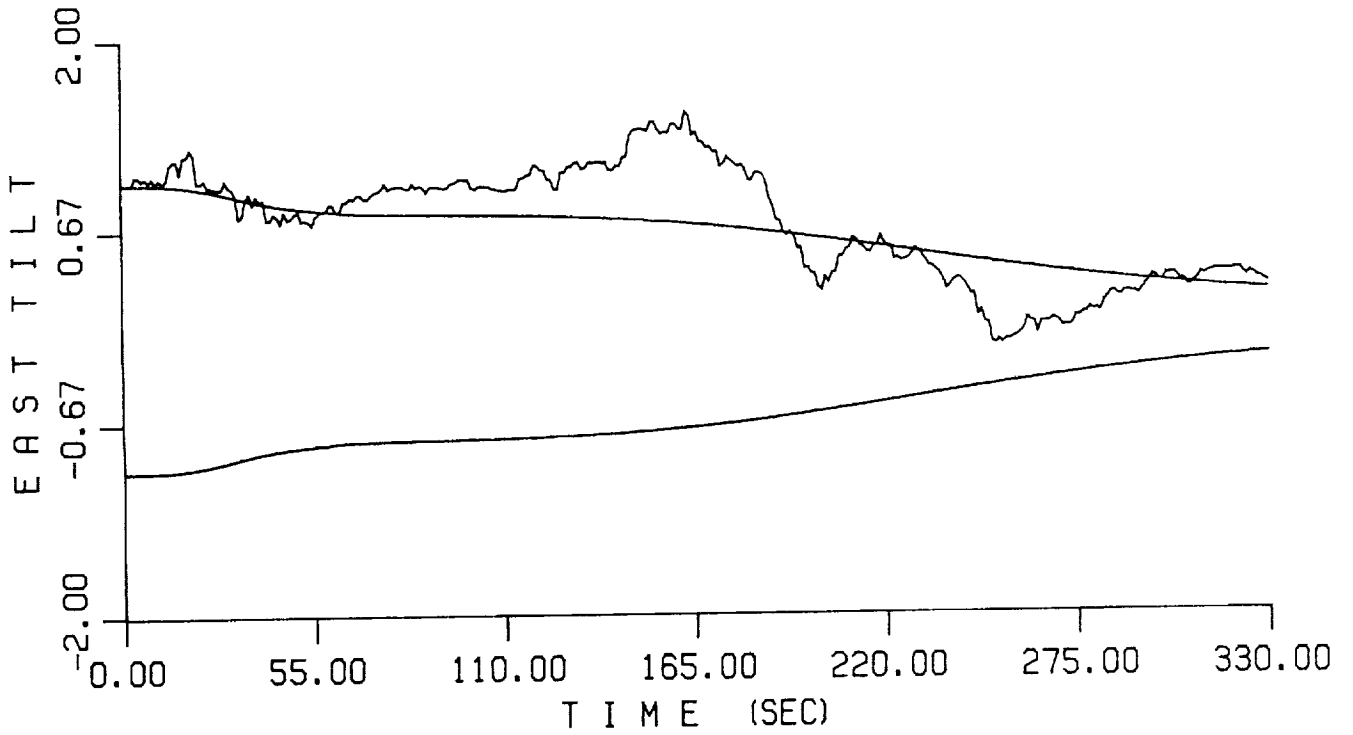


Fig. 39 : Time History of the East Tilt Error and its Covariance. Case I : Good Initial Conditions.

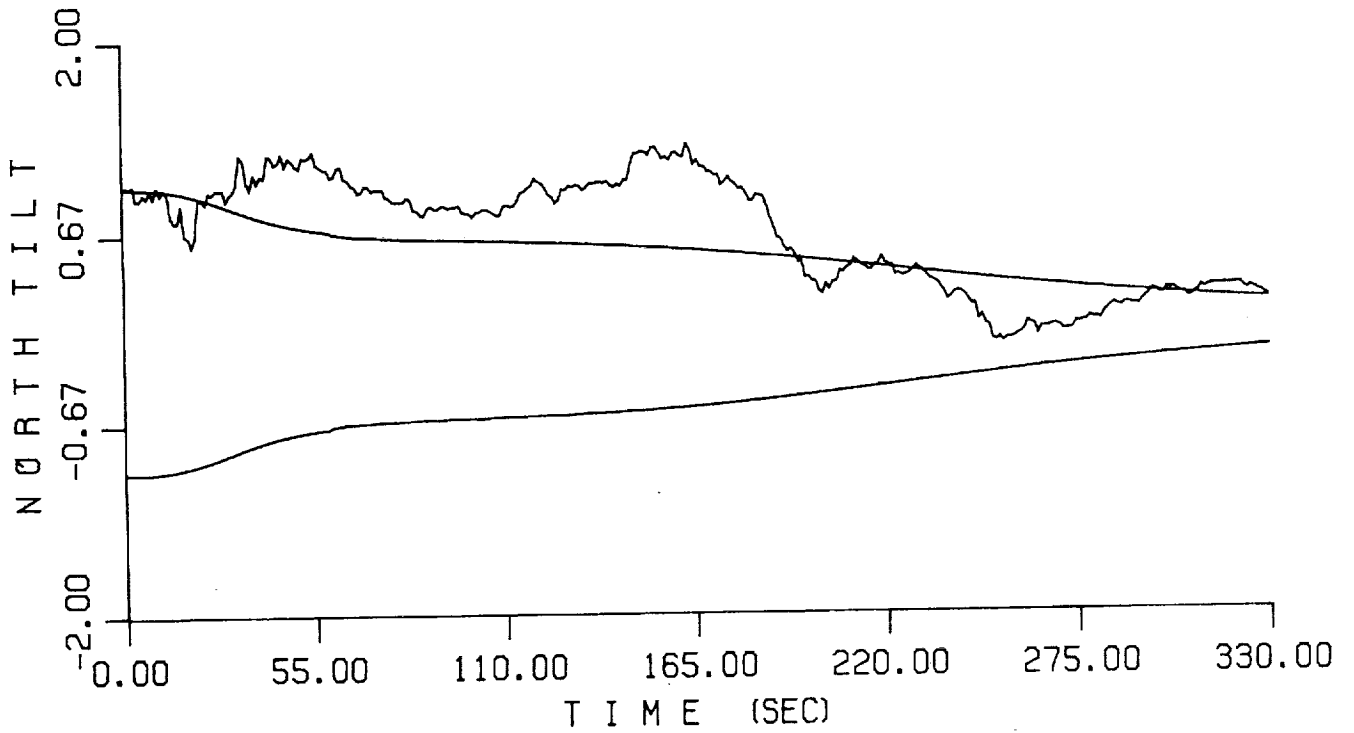


Fig. 40 : Time History of the North Tilt Error and its Covariance. Case I : Good Initial Conditions.

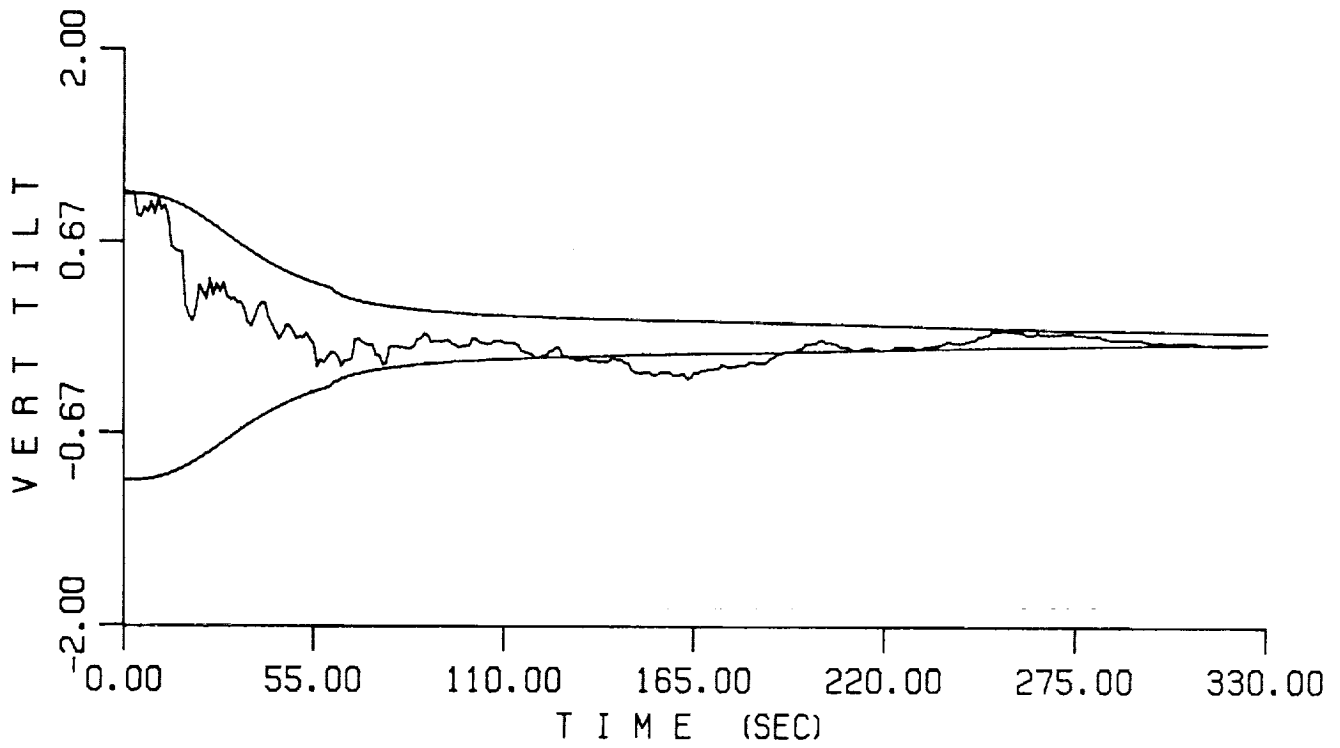


Fig. 41 : Time History of the Vertical Tilt Error and its Covariance. Case I : Good Initial Conditions.

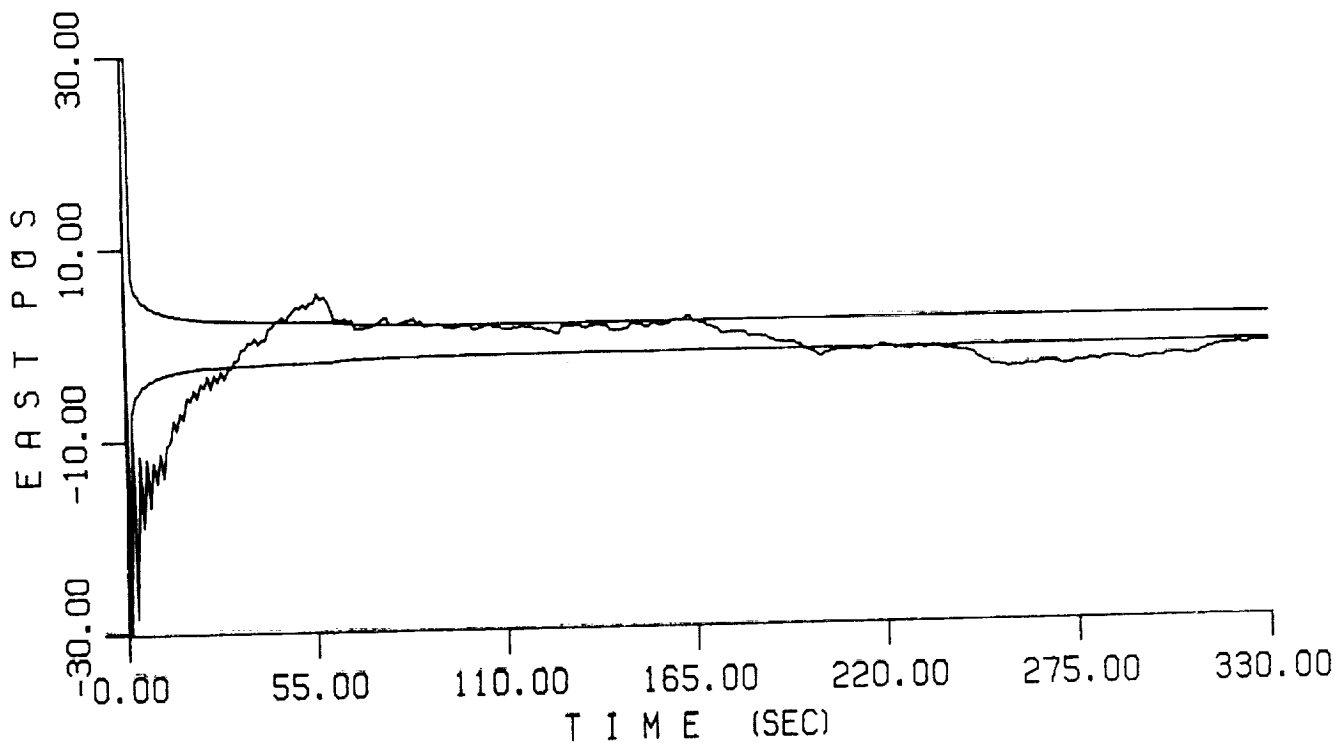


Fig. 42 : Time History of the East Position Error and its Covariance. Case II : Poor Initial Conditions.

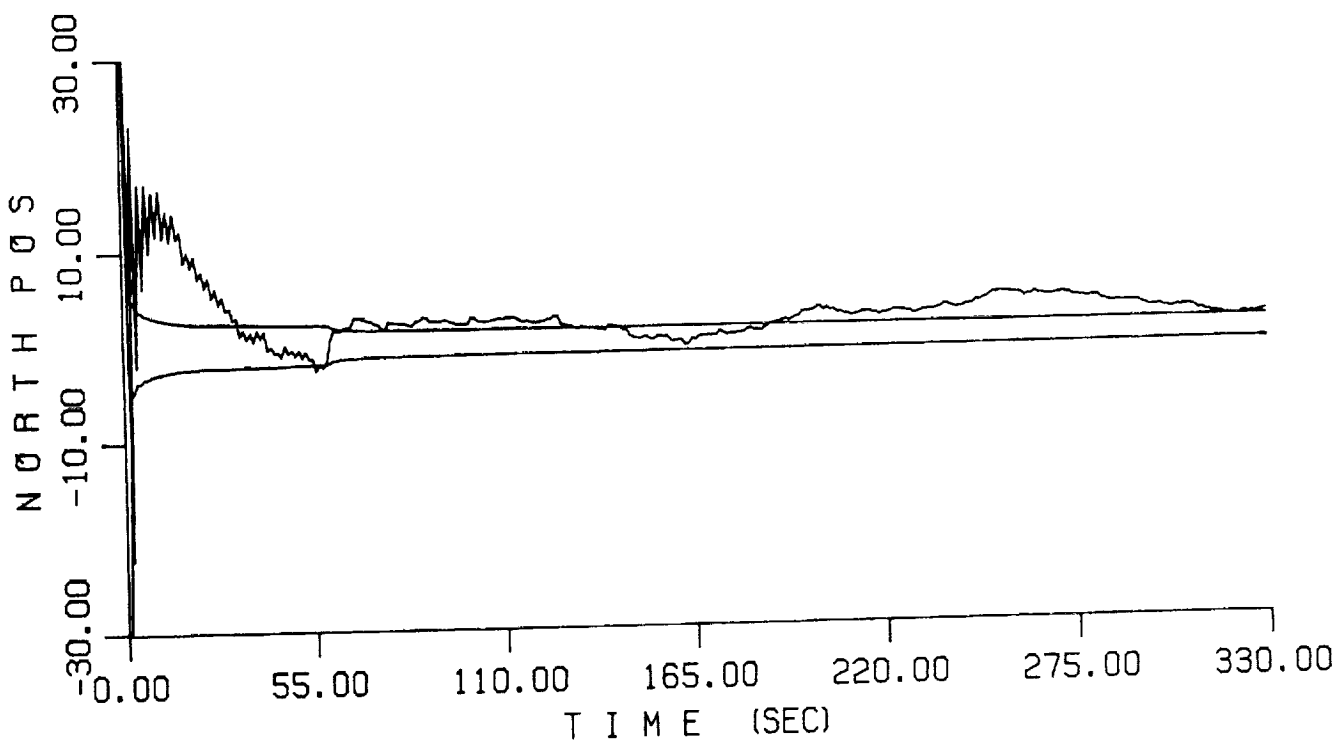


Fig. 43 : Time History of the North Position Error and its Covariance. Case II : Poor Initial Conditions.

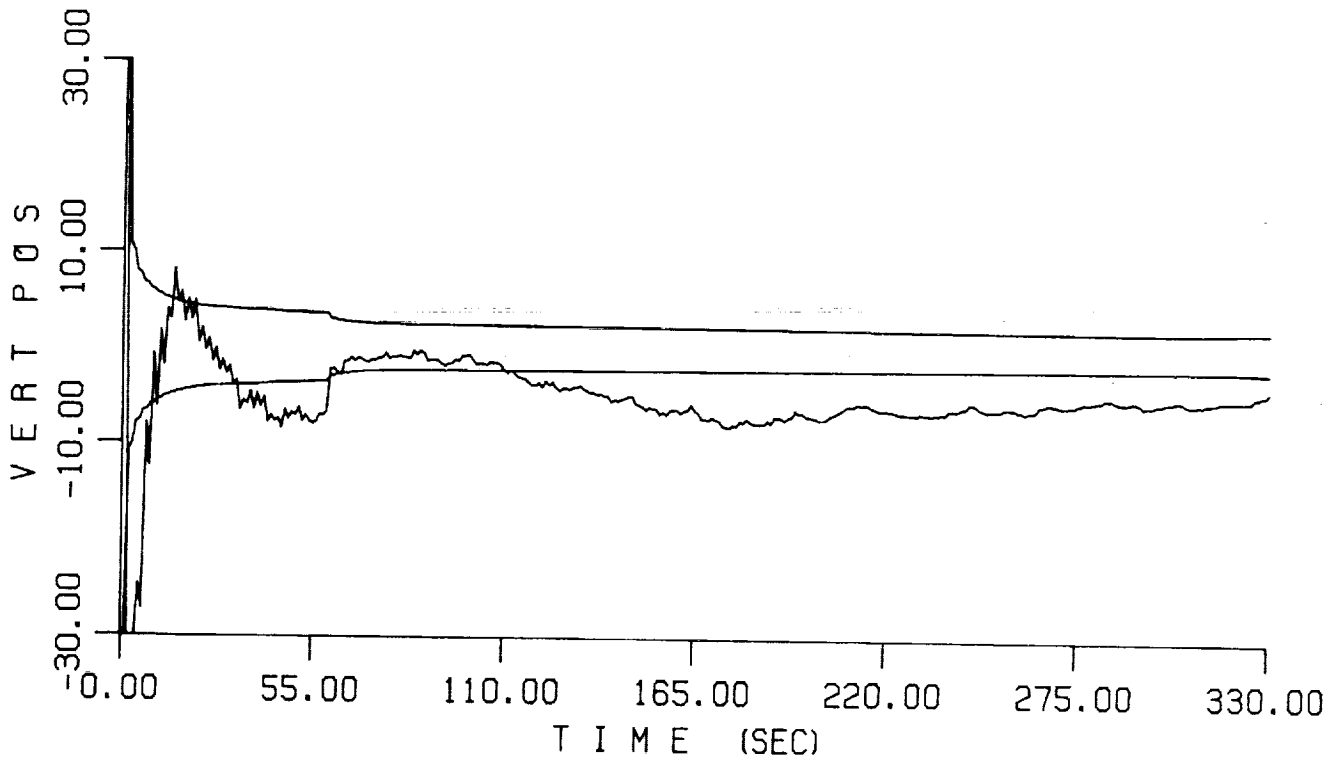


Fig. 44 : Time History of the Vertical Position Error and its Covariance. Case II : Poor Initial Conditions.

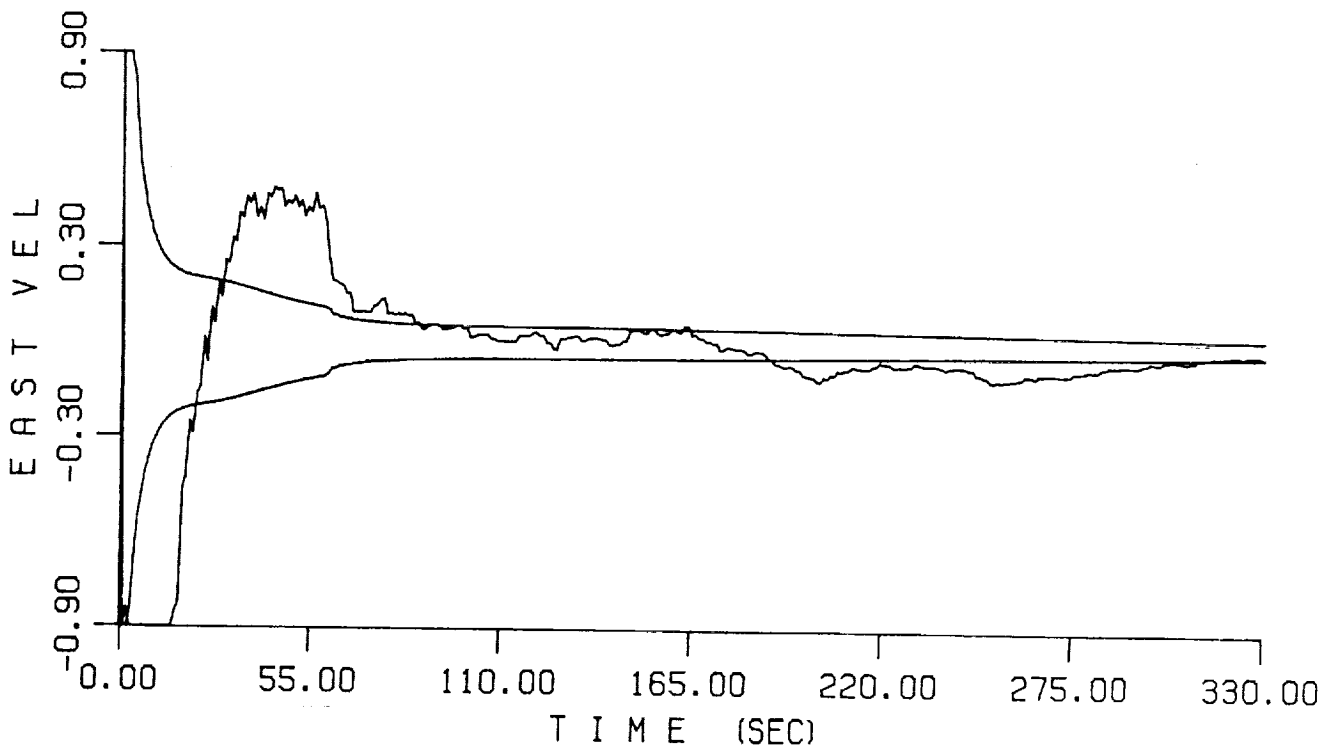


Fig. 45 : Time History of the East Velocity Error and its Covariance. Case II : Poor Initial Conditions.

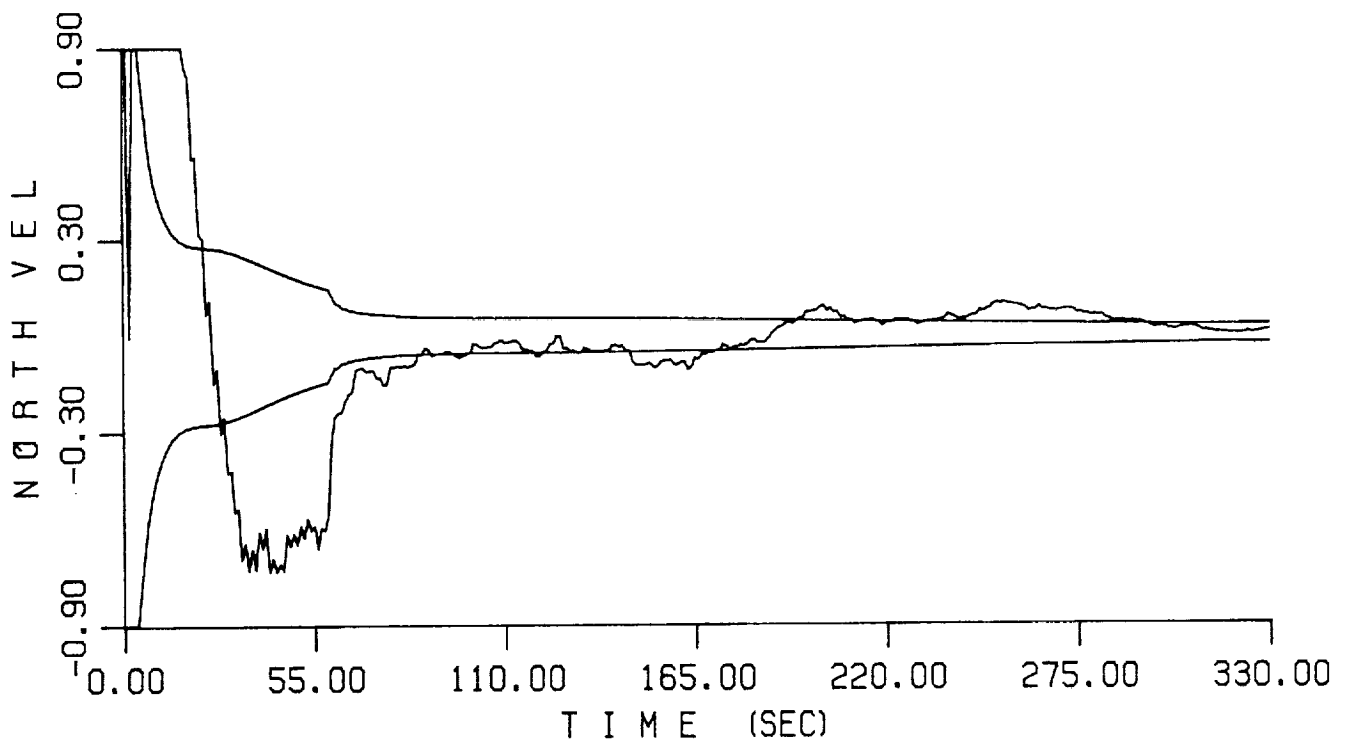


Fig. 46 : Time History of the North Velocity Error and its Covariance. Case II : Poor Initial Conditions.

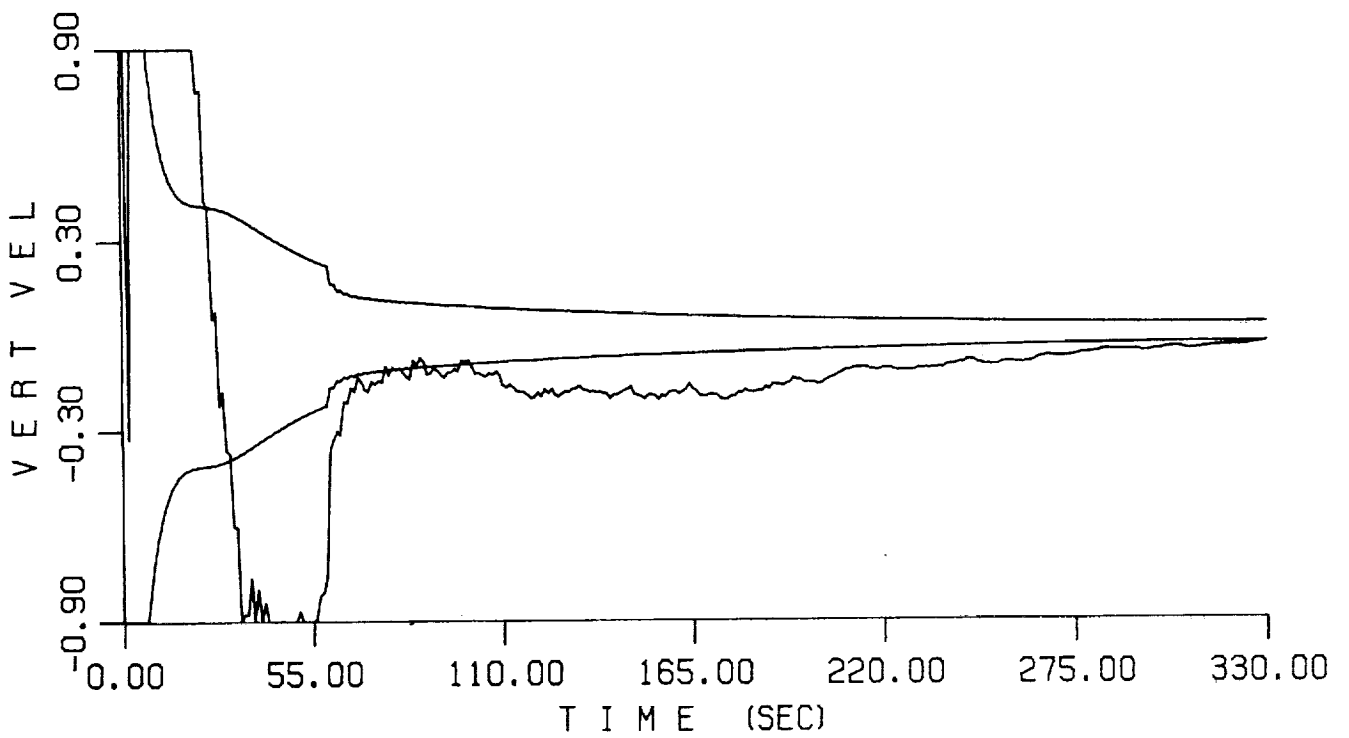


Fig. 47 : Time History of the Vertical Velocity Error and its Covariance. Case II : Poor Initial Conditions.

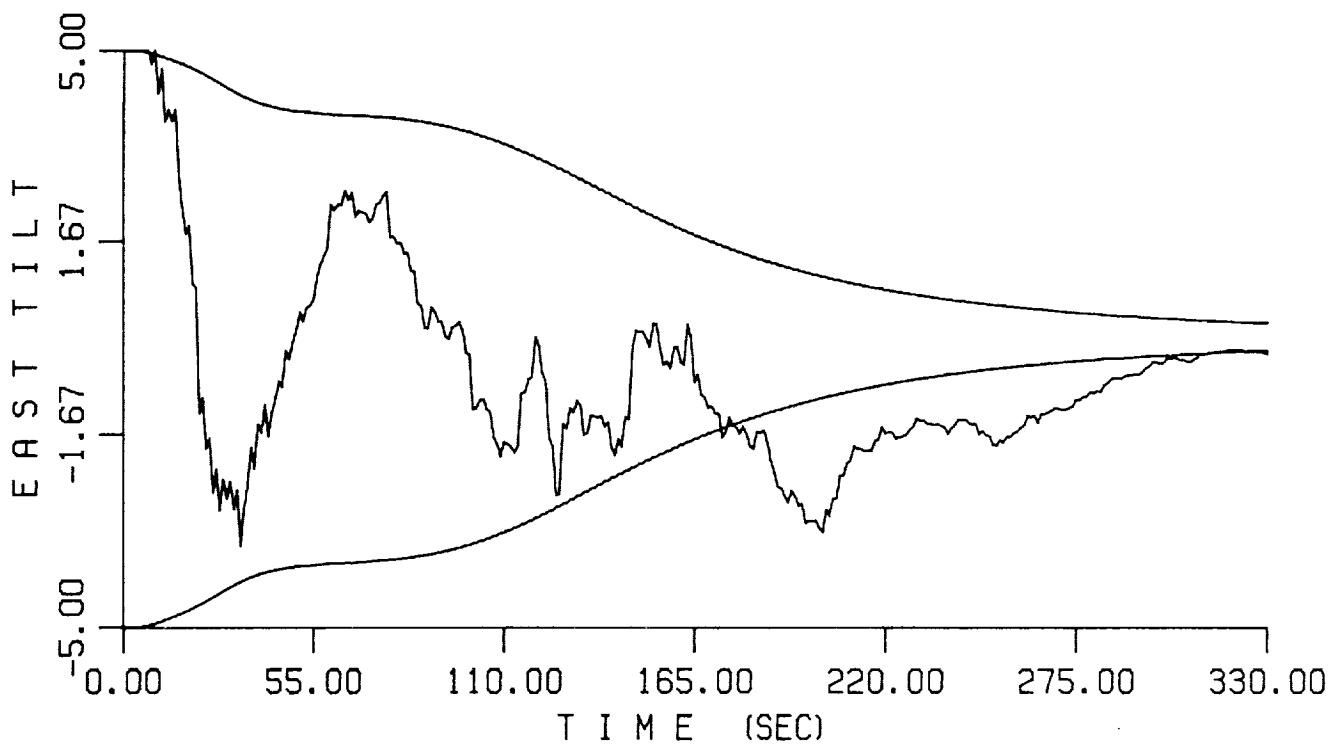


Fig. 48 : Time History of the East Tilt Error and its Covariance. Case II : Poor Initial Conditions.

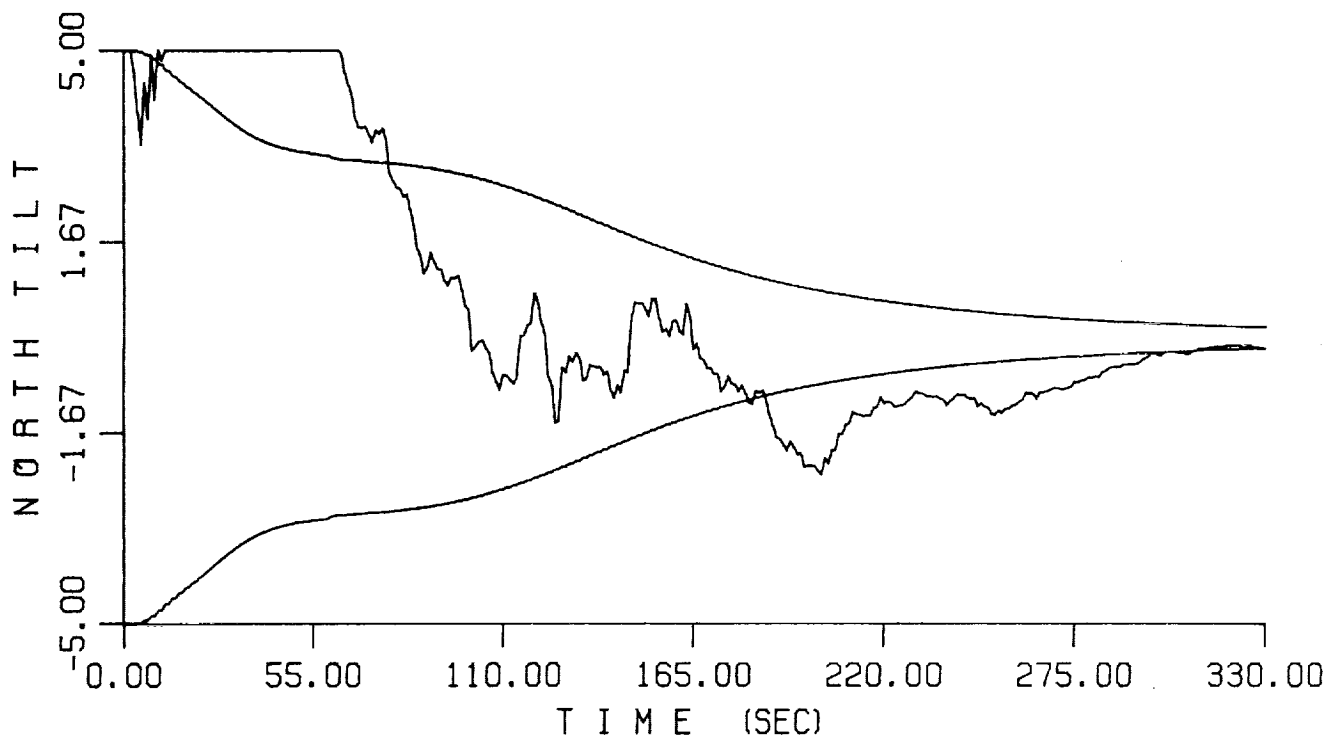


Fig. 49 : Time History of the North Tilt Error and its Covariance. Case II : Poor Initial Conditions.

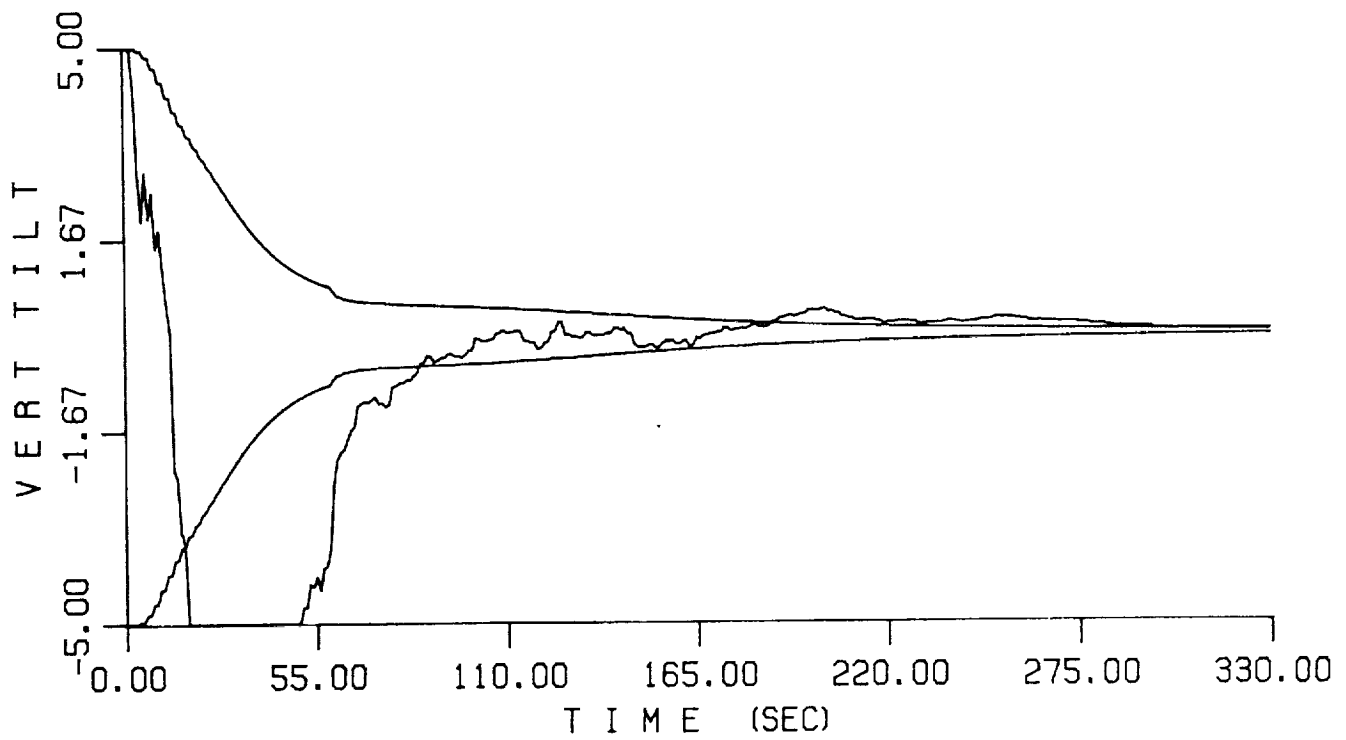


Fig. 50 : Time History of the Vertical Tilt Error and its Covariance. Case II : Poor Initial Conditions.

### **3.6 Memory and Throughput Analysis**

In order to successfully demonstrate the feasibility of the proposed autonomous integrated GPS/INS navigation experiment, efficient algorithms must be identified and demonstrated that meet performance requirements and do not stress available computer resources. We carried out, under Phase-I, the analysis that identifies the required software, interfaces between existing modules onboard the OMV and the new navigation software, and the memory and throughput estimates of this software. The following sections address these results in detail.

#### **Required Software**

The current baseline GPS/INS processing for the OMV was shown in Figure 1. In this, a loosely-coupled GPS/INS system, the GPS position and velocity is used to update or reset the INS position and velocity solution. In a tightly-coupled GPS/INS system (Figure 2), the GPS measurements are processed in an integrated navigation filter which estimates errors in position, velocity, attitude, and INS instrument errors such as gyro bias drifts and accelerometer scale factors. The INS instrument errors can thus be calibrated, providing superior navigation solution at all phases of the mission. It is this integrated navigation filter and the interfaces to the baseline TRW OMV navigation processing which is investigated here.

The functions performed by the Integrated GPS/INS Navigation Error Filter, shown in Figure 2, are:

Implementation of the Kalman Filter equations  
(propagation of the error states with time, and  
incorporation of the GPS measurements)

Formatting of data for I/O to other parts of the system

Computation of GPS satellite positions and velocities for predicted range and predicted delta-range computations

All of the algorithms required to meet the above functions are available by extracting the existing modules from the Mayflower integrated GPS/Inertial Navigation System Simulator (GINSS). Those modules extracted from GINSS (by name) and the functions of each module are listed in Table 3.

**Table 3: Required Software Modules for Proposed Navigation Filter**

MODULE	SOFTWARE FUNCTION
BFTRANS	Transforms input vectors and matrices to filter coordinate system
BFFMX	Computes the System Dynamics Matrix
BFPHIMTX	Computes the State Transition Matrix
BFQMX	Computes Process Noise Matrix
TUCOV	Performs the time propagation of the error states using the U-D factorization implementation
BFHMTX	Computes predicted measurements (range and delta-range) and computes the sensitivity vector
BFRESID	Computes the measurement residuals
MUCOV	Performs the measurement incorporation into the Kalman Filter using the U-D factorization
BPROPGPS	Computes GPS satellite positions and velocities from ephemeris data. Includes a polynomial interpolation routine.

The above modules meet all the processing requirements to implement the Integrated GPS/INS Navigation Filter. These modules were combined into a single file, and the interfaces were modified to conform to the new functionality required by the changed context of their environment. This file was used to estimate memory and throughput of the Integrated GPS/INS Navigation Error Filter, as detailed in the following two sections.

The Kalman Filter in this software is implemented by using the U-D factorization algorithms (see Section 3.3.4). This results in near double-precision accuracy while computing in single-precision floating point arithmetic. Also, no negative numbers can be computed for the main diagonal of the covariance matrix as can happen with the conventional Kalman Filter implementation. Published results [13] show no negative impact in throughput by using this implementation, as opposed to the conventional implementation.

### Memory Requirements Analysis

In order to estimate the memory requirements for the new software, the extracted sections of code from GINSS (listed in Table 3) were used. This code was then compiled and linked using Digital Equipment Corporation's FORTRAN version 5.1. The size of the resultant executable file is shown in Table 4. On another program, Mayflower has written FORTRAN and Ada benchmarks (which perform the same functions) in order to obtain information on code storage requirements and throughput inefficiencies which might be imposed due to Ada compiler immaturity. Using an unoptimized Ada compiler we found roughly a 90% penalty in executable file size. While this consideration would increase the memory requirements for code

storage to over 14K, we estimate the required size to be nearer 7.5K for the following reasons: 1) The code as tested was not optimized for real-time operation; 2) Ada compilers targeted for real-time code production produce tight, efficient code.

**Table 4: Executable File Size**

Compiler	Size of .EXE (16-bit words)
DEC	7.5K

For an estimate of the data memory requirements, we looked at two different approaches to arrive at a number for the integrated filter. The first involves manually going through the code, and counting variables and arrays to come up with an estimate of the data memory requirements. This first method results in a value of 2.95K 16-bit words for the data size. In the second approach, we used published formulae [13, 14] based on types of computations used to implement the Kalman Filter, number of states, and number of measurements available at one time. Using the formulae resulted in a value of 2.90K 16-bit words for the data size. These two values are summarized in Table 5. Both of these numbers include the storage required for GPS satellite ephemeris, position, and velocity values.

**Table 5: Data Memory Requirement**

Method	Data Size (16-bit words)
1. Counting	2.95K
2. Formula	2.90K

## Throughput Analysis

The throughput analysis was completed using the same code used for the memory requirement estimate. The FORTRAN code was analyzed to define the number of times each statement would be executed per filter cycle (one time propagation and two measurement incorporations). Then the operations in each statement were counted and multiplied by the number of times the statements are executed per filter cycle. This is done for every line in a program, and then all program totals are summed. The results of this procedure is shown in Table 6.

There are 3 columns in Table 6. The first is the total number of operations of the designated type that take place during one filter cycle (which corresponds to one second of real-time). Using details of the OMV's onboard computer (OBC) 444R<sup>2</sup> instruction set, the operation counts can be converted to the number of processor cycles. These numbers are shown in the second column of the Table. For the operations of array indexing and loads, two numbers are shown; worst and realistic cases. The worst case assumes every array element's address must be computed individually, and then that array element must be loaded as a separate operation. This is very unrealistic for filter operation, as explained in the following paragraph and so realistic numbers (less by a factor of four) are included for these two operations. With the above assumptions the total number of cycles required is  $1.2 \times 10^6$ . Assuming a 6 MHz clock frequency, this cycle loading represents 20% of the available throughput of one processor.

Table 6 reveals that close to 50 percent of CPU cycles are spent computing the memory locations of the variable arrays used in the filter, and in loading those values into registers where they can be used in computations. These values reflect no consideration for memory access

**WORST CASE AND REALISTIC CASE (In Parenthesis)**  
**THROUGHPUT ESTIMATE FOR PROPOSED 17-STATE**  
**NAVIGATION FILTER WITH A 1-SECOND, 2-MEASUREMENTS UPDATE**

Instruction	Number of Operations	Number of 444R <sup>2</sup> Cycles	Percentage of Estimated Total Cycles
Array indexing (1 SP add and 1 SP multiply)	25,000	5.71 x 10 <sup>5</sup> (1.43 x 10 <sup>5</sup> )	32
FP adds	21,300	3.20 x 10 <sup>5</sup>	18
FP multiplies	23,500	3.05 x 10 <sup>5</sup>	17
FP loads	32,000	2.23 x 10 <sup>5</sup> (0.56 x 10 <sup>5</sup> )	13
Other (tests, branches, increments)	56,000	3.58 x 10 <sup>5</sup>	20
TOTAL		1.8 x 10 <sup>6</sup> (1.2 x 10 <sup>6</sup> )	100

**Table 6: Throughput for Navigation Filter**

optimization, and assume addresses must be computed for every individual array element. This clearly is very unrealistic for real-time code. Also, the values in Table 6 assume all elements in the matrices are non-zero, and thus need to be used in the computations. Because of sparseness in the matrices, many multiplications and additions need not be carried out. Although we have coded our filter implementation to skip operations when matrix elements are equal to zero, the numbers in Table 6 assume every matrix operation will be carried out. For example, roughly 60 percent of the elements in the state transition matrix are zero. This will reduce the number of computations involved by at least a factor of two. Therefore, the 20% loading factor which was stated in the previous paragraph is very conservative for real-time code which will be optimized for its specific function.

### **3.7 Experiment Validation Test Plan**

The validation and testing of the reconfigurable integrated GPS/INS navigation error filter will take place in three stages. These three stages are:

- 1) Reconfigurable filter performance testing
- 2) Validation of knowledge-based resource allocation expert system
- 3) Testing of real-time software with simulated or real spacecraft telemetry data

Each stage is briefly described below:

- 1) During the development of the navigation error filter, GINSS will be relied upon to provide most of the testing and validation. The Monte Carlo capabilities have been recently demonstrated and will be used

extensively to verify the different modes of operation of the reconfigurable filter. The capability to choose what states to estimate will be invaluable during the early stages of this effort.

2) Different mission scenarios will be run in GINSS to validate the operation of the knowledge-based resource allocation in selecting the appropriate filter states to use for different mission phases.

3) We will either simulate telemetry data or obtain real data from NASA for one of the advanced STS missions. This will be used to test that all data interfaces are correct, the software performs as expected (using GINSS Monte Carlo statistics, and performance evaluations from ground stations, and other references where possible).

## SECTION 4

### SUMMARY - CONCLUSIONS

This report documents the results of a study on an autonomous integrated GPS/INS navigation experiment for the Orbit Maneuvering Vehicle (OMV). This investigation was carried out by Mayflower Communications Co., Inc. as an SBIR Phase I effort under Contract No. NAS8-38031. In this section, the results of the SBIR Phase I are summarized and conclusions are drawn.

The navigation and attitude update requirements for several NASA missions were reviewed during the Phase I study. Specific attention was devoted to the OMV, the OTV/STV, the Space Station and the Earth Science Geostationary Platforms. Careful examination of the aforementioned requirements established the applicability of the studied experiment to a wide variety of future NASA missions.

An important aspect of the Phase I investigation was to ensure that the appropriate interfaces between the GPS receiver, the OMV OBC and the telemetry data will be available for the demonstration of the experiment. Review of OMV documents and discussion with TRW personnel verified the availability of these interfaces. It was concluded that both the 1-second-rate and the slower-rate data, required for a ground demonstration of the navigation experiment will be available at the telemetry downlink.

A tightly-integrated GPS/INS navigation filter design was presented as an alternative to the current OMV configuration in which GPS signals are used to compute the vehicle's position and velocity and the IMU gyros are utilized to

provide inertial attitude reference. The inherent synergism of the GPS and the INS is taken into consideration and the outcome is improved navigation solution and attitude determination. The error models associated with the Rockwell International GPS receiver as well as the Singer-Kearfott SKIRU IV unit are presented.

There are times, during the OMV mission, at which prediction of the vehicle's orbit is required. Currently, this task is performed by the OMV OBC using a fourth order Runge-Kutta integrator, where the second degree zonal harmonic  $J_2$  is used to model the geopotential and the atmospheric drag acceleration is an input constant. As far as the geopotential modelling is concerned, we compared six hour arcs of an (8,8) reference orbit to both a  $J_2$  and a (2,2) orbit. The conclusion was that the (2,2) orbit yields smaller prediction errors than the  $J_2$  orbit by a factor of 2.5 or larger. Furthermore, this improvement was introduced at a minimal computational cost, since the additional throughput required to implement it is only 42  $\mu$ sec per update. As far as the atmospheric drag modelling is concerned, comparison of a Keplerian orbit to a drag perturbed orbit indicated that the Root Sum Square error in coordinates is approximately 400m and in velocity is 0.5 m/sec after six hours. This is a significant effect and appropriate models which will not introduce a large computational burden on the OBC should be examined.

A study to determine the visibility of the GPS satellites to the OMV GPS antennae was carried out. The primary GPS constellation of 21 satellites [27] was used for this investigation. Twelve hour orbital arcs were generated to cover a full period of the GPS satellites. An antenna look angle of  $110^\circ$  and two OMV orbital altitudes (250 nmi and 1000

nmi) and two inclinations ( $27^\circ$  and  $55^\circ$ ) were utilized. The GPS satellite selection and the computation of the Geometric Dilution of Precision (GDOP) was carried out once per minute, due to the rapidly changing geometry. We examined the antenna switching idea, according to which, whenever the visibility to one antenna became poor, OBC control or ground commands could be used to switch to the other antenna.

Without antenna switching, both the number of the visible GPS satellites and the GDOP are improved at the 1000 nmi orbital altitude as compared to the 250 nmi altitude. On the other hand, the orbital inclination influences the results only marginally. With antenna switching, both the number of the visible GPS satellites and the GDOP are marginally influenced by the orbital altitude and inclination. Furthermore, antenna switching almost doubles the number of visible GPS satellites and it eliminates areas with poor geometry.

The integrated GPS/INS navigation filter was implemented as an extended Kalman filter to estimate navigation errors, dominant IMU instrument errors and dominant GPS clock errors. The 17 error states included for the OMV application are 3 for position, 3 for velocity, 3 for attitude, 3 for gyro bias drift, 3 for accelerometer scale factor and 2 for GPS clock. Two new features were introduced in our filter. The first one was the implementation of the U-D factor equations for the time and measurement update of the states and the covariances and the second one was the incorporation of the second degree zonal harmonic in the filter.

The U-D factor formulation of the filter introduces two improvements. The first one is that it guarantees positive definiteness of covariance matrices. The conventional

formulation of the Kalman filter may result in indefinite covariance matrices due to numerical instabilities. The U-D factor formulation is designed not to suffer from similar shortcomings, which improves the robustness of the filter. The second improvement is that the U-D factor formulation yields near double-precision accuracy with single precision arithmetic, hence, it lowers significantly the memory requirements.

Mayflower's GPS Inertial Navigation System Simulation (GINSS) software was used to evaluate the performance of the integrated navigation filter for the OMV high-thrust trajectory. Two cases were considered. In the first case it was assumed that a GPS update was available prior to the start of the burn such that the position, velocity, tilt and clock bias were accurately known. In the second case it was assumed that a period of GPS outage had elapsed which resulted in deterioration of the navigation parameters (the latter case corresponds to a GPS signal acquisition specification). The duration of the burn was 5.5 minutes. The results from both test cases indicated excellent performance of the filter. The OMV navigation performance specification (Table 1) was met with ample margin even after a GPS outage. Furthermore, attitude update accuracy comparable to horizon and sun sensors was achieved without the restriction of maneuvering the vehicle such that the sun sensor points within 2 degrees of the sun.

The memory and throughput requirements to implement the integrated GPS/INS navigation filter in the OMV OBC were analyzed. In order to do this, the existing modules were extracted from GINSS and they were combined in a single file, after modifying the interfaces to conform to their new environment. The resulting file was compiled and linked using

DEC's FORTRAN version 5.1 and the size of the executable file was 7.5K 16-bit words, which is our estimate for the memory requirement of the software. The memory requirement for the data was arrived at in two ways. At first, manually going through the code and, secondly, via published formulae. The estimates were 2.95K 16-bit words from manual counting and 2.90K 16-bit words from the formulae. On the other hand, the aforementioned file was used to estimate the throughput, which was  $1.8 \times 10^6$  444R<sup>2</sup> cycles for a worst case and  $1.2 \times 10^6$  444R<sup>2</sup> cycles for a realistic case.

The final aspect of this investigation was to develop a testing and validation plan for the experiment. This plan includes testing of the performance of the reconfigurable filter, validation of the knowledge-based resource allocation expert system and testing of real-time software with simulated or real telemetry data.

Mayflower is planning on submitting a follow-on SBIR Phase II Proposal on the autonomous integrated GPS/INS navigation experiment for the OMV/STV. The focus of the proposed SBIR Phase II research will be a proof-of-concept experiment demonstration of an autonomous integrated GPS/INS navigation system which can be readily implemented in real-time onboard computers to improve the total navigation performance of advanced Space Transportation Systems such as the OMV, the AOTV, the Space Station and the Shuttle-C. The autonomous aspect of the proposed experiment refers to the software reconfigurability feature of the integrated filter to provide optimum performance taking into account changes in the mission scenario, thus allowing extreme flexibility in mission contingency planning.

The specific technical objectives of the SBIR Phase II will be to develop the integrated filter algorithms for absolute and relative navigation and for attitude determination. These algorithms will be designed and implemented in Ada for ease of transportability to various NASA missions and will be tested using simulated telemetry data. A real-time, knowledge-based, resource allocation expert system will be developed to implement the automatic reconfigurability of the navigation filter. The feasibility and applicability of the advanced integrated GPS/INS navigation system will be analyzed for a on high altitude, high thrust missions such as the Space Transfer Vehicle (STV). A follow-on Phase III program is expected to implement the Phase II developed software design and navigation processing technology in a future NASA/DoD mission.

## 5. REFERENCES

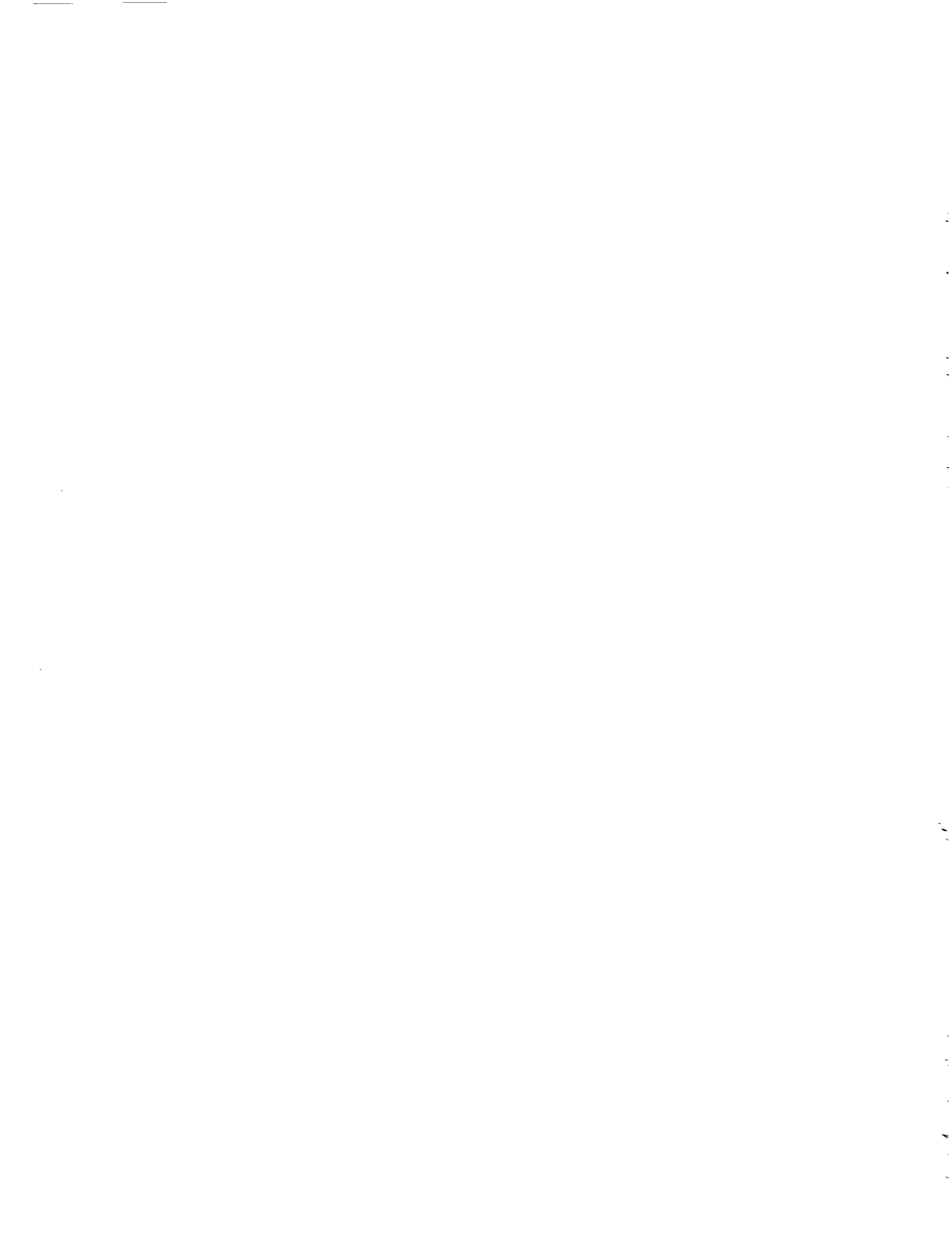
1. Wagner, R.E. and A.N. Bladsel, "An Approach to Autonomous Attitude Control For Spacecraft", Advances in the Astronautical Sciences, Volume 66, Proceedings of the Annual Rocky Mountain Guidance and Control Conference, January 30 - February 3, 1988, Keystone, Colorado, pp 51-64
2. Upadhyay, Triveni N. and Harley Rhodehamel, OMV Attitude Update Using GPS: Feasibility Study, Mayflower Communications, Company, Inc., Final Report No. MCC-R-88010, Contract No. NAS8-36363, NASA Marshall Space Flight Center, February 1988
3. Upadhyay, Triveni N., Harley Rhodehamel and A. Wayne Deaton, "Feasibility of Using GPS Measurements for OMV Attitude Update", Proceedings Institute of Navigation, National Technical Meeting, Santa Barbara, CA, January 1988
4. Maki, Stanley C., "Problems and Solutions for GPS Use Beyond the 12 Hour Orbit", Proceedings Institute of Navigation, National Technical Meeting, Santa Barbara, CA, January 1988, pp 187-193
5. Maki, Stanley C., "Optimization of a GPS User Experiment at GEO", Proceedings of the Satellite Division's International Technical Meeting, Institute of Navigation, Colorado Springs, CO, September 19-23, 1988, pp 203-210
6. Equipment Specification OMV: GPS Receiver Set, TRW CI No. 75-0202P, June 1988
7. Equipment Specification for OMV Inertial Measurement Unit, TRW, CI No. 75-0203P, November 1987
8. OMV Preliminary Design Review, Volume 4 - Avionics, Part 4 - Guidance, Navigation and Control, TRW Space & Technology Group, NASA Contract No. NAS8-36800, Marshall Space Flight Center, 22 August 1988
9. Ward, Phil and J. Rath, Spacecraft Applications of Advanced Global Positioning System Technology, Texas Instruments, Inc., Final Report U1-780130-F, Contract No. NAS9-17781, NASA Johnson Space Center, June 1988

## REFERENCES CONTINUED

10. Daley, Philip, C. and Allison L. Thornbrugh, "Autonomous Spacecraft Operations - Problems and Solutions", AIAA - Computers in Aerospace Conference, 6th, Wakefield, MA, October 7-9, 1987, pp 332-336
11. Donzelli, P., B. Ankermoeller, B. Sorensen and R. Katzenbeisser, Expert System Study for Spacecraft Measurement, Final Report, Dornier-Werke G.m.b.H., Friedrichshafen, West Germany, February 1987 (NTIS HC A06)
12. OTV Contract Definition and System Analysis Study, Final Review, Volume II, Part II Technical Summary, Martin Marietta, July 1986
13. Gura, I.A. and Bierman, A.B., "On Computational Efficiency of Linear Filtering Algorithms", Aerospace Report No. TR-0059(6521-01)-1, November 1970
14. Thornton, Catherine L. and Bierman, Gerald J. "UDU<sup>T</sup> Covariance Factorization for Kalman Filtering", Control and Dynamic Systems, Vol. 17, 1980
15. Rose, R.E., H. Schmeichel, C.P. Shortwell and R.A. Werner, "Automated Low-Thrust Guidance for the Orbital Maneuvering Vehicle", Proceedings of the Annual Rocky Mountain Guidance and Control Conference, Keystone, CO, Vol. 66, 1988
16. Upadhyay, Triveni N. and Harley Rhodehamel, "Autonomous Integrated GPS/INS Navigation Experiment for OMV", Proposal, SBIR Phase I, Mayflower Communications Company, Inc., Reading, MA, 1988
17. NASA's Earth Science Geostationary Platforms, A Program Status, October 1988
18. Upadhyay, Triveni N., George J. Priovolos, Wallace E. VanderVelde and Harley Rhodehamel, "STS-GPS Tracking Experiment for Gravitation Estimation: Feasibility Study", Final Report, AFGL-TR-89-0035, MCCI-TR-89-861002, Mayflower Communications Company, Inc., Reading, MA, February 1989

## REFERENCES CONTINUED

19. Marsh, J.G., et al., "An Improved Model of the Earth's Gravitational Field: GEM-T1", NASA Technical Memorandum 4019, 1987
20. French, R., "VAX Computer Implementation of a Preliminary Version of the GRAM Subroutine for AFE Simulations", NASA/MSFC, Huntsville, Al, May 1988
21. Yunck, Thomas P., William G. Melbourne, C.L. Thornton, "GPS-Based Satellite Tracking System for Precise Positioning",. IEEE Trans. on Geoscience and Remote Sensing, Vol. GE-23, No. 4, July 1985
22. Gelb, A. (ed.), Applied Optimal Estimation, The Analytic Sciences Corporation, Reading, MA, 1986
23. Windall, W.S., P.A. Grundy, "Inertial Navigation System Error Models", DTIC, TR-03-73, May, 1973
24. Heiskanen, W.A., H. Moritz, Physical Geodesy, W.H. Freeman and Co., San Francisco, CA, 1967
25. Rapp, R.H., "Geometric Geodesy - Part I", Classnotes, GS658, Department of Geodetic Science & Surveying, OSU, Columbus, OH, March 1984
26. Torge, W., Geodesy, Walter de Gruyter, Berlin - New York, 1980
27. Green, G.B., P.D. Massatt, H.W. Rhodus, "The GPS 21 Primary Satellite Constellation", Journal of the Institute of Navigation, Vol. 36, No. 1, Spring, 1989
28. Slides from NASA Symposium on GPS Space Applications, hosted by Jet Propulsion Laboratory, Pasadena, CA, November 1987







# Report Documentation Page

1. Report No. NASA CR-4267		2. Government Accession No.		3. Recipient's Catalog No.	
4. Title and Subtitle Autonomous Integrated GPS/INS Navigation Experiment for OMV: PHASE I Feasibility Study				5. Report Date January 1990	
				6. Performing Organization Code	
7. Author(s) Triveni N. Upadhyay, George J. Priovolos, and Harley Rhodehamel				8. Performing Organization Report No. MCCI-TR-89-891002	
				10. Work Unit No. M-621	
9. Performing Organization Name and Address Mayflower Communications Company, Inc. 80 Main Street Reading, MA 01867				11. Contract or Grant No. NAS8-38031	
				13. Type of Report and Period Covered 01-18-89 - 09-30-89 Final Contractor Report	
12. Sponsoring Agency Name and Address National Aeronautics and Space Administration Washington, DC 20546				14. Sponsoring Agency Code	
15. Supplementary Notes NASA Technical Monitor: A. Wayne Deaton, Systems Analysis and Integration Laboratory, Marshall Space Flight Center, MSFC, Alabama 35812 GPS - GLOBAL POSITIONING SYSTEM INS - INERTIAL NAVIGATION SYSTEM OMV - ORBITAL MANEUVER VEHICLE					
16. Abstract The Phase I research focused on the experiment definition. A tightly-integrated GPS/INS navigation filter design was analyzed in Phase I and was shown, via detailed computer simulation, to provide precise position, velocity and attitude (alignment) data to support navigation and attitude control requirements of future NASA missions. The application of the integrated filter was also shown to provide the opportunity to calibrate inertial instrument errors which is particularly useful in reducing INS error growth during times of GPS outages. While OMV provides a good target platform for demonstration and for possible flight implementation to provide improved capability, a successful proof-of-concept ground demonstration can be obtained using any simulated mission scenario data, such as STV, Shuttle-C, Space Station. OMV - ORBITAL MANEUVER VEHICLE ORBITAL MANEUVER VEHICLE					
17. Key Words (Suggested by Author(s)) GPS           Space Transportation System INS OMV Autonomous Navigation Filter			18. Distribution Statement Unclassified/Unlimited  Subject Category: 04		
19. Security Classif. (of this report) Unclassified		20. Security Classif. (of this page) Unclassified		21. No. of pages 91	22. Price A05

